NOVA SCHOOL OF SCIENCE & TECHNOLOGY

DEPARTAMENT OF CHEMISTRY

GONÇALO FILIPE CARRO PEDRO

BSc in Applied Chemistry

EXPLORING THE BEHAVIOUR OF SIX DIFFERENT DANSYL-BASED DYES AS ACTIVE MOLECULAR TOOLS

MASTER IN BIOORGANIC CHEMISTRY

NOVA University Lisbon

November, 2023

NOVA SCHOOL OF SCIENCE & TECHNOLOGY

DEPARTAMENT OF CHEMISTRY

EXPLORING THE BEHAVIOUR OF SIX DIFFERENT DANSYL-BASED DYES AS ACTIVE MOLECULAR TOOLS

GONÇALO FILIPE CARRO PEDRO

BSc in Applied Chemistry

Adviser: Carlos Lodeiro Y Espiño
Associate Professor with Habilitation, NOVA University Lisbon

Co-adviser: Elisabete de Jesus Oliveira
Assistant Researcher, NOVA University Lisbon

Examination Committee:

Chair: Luísa Maria da Silva Pinto Ferreira,
Assistant Professor with Aggregation, FCT-NOVA

Rapporteurs: Carla Isabel Madeira dos Santos,
Junior Investigator, Instituto Superior Técnico, Universidade de Lisboa

Adviser: Carlos Lodeiro Y Espiño,
Associate Professor with Aggregation, FCT-NOVA

MASTER IN BIOORGANIC CHEMISTRY

NOVA University Lisbon
November, 2023

Exploring the behaviour of six different dansyl-based dyes as active molecular tools

ACKNOWLEDGMENTS

I would like to start by expressing my appreciation to my supervisors, Prof. Carlos Lodeiro and Dr. Elisabete Oliveira, for allowing me to develop this project within the BIOSCOPE research group. Prof Carlos Lodeiro's constant support, guidance and shared passion for science were instrumental and I would like to thank him for always pushing me forward and believing in me. I would also like to thank Dr. Elisabete Oliveira for the support, for always pushing for high standards in our work and for always being so honest and direct. Both have not only made me appreciate the world of science but also instilled in me a work ethic of hard work and dedication that I will forever be thankful for. Moreover, I would like to extend my thanks to Prof. Atanas Kurutos and all the team from Bulgaria for all the enriching chemistry discussions and for sharing the compounds that were studied and made this thesis possible.

A special thanks to Frederico Duarte for patiently guiding me through the entire project. His constant presence and willingness to help have been invaluable and I am also very grateful for the friendship that we have developed.

I extend my gratitude to the remainder of the BIOSCOPE Group who always offered me assistance and definitely contributed to the development of this project, with a special thanks to Prof. José Luís Capelo for his constant support and for always pushing me and driving me forward.

I would also like to thank all the institutions that made this work possible by providing the necessary resources, namely FCT-NOVA, LAQV-REQUIMTE and PROTEOMASS Scientific Society.

To all my friends who I cannot thank enough, thank you for being there for me and for all the moments we shared during these years. You all have been an enormous source of support and encouragement throughout the journey and are a part of this achievement.

Finally, I extend my deepest thanks to my family for their unwavering support, regardless of the distance, and for all the sacrifices they made to provide me with the opportunity to do this project. Without their support, this achievement would not have been possible.

"Power is given only to those who dare to
lower themselves and pick it up."
Fyodor Dostoyevsky

ABSTRACT

Following the vast array of applications and great optical properties of the dansyl fluorophore, six novel dansyl-based compounds **L1** to **L6** have been synthesized and fully characterized in solution, solid-state and supported in a PMMA polymer matrix with the aim of discovering new luminescent sensing systems for environmental pollutants.

Within this study, we present an in-depth analysis of the photophysical properties of **L1** to **L6** in five different solvents, revealing their distinctive positive solvatochromic behavior. We also explore their acid-base sensing capabilities in both a CH_3CN solution and within a PMMA polymer matrix. Remarkably, these compounds exhibit an on-off emission response to highly acidic solutions and demonstrate excellent reversibility when exposed to ammonia.

The metal sensing behaviour was examined in CH_3CN solution with all compounds showing notable sensibility for Hg^{2+} and Cu^{2+} ions, and one compound also showing sensibility for Ag^{+} ions. The increase in concentration of metal ions was found to induce variations in absorption spectra and substantial fluorescence emission quenching.

Furthermore, in anion sensing studies, compounds **L4** to **L6** displayed exceptional sensibility for CN^{-} and F^{-} ions as evidenced by spectral changes and emission quenching during spectrophotometric and spectrofluorimetric titrations.

In the modern days of chemistry, the search for novel luminescent sensors has gained significant momentum due to the advantages they offer over conventional methods. The present study introduces an innovative system with a wide range of potential applications in the field of environmental monitoring, enabling the detection of various pollutants and toxic agents.

Keywords: Spectroscopy, Luminescence Probes, Dansyl-derivatives, Acid, PMMA Doped Films, Heavy Metals, Toxic Anions

RESUMO

Com base na versatilidade e excelentes propriedades ópticas do fluoróforo dansilo, foram sintetizados e caracterizados seis novos compostos baseados no dansilo (**L1** a **L6**) em solução, no estado sólido e suportados numa matriz de PMMA, com o objetivo de descobrir novos sistemas de deteção luminescente para sistemas poluentes.

Neste estudo, apresentamos uma análise aprofundada das propriedades fotofísicas de **L1** a **L6** em cinco solventes diferentes, revelando o seu comportamento solvatocrómico positivo. Também explorámos as suas capacidades de deteção ácido-base tanto numa solução de CH_3CN como numa matriz de polímero PMMA. De forma notável, estes compostos apresentam uma resposta de emissão *on-off* a soluções altamente ácidas e demonstram uma excelente reversibilidade quando expostos a amoníaco.

O comportamento de deteção de metais foi estudado em solução de CH_3CN, na qual todos os compostos mostraram uma sensibilidade notável aos iões Hg^{2+} e Cu^{2+}, e um composto a mostrar também sensibilidade a iões Ag^{+}. Verificou-se que a presença dos iões metálicos induz variações nos espectros de absorção e uma diminuição substancial da intensidade de emissão. Nos estudos de deteção de aniões, os compostos **L4** a **L6** mostraram sensibilidade excecional para os iões CN^{-} e F^{-}, tal como evidenciado pelas alterações espectrais e pela diminuição da emissão durante as titulações espectrofotométricas e espectrofluorimétricas.

Nos dias modernos da química, a procura de novos sensores luminescentes tem vindo a ganhar um impulso significativo devido às vantagens que apresentam sobre métodos tradicionais. Este estudo introduz um sistema inovador com uma vasta gama de aplicações potenciais na área ambiental, permitindo a deteção de poluentes e agentes tóxicos.

Palavras chave: Espectroscopia, Sondas Luminescentes, Derivados de Dansilo, Ácido, Filmes Dopados de PMMA, Metais Pesados, Aniões Tóxicos

SCIENTIFIC COMMUNICATIONS

Oral Communications

1 - Gonçalo Pedro, Frederico Duarte, Georgi Dobrikov, Atanas Kurutos, Hugo M. Santos, José Luis Capelo-Martinez, Elisabete Oliveira, Carlos Lodeiro

"Detecting toxic molecules and ions, ranging from cyanide to mercury, using a solvatochromic derivative of dansyl"

5th International Caparica Conference on Pollutant Toxic Ions and Molecules (PTIM)

Caparica, Portugal – 6th -9th November 2023

Shotgun Communication – www.ptim2023.com

Poster Communications

1 - Frederico Duarte, Gonçalo Pedro, Georgi Dobrikov, Atanas Kurutos, Hugo M. Santos, José Luis Capelo-Martinez, Elisabete Oliveira, Carlos Lodeiro

"From Blue to Green: Solvent and acid effects on novel emissive molecular probes of dansyl-based dyes."

16th International Workshop on Sensors and Molecular Recognition (IWOSMOR)

Valencia, Spain – 6th -7th July 2023

Poster Communication – www.iwosmor.com

SCIENTIFIC PAPERS

"Optical Evaluation of Dansyl Derivatives and Their Implementation in Low-Cost and Flexible Dye-Doped PMMA Platforms for Efficient Detection of Hazardous Chemical Vapors"

Gonçalo Pedro, Frederico Duarte, Georgi Dobrikov, Atanas Kurutos, Hugo M. Santos, Jose Luis Capelo-Martinez, Elisabete Oliveira, Carlos Lodeiro

Submitted 11/2023

CONTENTS

LIST OF FIGURES

List of Tables

List of Equations

ACRONYMS

AIEE	Aggregation Induced Enhanced Emission
CHEQ	Chelation Enhancement Quenching Effect
DMSO	Dimethyl Sulfoxide
DNSC	Dansyl Chloride
EDTA	Ethylenediaminetetraacetic Acid
ESI-Qq-TOF	Electrospray Ionization Quadrupole-Quadrupole Time Of Flight
FTIR	Fourier-Transformed Infrared
GSH	Glutathione
IC_{50}	Half Maximal Inhibitory Concentration
ICP-MS	Inductively Coupled Plasma Mass Spectrometry
LOD	Limit of Detection
LOQ	Limit of Quantification
MCF-7	Michigan Cancer Foundation-7 (Breast Cancer Cell Line)
MS	Mass Spectrometry
NEM	N-Ethylmaleimide
NMR	Nuclear Magnetic Resonance
PFA	Perfluoroalkoxy Alkane
PMMA	Poly(methyl methacrylate)

ppb	Parts Per Billion
ppm	Parts Per Million
PVP	Polyvinylpyrrolidone
SBS	Styrene-butadiene-styrene
SK1	Sphingosine Kinase 1
THF	Tetrahydrofuran
US EPA	United States Environmental Protection Agency
UV-Vis	Ultraviolet-Visible

SYMBOLS

Φ_f	Sample fluorescence quantum yield
Φ_r	Standard Quantum Yield
υ_0	Value of absorption and/or emission in a reference solvent
A	Absorbance
b	Cell path length
c	Concentration
I_{norm}	Normalized emission intensity
k_r	Radiative rate constant
k_{nr}	Non-radiative rate constant
P	Energy per second per unit of area entering sample
P_0	Energy per second per unit of area emerging from sample
S_0	Ground state
S_1	Lowest excited singlet state
T	Transmittance
T_1	Lowest excited triplet state
α	Solvent hydrogen bond donor acidity
β	Solvent hydrogen bond acceptor basicity
ε	Molar extinction coefficient

π^*	Solvent dipolarity/polarizability
τ_f	Fluorescence lifetime

1

INTRODUCTION

1.1 Absorption and Fluorescence Spectroscopy: Key Concepts

1.1.1 Light Absorption

When a molecule absorbs a photon, it experiences an increase in its energy level, transitioning to an excited state. However, upon emitting a photon, the molecule experiences a decrease in its energy level, returning to the lowest energy state, commonly referred to as the ground state. The specific wavelength of absorbed light is crucial because it represents the molecular processes that can occur. Visible and ultraviolet radiation, which play a central role in this master thesis, promote the excitation of electrons to higher-energy orbitals. Another example is infrared radiation, which induces molecular vibrations. On the other hand, short-wavelength radiation, such as X-rays and gamma-rays, can lead to bond cleavage and ionization in molecules.[1]

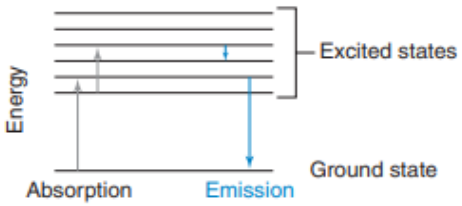

Figure 1. Absorption and emission effects on energy

1.1.2 Lambert-Beer Law

When a sample is exposed to light, the irradiance of the beam decreases as the sample absorbs light. The quantification of irradiance can be achieved through transmittance (**T**), which denotes the ratio of light passing through the sample. Transmittance is calculated by considering P_0, the energy per second per unit area of the incident light beam entering the sample, and **P**, the energy per second per unit area of the light beam emerging from the sample. [1]

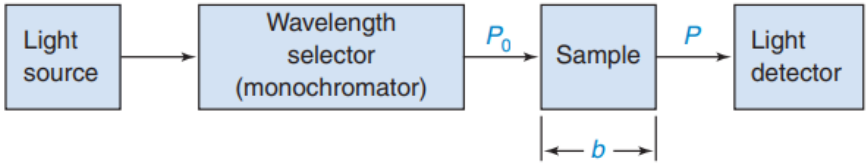

Figure 2. Single-beam spectrophotometry. [1]

$$T = \frac{P}{P_0} \qquad \text{(Equation 1 [1])}$$

Absorbance is considerably more practical to use than irradiance since it relies on two variables that can be easily manipulated during an experiment.

The Lambert-Beer law, a basis principle in spectroscopy and analytical chemistry, elucidates the correlation between the absorption of light by a solution and the concentration of the absorbing species within that solution. This fundamental concept provides a framework for understanding and analyzing the behavior of absorbing species in solution (refer to equation 3).

$$A = \log\left(\frac{P_0}{P}\right) = -\log T \qquad \text{(Equation 2 [1])}$$

$$A = \varepsilon bc \qquad \text{(Equation 3 [1])}$$

In equation 3, **c** denotes the concentration of the sample, **b** represents the path length of the cell and **ε** (epsilon) the molar extinction coefficient, which is an inherent property of the species. Lambert-Beer law is widely used in analytical chemistry for quantitative analysis of various compounds. While the Lambert-Beer Law is highly useful, it requires a homogeneous solution

of the absorbing species, and the chemical system should follow the determined range of concentrations in order to avoid deviations from linearity.[2]

1.1.3 Jablonski Diagram

The Jablonski Diagram, displayed in Figure 3, serves as a valuable tool for defining the various processes that unfold when a system (molecule) absorbs energy, by illustrating the electronic states of the molecule and the transitions between them. In a molecule, electronic states are categorized into singlet states, where all electrons are spin-paired, and triplet states, where one set of electrons is spin-unpaired.

When a molecule is excited by light, it can occupy various vibrational levels within the electronic state and subsequently undergo processes that facilitate relaxation to a lower energy state. These processes can lead to the emission of a photon, such as fluorescence and phosphorescence, or the transfer of energy to other molecules through collisions, ultimately converting the energy into heat.

The different processes that can occur between states are: [1,3]

Vibrational relaxation: Transition to the lowest vibrational level inside the spin-state

Internal conversion (S_1 -> S_0): Nonradiative transition between states with same spin multiplicity

Intersystem crossing (T_1 -> S_0): Nonradiative transition between states with different spin multiplicity

Fluorescence (S_1 -> S_0): Transition with photon emission between states with same spin multiplicity

Phosphorescence (T_1 -> S_0): Transition with photon emission between states with different spin multiplicity

Singlet-singlet or Triplet-triplet transition: Excitation into higher singlet or triplet states upon absorbing a second photon (S_1-> S_2 or T_1-> T_2)

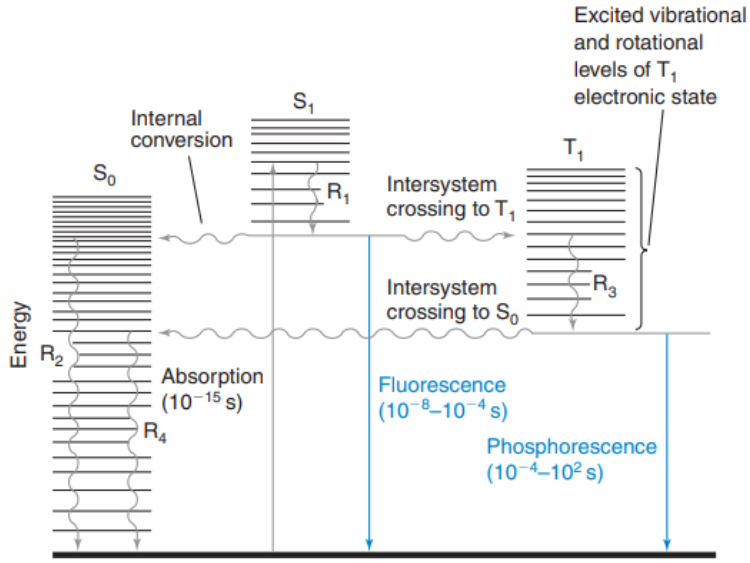

Figure 3. Jablonski Diagram - S_0 is the ground state, S_1 and T_1 are the lowest excited singlet and triplet states. Wavy arrows represent non-radiative transitions and straight arrows represent transitions involving photons. Adapted from [1]

1.1.4 Solvent effects and Stokes Shift

In a solution, a fluorophore can be enclosed within a solvation shell, engaging in interactions with the solvent's molecules. Upon exciting the fluorophore with a specific wavelength, the electronic distribution undergoes changes, giving rise to new bonding forces and dipole moments. Consequently, the solvent molecules need to adapt to a new equilibrium configuration. At room temperature, the vibrational transitions that occur become broader, resulting in a displacement of the fluorescence emission band compared to the absorption band. This displacement is known as the Stokes Shift, named in honor of the physicist George Gabriel Stokes, who made significant contributions to optics and fluorescence, aiding in the comprehension of this phenomenon. Since there is a loss of vibrational energy following light absorption, attributed to non-radiative relaxation processes, fluorescence emission always occurs at higher wavelengths, accounting for the observed Stokes Shift.[3]

1.1.5 Solvatochromic effect

Solvatochromism is a phenomenon that provides insights on the interactions between molecules and their surrounding environment, specifically the solvent in which they are dissolved. This phenomenon is evident through the alteration of a molecule's color, absorption or emission spectra when placed in different solvent environments. Solvatochromism serves as

a valuable tool for comprehending the electronic and structural attributes of molecules, as it unveils how the polarity and dielectric constant of a solvent can impact a molecule's energy levels, consequently leading to shifts in its photophysical properties. Depending on whether an increase in solvent polarity results in a red or blue shift, solvatochromism can manifest as either positive or negative, respectively.

Solvatochromism is widely employed across different domains of chemical and biological research to investigate both bulk and local polarity in macrosystems, such as membranes. Additionally, it is utilized to elucidate the conformation and binding of proteins.[4,5] Due to its importance in the forementioned fields, this phenomenon has been explored by our group in the past decade in several fluorophores, from arylthiophenes[6] to coumarins[7] and most recently in dansyls[8], which is the fluorophore of interest for this thesis.

The Kamlet-Taft equation is a widely used equation to describe and quantify solvatochromic effects, particularly the influence of solvent polarity on the behaviour of molecules. In Equation 4, the correlation between absorption and emission energies is illustrated with various solvent parameters. Here, ν_0 represents the absorption and/or emission value in a reference solvent, α denotes the solvent's hydrogen bond donor (HBD) acidity, β signifies the solvent's hydrogen bond acceptor (HBA) basicity, and π* represents the solvent's dipolarity/polarizability. The parameters a, b, and p, corresponding to the responses of the solute property to the solvent property, can be determined through a multiparametric fitting process.[5]

$$\upsilon = \upsilon_0 + a\alpha + b\beta + p\pi^* \quad \text{(Equation 4 [5])}$$

1.1.6 Fluorescence quantum yield and lifetime

Fluorescence quantum yields and lifetime are two crucial experimental parameters to measure in sensor molecules. The fluorescence quantum yield of a process is characterized as the proportion of emitted photons to the absorbed photons by the fluorophore. It is typically measured on a scale from 0 to 1, with 1 representing a 100% yield, where every photon absorbed results in the emission of a photon.

Quantum yield can be described by two rate constants: k_r, radiative rate constant, and k_{nr}, nonradiative rate constant, which comprise every possible decay mechanism (see Equation 5). Since photon-emitting decay mechanisms are the goal when searching for a high quantum-yield fluorophore, the non-radiative decay must be minimized ($k_{nr} \approx 0$).

$$\Phi_f = \frac{k_r}{k_r + k_{nr}} \quad \text{(Equation 5 [3])}$$

Experimentally, fluorescence quantum yields can be determined using either relative quantum yields (solution) or absolute quantum yields (solid state). The relative quantum yields are determined in comparison to a standard solution of known quantum yield, however, it's worth noting that this method can present certain challenges. This method requires a fluorescence standard with a precisely characterized quantum yield that emits and absorbs light in the same wavelength range as the sample is required. However, only a limited number of standards have been characterized with the necessary precision to ensure reliable measurements, including substances like quinine sulfate, fluorescein, and rhodamine.

The following equation can be used to calculate a sample's quantum yield using this method: A - area of sample's absorption spectra; A_r - area of standard's absorption spectra; n - sample refraction index; n_r - standard refraction index; Φ_r - standard quantum yield [3,9]

$$\Phi_f = \frac{A}{A_r}\Phi_r\left(\frac{n}{n_r}\right)^2 \quad \text{(Equation 6. [9])}$$

The fluorescence lifetime is the duration during which a molecule remains in its singlet excited state S_1 and can be calculated with the following equation:

$$\tau_f = \frac{1}{k_r + k_{nr}} \quad \text{(Equation 7. 3)}$$

1.1.7 Fluorescence quenching

Fluorescence intensity can be diminished by various processes, collectively referred to as quenching. This reduction in intensity can result from several factors, including: [1,10]

Collisional Quenching - The fluorophore in an excited state contacts with another molecule in solution (quencher) and returns to the ground state. Can happen when molecule-molecule interactions are strong enough to overcome the solvent interactions and prevent the molecule from being solvated. Can occur between identical molecules to form excimers or between different molecules to form exciplexes.

Photoinduced Electron Transfer - Excited state electron transfer between a donor and acceptor group

Energy Transfer - Energy transfers between electron donating molecules and electron accepting molecules.

Proton Transfer - Proton transfer between proton donating or accepting molecules with an acid or base, leading to protonation/deprotonation in the excited state.

Static Quenching - The fluorophore, while in the ground state, establishes a nonfluorescent complex with the quencher.

1.1.8 Fluorophore structure effects

Fluorophores with a rigid structure are effective at minimizing nonradiative decay by limiting rotation and vibration of the side groups, thereby maximizing their quantum yield. Conjugated electron-donating groups and electron-withdrawing groups play a role in charge transfer transitions, which further enhance the quantum yield. Structures containing heavy atoms should be avoided because of their strong spin-orbit coupling, which can lead to a high intersystem crossing rate constant. [1,10]

1.2 Luminescence-based molecular probes

Within the wide domain of analytical chemistry and molecular detection, luminescence-based molecular sensors or probes hold a prominent position as versatile and sensitive tools, providing valuable insights into intricate molecular interactions. Luminescence possesses distinct advantages for molecular sensing, including its sensitivity, selectivity, and non-invasive characteristics. These attributes explain the growing popularity of luminescence-based sensors in a wide range of fields, covering environmental monitoring, medical diagnostics, drug discovery, and food safety.

The principle behind these sensors revolves around the interaction between the luminescent probe and the analyte of interest. This interaction results in alterations in the luminescent properties of the system, particularly in its fluorescence, when subjected to external stimuli. These alterations can manifest as changes in emission intensity, wavelength, quantum yield, or fluorescence lifetime. The versatility of these systems allows their application across various domains, from tracking intracellular ions [11–13], to detecting pollutants in environmental samples [14–16] or even monitoring of biochemical interactions in organisms. [17–19]

1.2.1 Doped polymeric materials as sensors

As mentioned previously, luminescent sensors offer exceptional sensitivity and versatility. However, their use in the liquid state presents specific challenges and limitations, primarily related to stability, reusability, and adaptability to various environments. Integrating these systems into polymers effectively addresses these issues by providing a solid platform for their immobilization, thereby enhancing practicality. Additionally, this solid platform can improve stability, making them suitable for long-term applications. This strategy has opened up numerous possibilities for sensing applications, as doped polymers, in general, serve as robust and cost-effective matrices, offering rapid response times and system reversibility.[20]

Among the high number and types of polymeric matrices, polymethyl methacrylate (PMMA, chemical structure depicted in Figure 4) emerges as a promising candidate for luminescent sensing applications, due to its outstanding mechanical and optical properties that favour its application for optical devices, usually leading to enhanced fluorescence or phosphorescence. Additionally, this polymer is cost-effective and easy to prepare, facilitating an efficient production process [21]. Another popular polymer for sensing applications is styrene-butadiene-styrene, known as SBS. It is distinguished by its mechanical flexibility, elasticity, and robust adhesion properties, making it suitable for a variety of applications that may not be feasible with PMMA. Polyvinylpyrrolidone (PVP), on the other hand, is well-regarded for its biocompatibility, rendering it an excellent choice for incorporating luminescent probes into materials for biomedical applications. Additionally, PVP is hydrophilic, promoting water solubility and ease of dispersion for hydrophobic probes.[22]

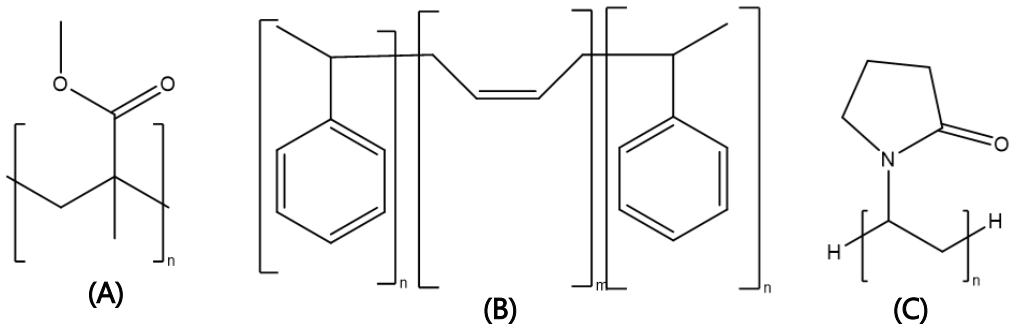

Figure 4. Polymeric structures of (A) PMMA, (B) SBS and (C) PVP

1.2.2 Luminescence-based acid-base sensors

The pH value, which represents the proton concentration, is a crucial factor in numerous chemical and biological processes and requires thorough regulation. Minor deviations can lead

to physiological damage and disrupt the normal functioning of biological systems. Therefore, precise monitoring of pH changes in organisms is crucial for medical applications and research in the biological sciences[19]. Furthermore, monitoring of pH levels is of utmost importance in industrial processes, where maintaining precise pH levels ensures efficient chemical reactions, consistent product quality and environmental compliance. [23]

Among traditional methods for pH measurement, luminescence-based acid-base sensors have emerged as valuable tools. They offer enhanced sensitivity and selectivity while remaining non-destructive and non-invasive and provide a quick response time and straightforward monitoring, making it possible to continuously track pH changes in systems requiring precise control.[24,25]

1.2.2.1 Previous studies in doped polymer materials as acid-base sensors

Our group has been working with doped polymer materials as sensors during the past years.[26,27] As a practical example recently we developed a low-cost colorimetric pH sensor, based on PMMA polymers doped with cyanines **1**, **2** and **3**. After exposing cyanine-doped PMMA polymers to low pH concentrations, the system showed a degree of spectral changes, from emission maximum shifts and emission enhancements (Figure 5B) as well as, the colour changes from green to yellow (Figure 5C). Moreover, as we can observe in Figure 5C, the system showed excellent reversibility, reverting to the natural green colour after being removed from the acid environment, proving this to be a reusable system. The authors reported that the sensing mechanism was due to the protonation of the indole nitrogen atom present in the cyanine group - acidic conditions lead to the protonation, inducing a strong increase in fluorescence, while basic conditions quenched the emission. Those results show that probes **1**-**3** are good candidates for naked-eye detection of low pH concentrations, with possible contributions for superacid sensing, enabling the continuous monitoring of polluted effluents in real-time or integration into quality control procedures within industrial processes.[28]

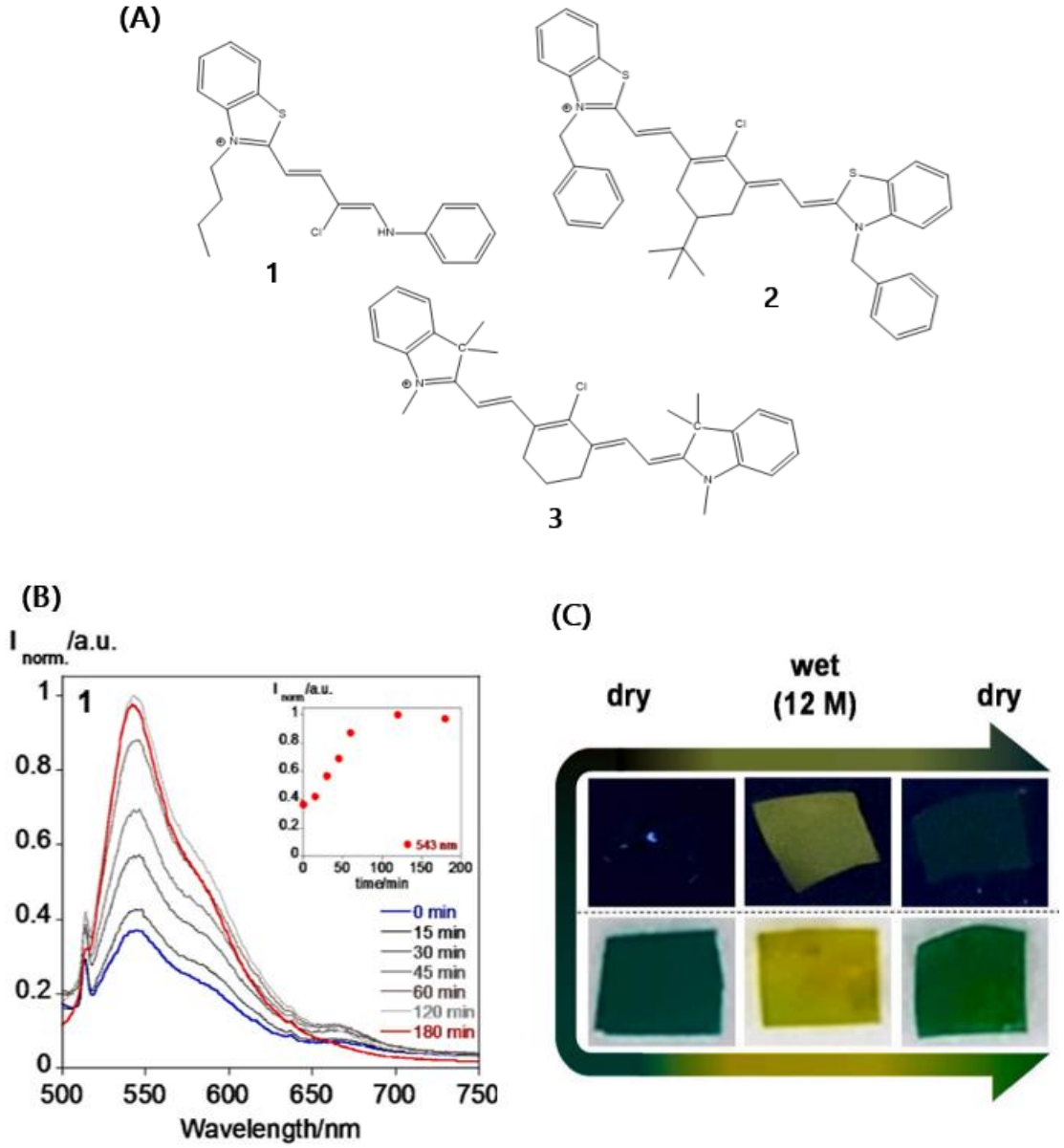

Figure 5 - (A) Chemical structure of compounds **1**, **2** and **3**. **(B)** Emission spectra of cyanine doped PMMA system after immersion in 12M HCl solutions for 15-180min. **(C)** Naked-eye(top) and under 365nm UV-light (bottom) images of cyanine doped PMMA system after immersion in 12M HCl solutions. Adapted from[28] .

1.2.3 Luminescence-based metal sensors

Due to the rapid expansion of industries along the years as well as the anthropogenic concentration of metals in mines and mineral explorations, a large amount of toxic and carcinogenic heavy metal ions has been discharged into the environment, leading to a progressively severe pollution of soil and groundwater, as metals have limited biodegradability.

The accumulation of heavy metals such as Hg^{2+}, Cd^{2+}, Ni^{2+} and Pb^{2+} in the environment poses significant threats to human health, as they induce immunotoxic and neurotoxic effects, potentially causing harm to the central nervous system and leading to the risk of organ failure.[29] On the other hand, even other metals such as Fe^{3+}, Cu^{2+} and Zn^{2+} are essential micronutrients in biological organisms, vital for enzymatic reactions, cellular signalling, DNA replication, in high concentrations results as well in toxic elements.[30]

Conventional methods for heavy metal detection mainly consist of atomic absorption and fluorescence spectrometry, and the more expensive and sophisticated inductively coupled plasma mass spectrometry (ICP-MS). Even though these analytical methods enable the sensitive and selective determination of heavy metals, they are time consuming, require sophisticated costly instrumentation and cannot perform real-time monitoring [31]. In contrast, fluorescence-based sensors have been highly regarded, due to their rapid, cheap, and simple use in detecting heavy metals.

Given the sensitivity of the sensors developed in this study towards Hg^{2+} and Cu^{2+}, it is key to explore the roles that these metals play.

Mercury as Hg^{+}, Hg^{2+} and organomercury is notable for its toxicity, and given its ability to accumulate in most parts of the human body, it can cause a large range of symptoms leading to death. Furthermore, human and animal studies that have established a connection between mercury toxicity and neurodegenerative diseases emphasize the critical need for detecting this metal in the environment. This is especially important as mercury is released as a byproduct of various industrial processes.[32]. The United States Environmental Protection Agency has established a maximum contaminant level for mercury in water at 2 parts per billion (ppb) [33].

Copper, as opposed to mercury, is an essential trace element in biological systems as it plays a vital role in various biological processes, serving as an important cofactor for a variety of enzymes involved in key biochemical reactions, including redox enzymes related to oxidative stress. Being essential for life, copper concentration in organisms is meticulously regulated, as a deficiency can led to health issues like anemia. Conversely, excessive copper intake can result in poisoning and give rise to a condition known as Wilson disease. The maximum contaminant level for copper in drinking water has been set at 1.3 parts per million (ppm) by the U.S. Environmental Protection Agency (EPA), which is a concentration 1000 times higher than the permitted level for mercury. [34]. Considering the substantial toxicity associated with both mercury and copper, it is imperative to closely monitor their presence in various environments.

Our research group has been working on metal ion detection with luminescence-based sensors for the past twenty years and based on this experience many examples based on macrocycles, acyclic molecules, free chromophores, conjugate sensors, etc. have been used. For instance, we recently explored a cationic porphyrin-based molecule **4** with the objective of metal sensing. The metal sensorial studies revealed that the system did not exhibit significant changes in the presence of Zn^{2+}, Cd^{2+} and Fe^{3+} ions. However, when Cu^{2+}, Pb^{2+} and Hg^{2+}ions were introduced the emission intensity in the two bands centered at 635 and 702nm decreased (see Figure 6B). The system also displayed a selective colorimetric response, with a specific color variation for each metal ion (Figure 6C), which was confirmed by the absorption spectra (Figure 6D). The absorption spectra showed the development of a new band for Pb^{2+} and $Hg^{2+}$and an increase in absorbance of the porphyrin band for Cu^{2+}. The detection limits by absorption for this system were found to be 3.6, 5.8 and 3.8 ppm for Cu^{2+}, Pb^{2+} and Hg^{2+}, respectively. Furthermore, the authors incorporated the system in mesoporous silica nanoparticles, achieving a detection limit of 2 ppb, with a naked-eye detection of 5 ppm. This system was also successfully applied for Hg^{2+} remediation in water, being able to extract the amount of ca. 69 mg/g, higher numbers than most of those reported in literature up to the publication date.[35]

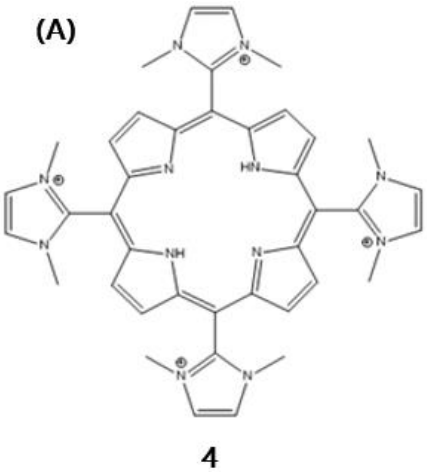

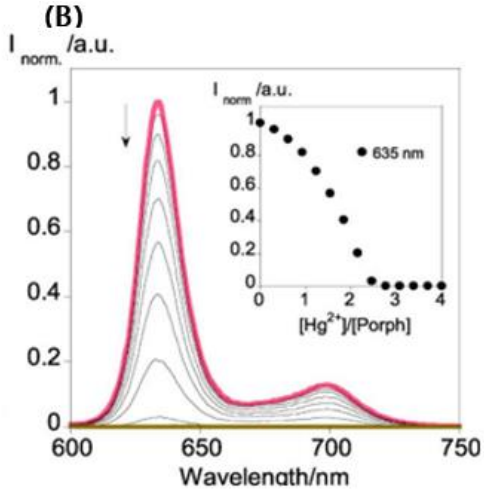

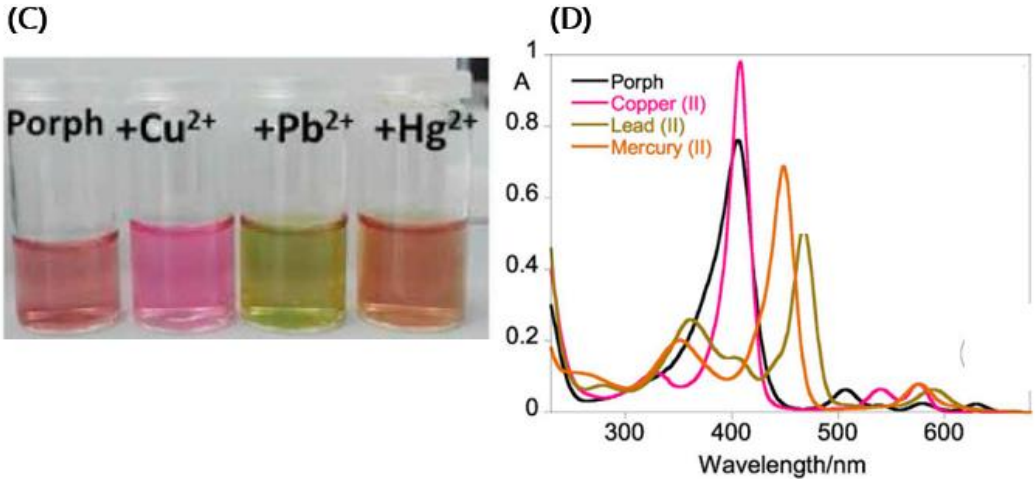

Figure 6 - **(A)** Chemical structure of compound **4**. **(B)** Spectrofluorimetric titration of **4** with addition of Hg^{2+}. **(C)** Colorimetric changes of solutions of **4** after addition of metal ions. **(D)** Absorption spectra of **4** upon addition of 1eq. of Cu^{2+}, Pb^{2+} and Hg^{2+}. Adapted from[35]

Exploiting the use of inorganic complexes as metal ion sensing, we reported some luminescent platinum complexes and tested them for metal sensing with eleven different metal cations, with the most interesting results being achieved by molecules **5** and **6**. Since these compounds possess free coordinative positions, it was interesting to investigate the effects of various metal cations. With compound **5**, the authors observed significant alteration in fluorescence emission only in the presence of Hg^{2+}, where the quenching of emission reaches a minimum upon the addition of 1 equivalent., which is consistent with the chelation enhancement of the quenching effect reported previously by our group[36] (Figure 7A). The authors suggested the interaction of Hg^{2+} with the structure to be like depicted in Figure 7B. Compound **6** was also evaluated for metal sensing, and surprisingly, the addition of Hg^{2+} led to an increase of the emission intensity (Figure 7C), reaching its maximum after addition of 2eq. of the cation. Additionally, there was a red-shift from 527 to 644nm, changing from a low-greenish emission to a bright red (Figure 7D). This red-shift was attributed to the formation of intermolecular Pt-Pt interactions as illustrated in Figure 7E, leading to an aggregation-induced emission enhancement (AIEE) response. Upon the addition of up to 7 equivalents of Hg^{2+}, the developed emission band decreased until the initial intensity was recovered. However, the emission maximum remained at 644nm, indicating that the molecules maintained their assembly via Pt-Pt interactions. The authors demonstrated that these systems are promising candidates for Hg^{2+} sensing. They also highlighted how similar molecules can respond differently to the same metal, employing distinct sensing mechanisms, whether through emission quenching or enhancement.[37]

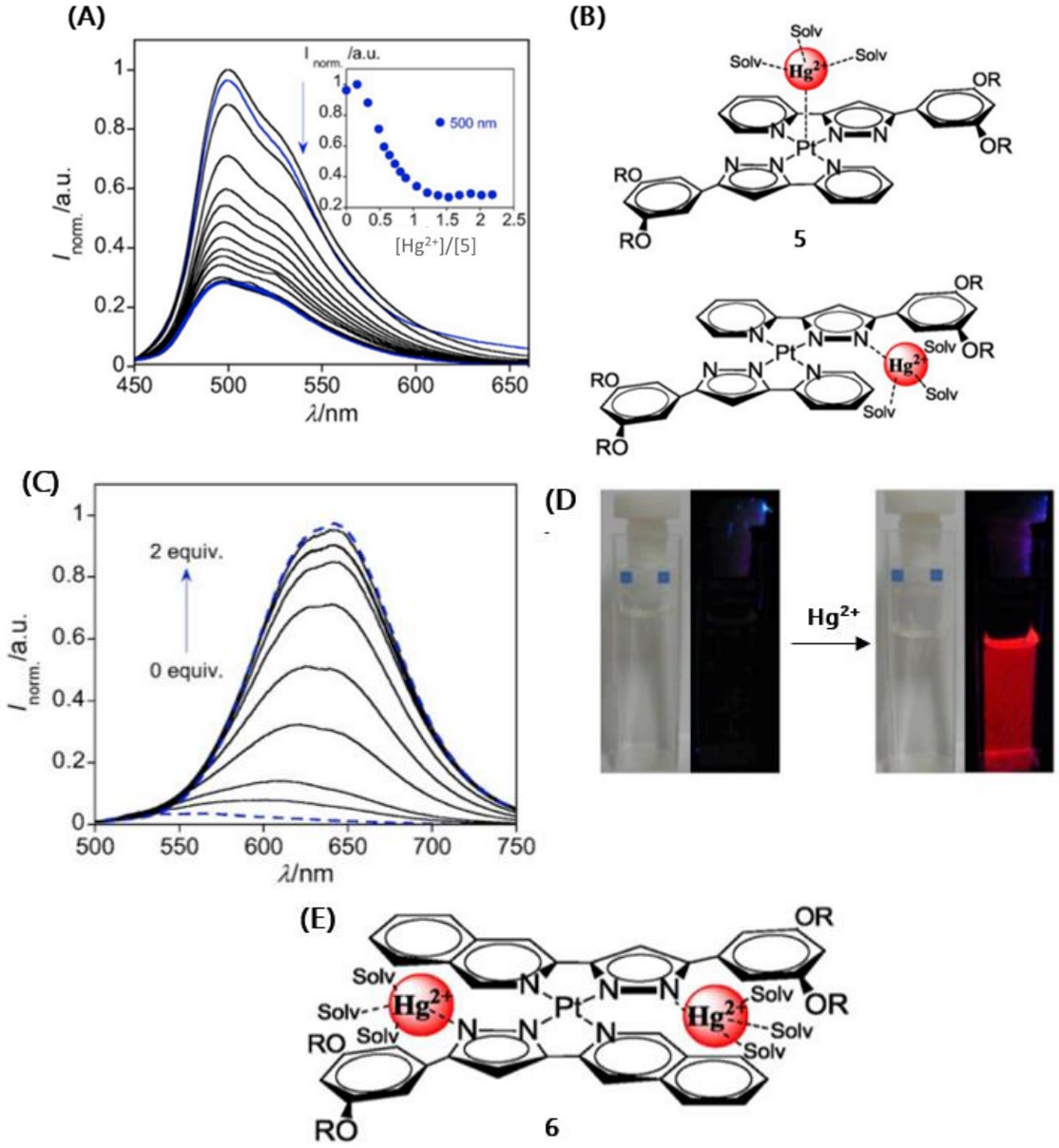

Figure 7 - **(A)** Spectrofluorimetric titration of **5** with addition of Hg^{2+}. **(B)** Proposed interaction mode of **5** with Hg^{2+}. **(C)** Spectrofluorimetric titration of **6** with addition of Hg^{2+}. **(D)** Colorimetric changes of **10** upon addition of Hg^{2+}. **(E)** Proposed interaction mode of **6** with Hg^{2+}Adapted from [37]

1.2.4 Luminescence-based anion sensors

The second group of important analytes in life and environmental samples are the anions. They are indispensable entities to life, as many biological processes depend on their presence or their transport. Anions such as PO_4^{3-}, SO_4^{2-} and HCO_3^- are essential for the normal functioning of living organism, participating in biochemical pathways such as nucleic acid and

aminoacid synthesis and pH regulation (respectively). Beyond the biological importance, anions are also involved in many industrial processes and are frequently found as harmful pollutants. The presence of excessive NO_3^-, Br^- and Cl^- in waterbodies can harm aquatic life and contaminate drinking water. Consequently, the need for developing anion sensors in complex media such as blood, cells, soil, and wastewater is of utmost importance. Due to their exceptional characteristics mentioned earlier, luminescent molecular sensors are ideal for this purpose.[38,39]

Given the exceptional sensitivity of the sensors developed in this work to fluoride and cyanide anions, it is important to investigate the roles of these entities.

Fluoride anions play a significant role in biological and medical processes, with their positive impact on dental health well-established. However, excessive exposure to fluoride can have detrimental effects on health, including kidney failure and skeletal defects. Additionally, several chemical warfare agents release fluoride through hydrolysis, making the detection of this anion crucial for identifying potential chemical weapon usage.[40]

Cyanide, on the other hand, is notorious as a lethal poison when ingested, as it inhibits cellular respiration by binding to cytochrome c oxidase, leading to oxygen deprivation. Consequently, there has been significant interest in developing methods for cyanide detection. The cyanide anion shares several characteristics with fluoride, particularly its similar basicity. This similarity accounts for the number of dual-sensing systems for both fluoride and cyanide that have been reported in the literature. [40]

As example in the last years the group developed a colorimetric probe using gallium (III) corrole complexes **7** and **8**. The authors conducted spectrophotometric and spectrofluorimetric titrations of both compounds with four different anions and found that the system exhibited exceptional sensitivity to cyanide and fluoride. The system produced notable changes in absorption and emission intensity and wavelength (Figure 8A, B) and underwent a color change in the case of the cyanide titration, visible to the naked eye, transitioning from green to colourless (Figure 8C). This color change was explained by the development of the 630nm band with addition of the anions, while the 590nm band disappeared. The authors achieved a limit of quantification (LOQ) of 1.00 and 1.01 μM (respectively) with complexes **7** and **8**, showing great promises for future applications in environmental samples.[41]

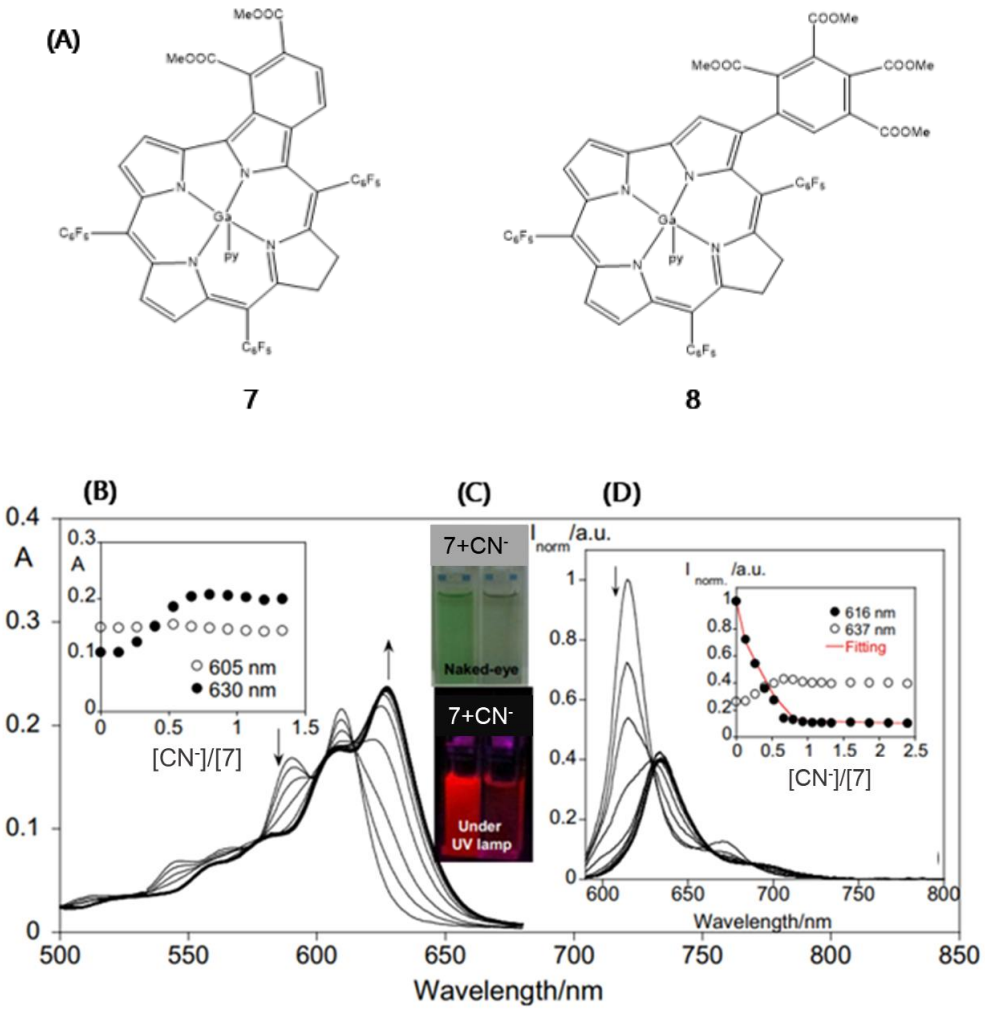

Figure 8 - **(A)** Chemical structure of compounds **7** and **8** **(B)** Spectrophotometric titration of **7** with addition of cyanide. **(C)** Colorimetric changes of **7** upon addition of cyanide **(D)** Spectrofluorimetric titration of **7** with the addition of cyanide. Adapted from[41]

More recently, during my bachelor's final research project we developed and studied a new coumarin-based boron emissive complex **9**. After conducting the anion sensing tests, we discovered that the system exhibited sensitivity to both cyanide and fluoride anions. Notably, the emission intensity was completely quenched upon the addition of one equivalent of CN^- or F^-. Furthermore, the system demonstrated a colorimetric response, shifting from a bright yellow to pink colour, accompanied by a simultaneous disappearance of the green emission (Figure 9B). This variation is consistent with the absorption spectra, where a decrease in the 469nm band is observed as a new band appears at ca. 550nm (Figure 9C). This phenomenon was explained by the loss of protons, resulting in the formation of a quinone base with enhanced conjugation (see Figure 9A), leading to a red shift in absorption. This explanation was demonstrated through NMR titration. [7]

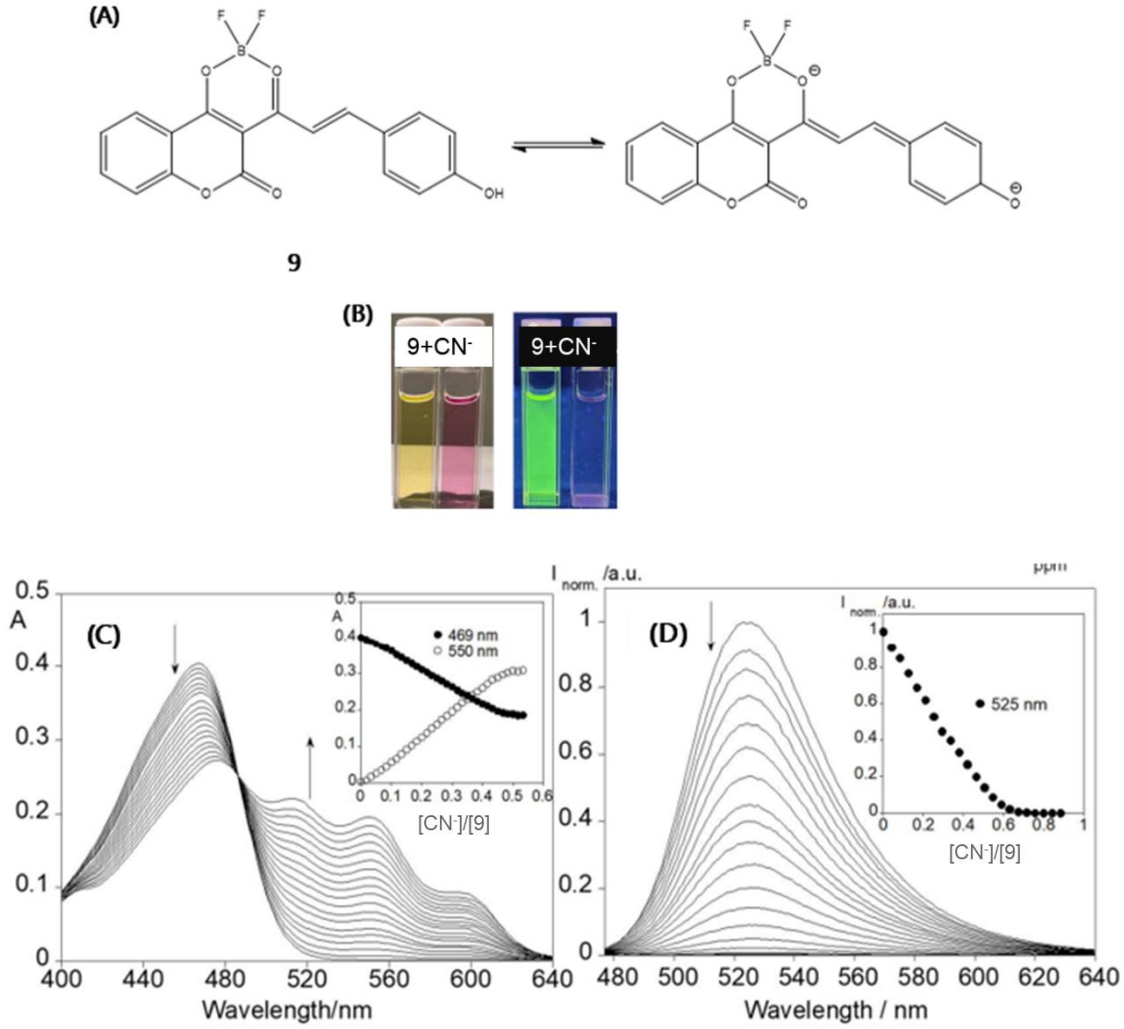

Figure 9 - **(A)** Chemical structure of compound **9** with proposed mechanism of anion sensing through deprotonation. **(B)** Colorimetric changes of **9** upon addition of cyanide. **(C)** Spectrophotometric titration of **9** with addition of cyanide **(D)** Spectrofluorimetric titration of **9** with the addition of cyanide. Adapted from[7]

1.3 Dansyl fluorophore: A short overview

Dansyl chloride, also known as 5-(dimethylamino)naphthalene-1-sulfonyl chloride (structure **10**), is a versatile reagent widely utilized in chemical and biological research. It has the unique property of reacting with primary amino groups, found in both aliphatic and aromatic amines, resulting in the formation of stable blue or blue-green fluorescent sulfonamide adducts. Furthermore, it can be employed to modify secondary amines.

Dansyl chloride plays a crucial role in various applications, most notably in the realm of amino acid analysis and protein sequencing. It is a valuable tool for scientists and researchers involved in these fields. Dansyl chloride is sometimes denoted by the acronym DNSC, simplifying its reference in scientific literature. Additionally, a similar derivative called dansyl amide is referred to as DNSA.

In addition, many fluorescent dyes containing the 5-(dimethylamino)naphthalene-1-sulfonyl group, commonly referred to as dansyl (structure **11**), have been extensively studied in various scientific fields owing to their outstanding optical properties. The sulfonic amide group in dansyl allows for easy incorporation into organic molecules, facilitating a wide range of applications. These dyes have found utility in diverse areas, including analytical chemistry, where they have been used as molecular sensors for metals and other ions.[42–44], to biosensors where they have been used for detection of biomolecules such as peptides and nucleic acids as referred before [45–47].

Additionally, applications using dansyl-based systems in bioimaging have also been extensively explored[48–50] , taking advantage of the fluorescent behaviour of the dansyl derivatives. These compounds exhibit high quantum yields, large Stokes shifts and good structural flexibility, which proves valuable for maintaining these properties under external stimuli such as pH and temperature.[51,52]

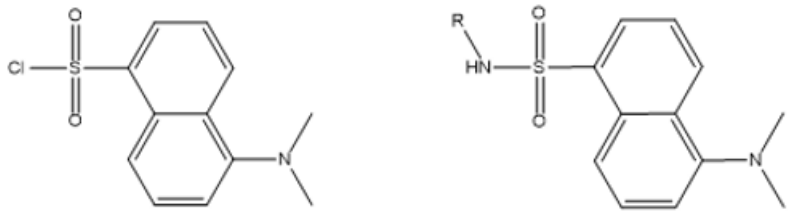

10 **11**

Figure 10 - Chemical structure of compounds **10** and **11**

Following the multifunctional applications of dansyl-based compounds, Eun-Young Park et. al. synthesized a dansyl-labeled sphingosine kinase 1 (SK1) inhibitor **12**. This compound was based on the PF-543 inhibitor **13**, which is recognized as the most potent SK1 inhibitor with a significant role in colorectal cancer, multiple sclerosis, and myocardial infection. Previous studies performed by Schnute et. al. [53] proved the importance of the phenylsulfonyl tail in the inhibitory effect of **13**, which led the authors to search for a possible improvement in the structure. The synthesis of the dansyl-PF-543 **12** was successful, with an overall yield of 27% and the IC_{50} studies proved that this new compound provided an improvement in the inhibitory activity, with a higher IC_{50} (Figure 10B). Moreover, UV-Vis and fluorescence spectroscopy studies of

compound **12** revealed maximum wavelength of emission at 470nm and a quantum yield of 0.11, which are appropriate results for biological studies, confirming that this structure represents a useful tool for spectroscopic analysis of the biological inhibitory activity. [54]

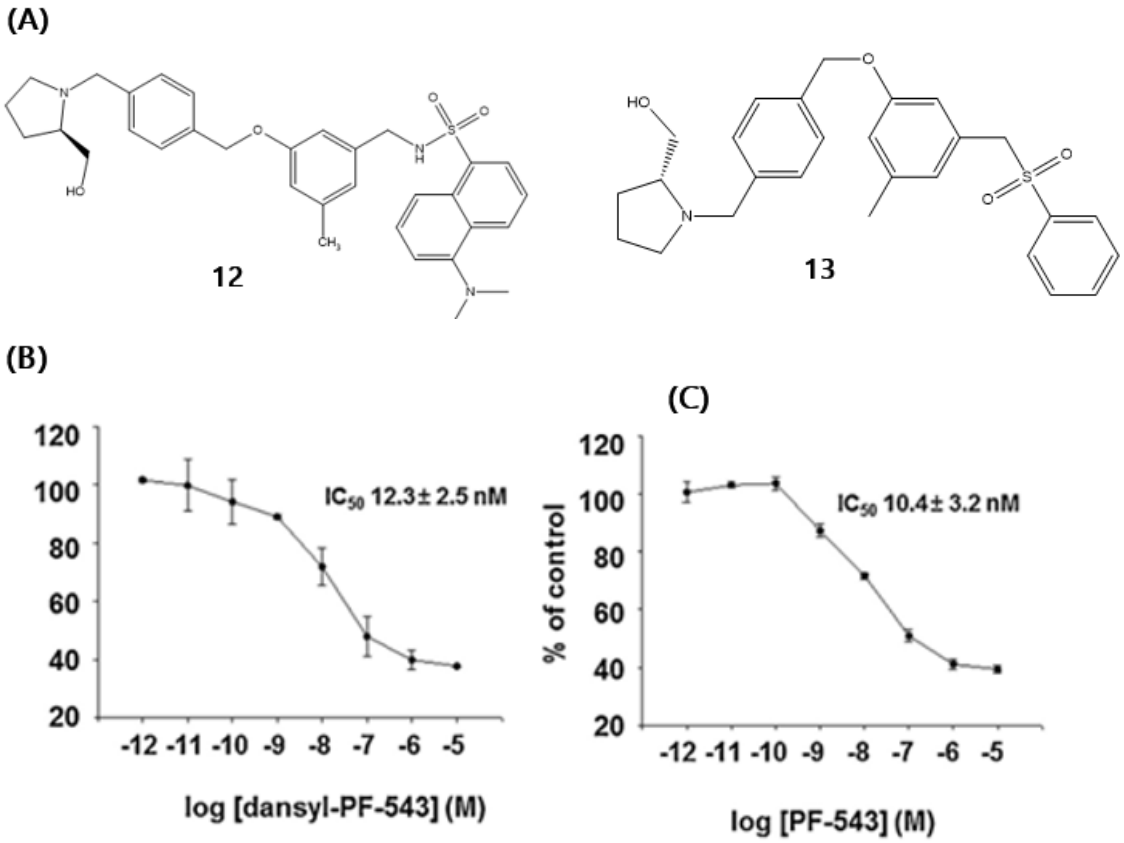

Figure 11 - (A) Chemical structures of compounds **12** and **13**. Effect of dansyl PF-543 **12 (B)** and **13 (C)** on SK1 activity, with respective IC_{50} values. Adapted from[54]

In the realm of colorimetric sensors, Kai-Bin Li and colleagues created a fluorescent and colorimetric sensor for cysteine (Cys) by combining a sulfonyl benzoxadiazole dye with dansyl chloride. They employed a piperazine group to link both moieties, resulting in compound **14**. This probe exhibited sensitivity to Cys with a nanomolar limit of detection and demonstrated selectivity for Cys, showing no interference from competing analytes and amino acids (see Figure 12B). When compared to previously developed Cys fluorescent probes, compound **14** provided one of the lowest limits of detection (LOD) and offered both colorimetric and fluorescent signals (unlike some other probes that only provided fluorimetric signals). It also displayed high selectivity for quantitative and qualitative detection. Furthermore, the authors conducted experiments by incubating living cells with compound 14 and Cys, following the removal of

thiol agents from the system using N-Ethylmaleimide. This demonstrated the potential use of this system for detecting naturally occurring in living cells (Figure 12C). [55]

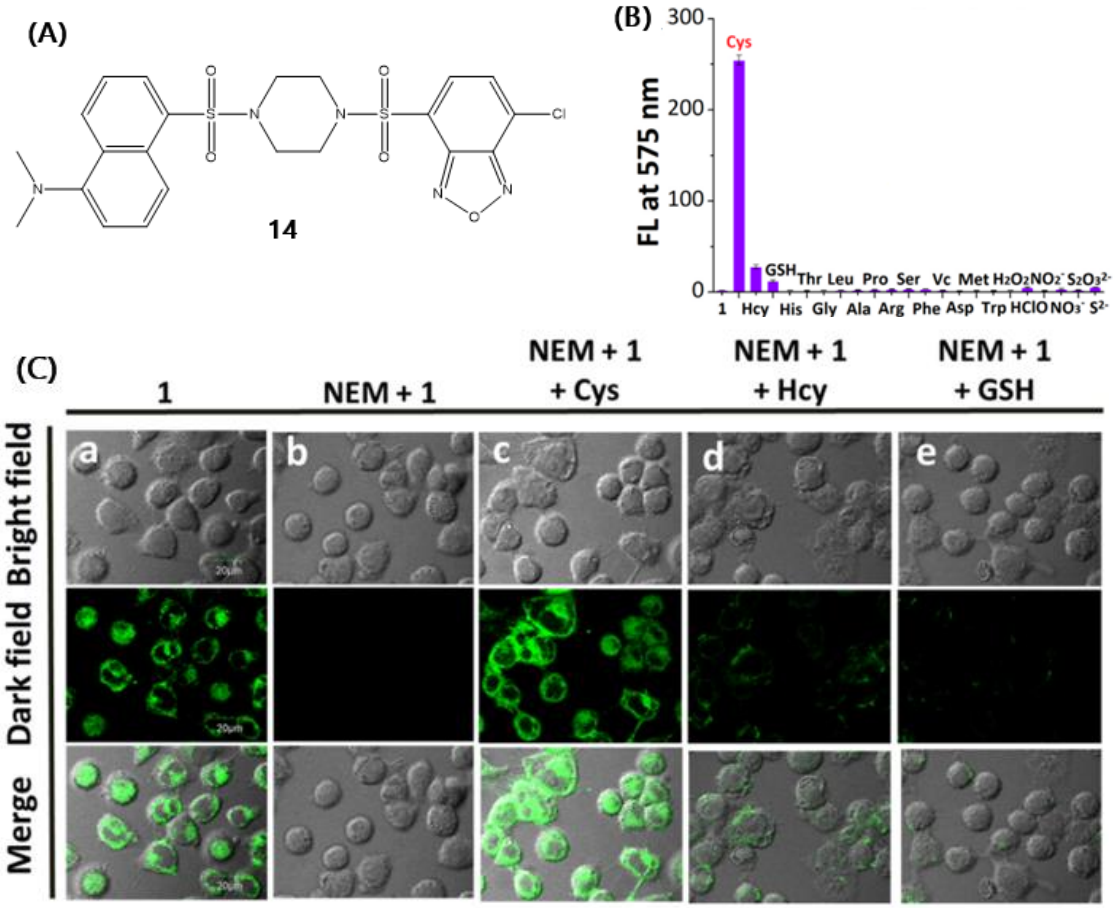

Figure 12 - (A) Chemical structure of compound **14**. **(B)** Selectivity evaluation of **14** (at a concentration of 5 μM) in the presence of competing analytes (at a concentration of 50 μM). **(C)** Fluorescent imaging depicting (a) 10 μM of compound **14**, (b) 10 μM of **14** following treatment with 0.5 mM of NEM for 30 minutes. (c) 10 μM of compound **14** after 0.5 mM of NEM treatment for 30 minutes along with 0.5 mM of Cys, (d) Hcy, and (e) GSH under identical conditions in live MCF-7 cells. Adapted from [55]

Moving to the nanoscale, Richard C. Knighton et. al. employed the dansyl fluorophore for the detection of sulfur-containing chemical warfare agents. This was accomplished by binding the fluorophore to gold nanoparticles through imidazole and amine groups, resulting in conjugate **15** capable of detecting micro-molar concentrations of the toxic gas. The developed system leveraged the binding energies of various ligands with the gold nanoparticle surface. When the fluorophore was in proximity to the nanoparticle surface, it experienced quenching through an energy transfer process. However, when the system was exposed to a sulfide agent,

the weak surface interaction allowed the fluorophore to detach from the surface, leading to the activation of fluorescence and the binding of the sulfide to the nanoparticle. This switching on of fluorescence was observed through fluorescence spectroscopy, where the authors noted a significant enhancement of fluorescence upon the addition of the sulfide agent (see Figure 13A). Additionally, NMR analysis revealed that only bands corresponding to the dansyl fluorophore were observed upon the addition of 10 equivalents of the sulfide agent (see Figure 13B). The system also exhibited a color shift upon the addition of the sulfide agent, transitioning from a dark orange color to colorless. [56]

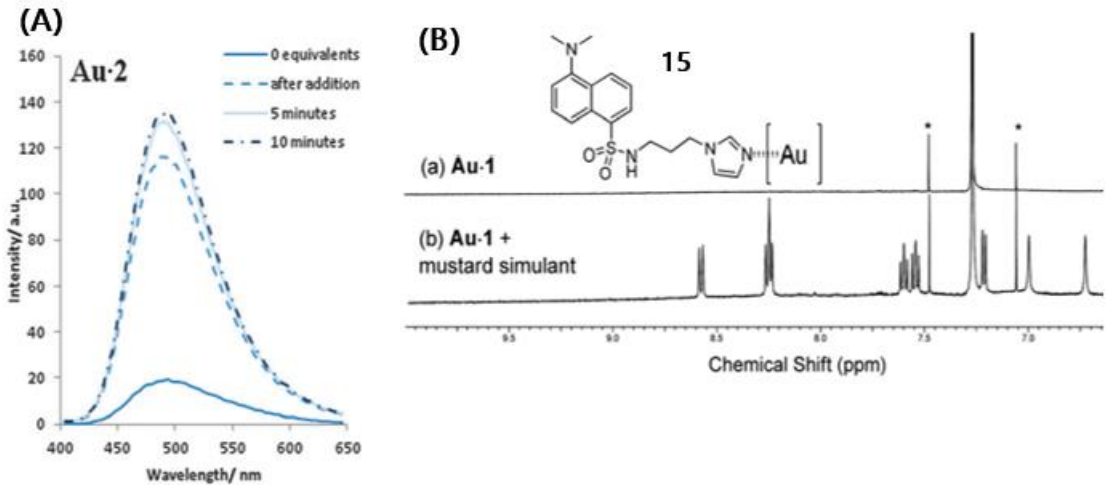

Figure 13 - (A) - Fluorescence spectra of the nanoparticle-dansyl system before and after addition of sulfide agent. **(B)** - ^{1}H NMR spectra of the nanoparticle-dansyl system (a) and (b) the nanoparticle-dansyl system in the presence of 10eq. of sulfide agent. Adapted from [56].

1.3.1 The use of Dansyl-based compounds as acid probes

Dansyl-based compounds have been recognized as effective acid sensors, primarily because of the presence of a tertiary amine that can be protonated. This protonation induces an intramolecular charge transfer, resulting in fluorescence quenching. The tertiary amine's presence promotes pH-responsive emission, enabling the detection of pH variations. As a result, numerous dansyl-based fluorescence pH probes have been developed and documented in the literature.[57]

Yu Liu and collaborators developed a dansyl derivative probe, labeled as compound **16**, which featured a bromo-butane amine moiety. This probe exhibited good selectivity and sensitivity over a pH range from less than 4 to greater than 2. In solution, it emitted a yellow color that gradually diminished as the pH decreased, ultimately becoming completely quenched at

pH less than 2 (as observed in Figure 14B). Furthermore, the authors successfully detected intracellular pH changes using this probe (as shown in Figure 14C), highlighting its potential for applications in acidic biological environments[57].

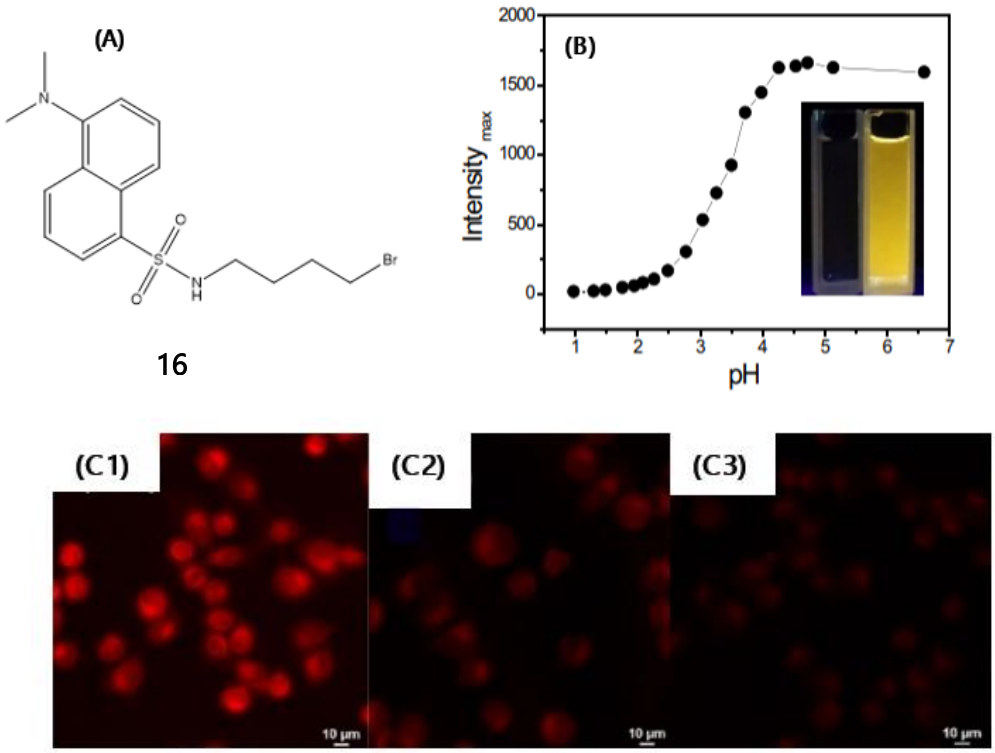

Figure 14 - (A) Chemical structure of compound **16. (B)** Variation of fluorescence intensity at 557nm with pH changes. **(C)** Fluorescence microscope images of cells at pH 3.6 (**C1**), pH 3.0 (**C2)** and pH 2.0 **(C3)**. Adapted from[57]

Improving on previously reported systems, Chunming Sha and colleagues reported fluorescent pH probe **17** from dansyl chloride and thiosemicarbazide. This probe demonstrated high selectivity and sensitivity in the pH range from 10.88 to 1.98, with an almost linear decrease with the reduction of pH value in the pH range of 7.45 to 1.98 (as illustrated in Figure 15B). The authors also confirmed that the system displayed anti-interference capabilities when tested with various biologically and environmentally relevant ions, underscoring its value for selective sensing applications. Furthermore, the system exhibited reversibility, as evidenced by alternating additions of HCl and NaOH, displaying an "alkali-on, acid-off" response by the probe, as depicted in Figure 15C.[58]

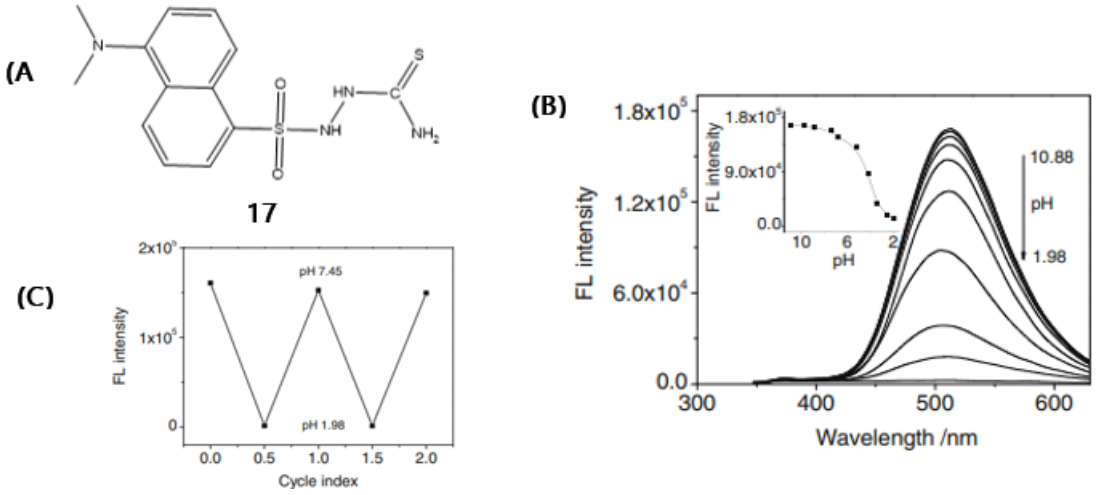

Figure 15 - (A) Chemical structure of compound **17 (B)** Fluorescence spectra of **17** with various pH and inset showing relationship between maximum fluorescence at 510nm and pH **(C)** Reversibility of the fluorescence detection of pH. Adapted from [58]

1.3.2 The dansyl moiety as Cu^{2+} and Hg^{2+} sensor.

The dansyl moiety has been extensively studied in the literature for its sensing capabilities, especially regarding metal ions such as copper and mercury. Paramagnetic transition metal ions with an unfilled d orbital shell, like Cu^{2+}, are typically identified using spectrophotometric and spectrofluorimetric techniques through a phenomenon known as the chelation enhancement of quenching effect (CHEQ). This effect results in the quenching of fluorescence emission when the metal is detected. Hg^{2+} exhibits a similar behavior, where the fluorescence quenching occurs; however, as a diamagnetic d^{10} metal, this quenching can also be explained by spin-orbit coupling. Spin-orbit coupling serves as a primary pathway for nonradiative transitions, contributing to the quenching observed in the presence of Hg^{2+} [8]. Recently our group has reported these behaviors when developing two novel dansyl derivatives **18** and **19** and testing them for metal sensing. The authors observed that both compounds exhibited modifications in their photophysical characteristics in the presence of Cu^{2+} and Hg^{2+}, resulting in a quenching of the emission signal. This behavior is illustrated in Figure 16B for Hg^{2+}. Upon calculating stability association constants and analyzing the stoichiometry, the results suggested the presence of a mononuclear species for the metals in both compounds, with the presence of heteroatoms playing a crucial role for sensing. Compound **18** displayed a LOD and LOQ of 2.5uM and 4.5 uM, respectively, towards Hg^{2+} ions. [8]

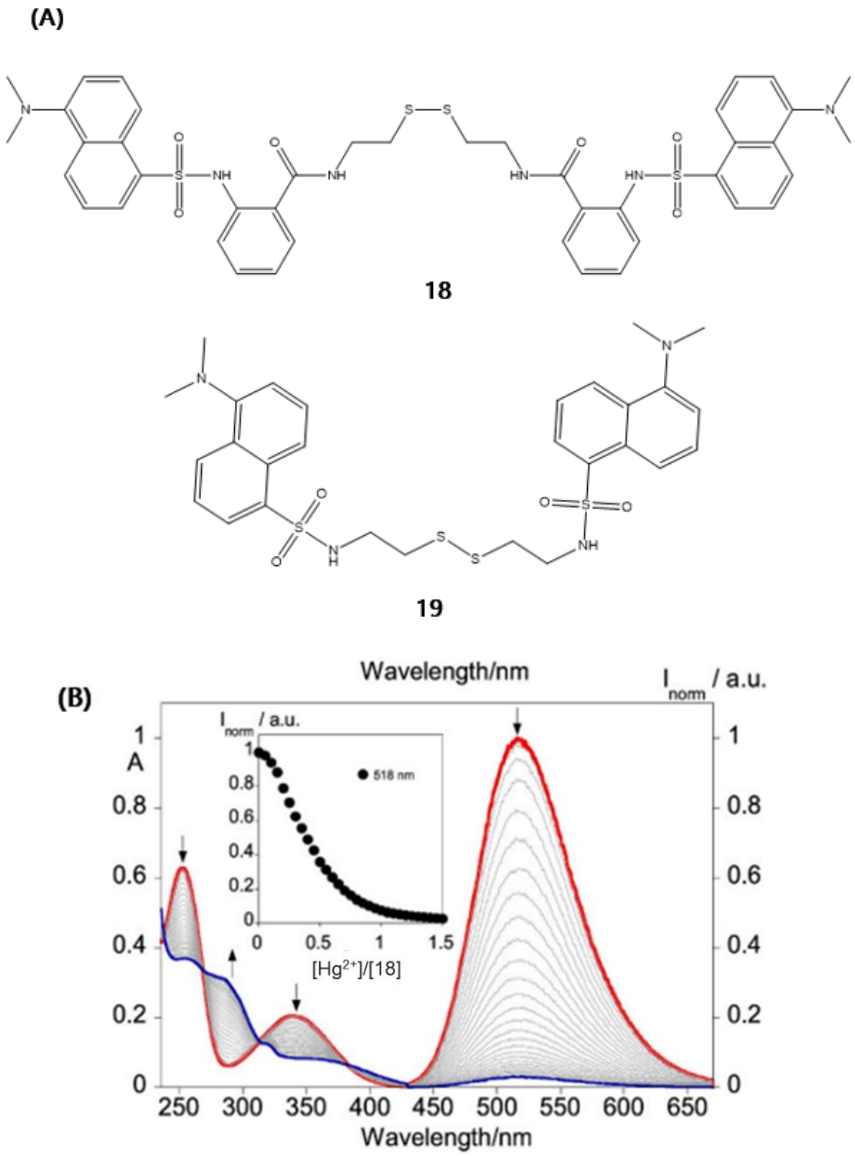

Figure 16 - (A) Chemical structure of compounds **18** and **19 (B)** Spectrofluorimetric titration of **18** with addition of Hg^{2+} Adapted from [8]

1.3.3 Dansyl derivatives as CN^- and F^- sensors

Dansyl derivatives have been extensively explored in the literature for sensing cyanide and fluoride ions, and their sensing mechanisms can vary. In a study by Eunhye Jeong and colleagues, they developed an ensemble system that combined an imidazolium-bearing dansyl-based probe labeled as compound **20** with substrate **21**. After conducting anion sensing tests, they discovered that the system exhibited high selectivity and sensitivity to cyanide. Remarkably, instead of the typical emission quenching seen in many other probes, this system

displayed a significant fluorescence emission enhancement, as depicted in Figure 17B. The authors proposed that the CN^- ion did not directly interact with the probe but formed an addition product with substrate **21**, resulting in the formation of supramolecular assemblies. This explained the high association constants and the enhancement of emission. The system demonstrated exceptional sensitivity with a limit of detection (LOD) of 200 nM (5.2 ppb), making it one of the lowest LODs achieved for cyanide sensing to date. [59]

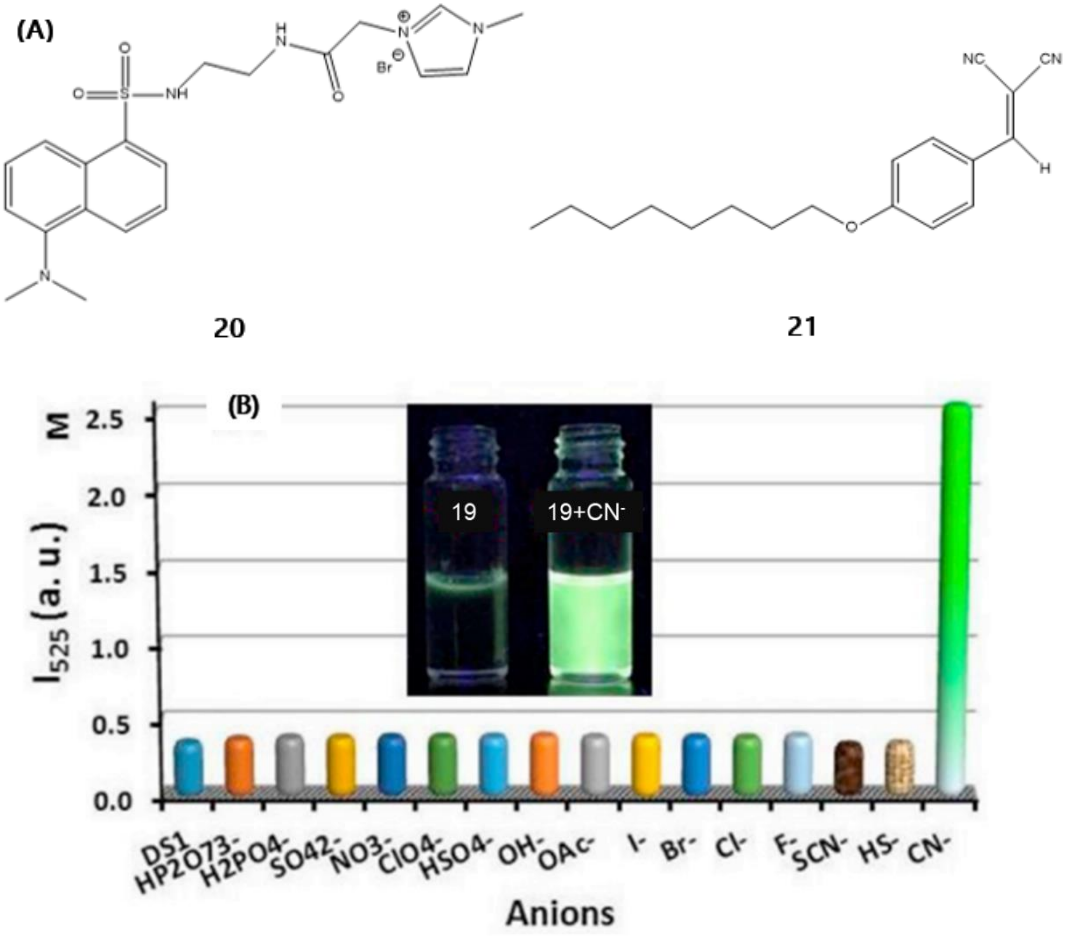

Figure 17 - (A) Chemical structure of compounds **20** and **21 (B)** Fluorescence intensity of **19** in the presence of various anionic species. Adapted from [59]

Using orcinol-dansyl compound **22**, Kwanmuang and coworkers developed a novel system for fluoride ion detection, however, the authors reported a different sensing mechanism from the previously mentioned one. In this system, the addition of fluoride caused the deprotonation of **22**, which was proven by NMR studies. Additionally, complexation between fluoride ions and compound **22** was reported. This complexation led to internal charge transfer

processes and, subsequently, the formation of a new absorption band and the quenching of fluorescence emission, as shown in Figure 18B.[60]

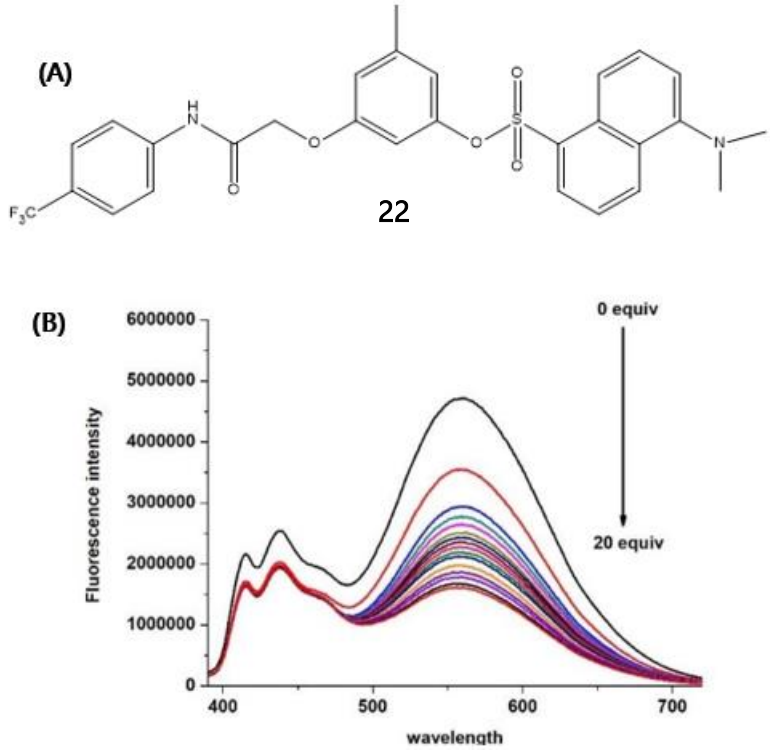

Figure 18. (A) Chemical structure of compound **22 (B)** Fluorescence spectra of **22** upon addition of F^- Adapted from [60]

2

OBJECTIVES

Inspired by the previously explained studies, in this work we have studied six new dansyl-based compounds, represented in Figure 19. In the frame of an international collaboration, all compounds studied in this Master Thesis have been synthesized in the group of Dr. Atanas Kurutos and Dr. Georgi Dobrikov from the Bulgarian Academy of Sciences in Sofia, Bulgaria. We have characterized and explored in different solvents in solution, solid state, and have prepared several polymeric supported materials in our group in FCT NOVA - Caparica. The focus of this master thesis was to explore all these new molecules as multifunctional materials in solution, solid state and supported in polymers as new colorimetric and fluorimetric sensors for pollutant cations and anions.

Among these compounds, **L1**, **L2**, and **L3** have shown remarkable abilities for metal sensing.

Both **L1** and **L3** have a strategic arrangement of an amine group near a sulfur group, facilitating the formation of a stable chelate unit to coordinate with a wide range of metal ions. This arrangement provides donor sites and free electrons for metal chelation. Compound **L2** features the amine group in proximity to an amide group, which also offers good donor sites for metal binding. However, for comparative purposes, all six compounds were tested for their metal sensing capabilities.

On the other hand, compounds **L4**, **L5**, and **L6** contain multiple amine groups in their structures, which make them suitable for anion sensing. These amine groups provide several sites that can interact with anions through hydrogen bonding or undergo deprotonation, leading to variations in the photophysical properties of the compound. Additionally, electrostatic interactions can occur as the anion interacts with the positively charged amine groups. These favorable properties led to the testing of compounds **L4**, **L5**, and **L6** for anion sensing.

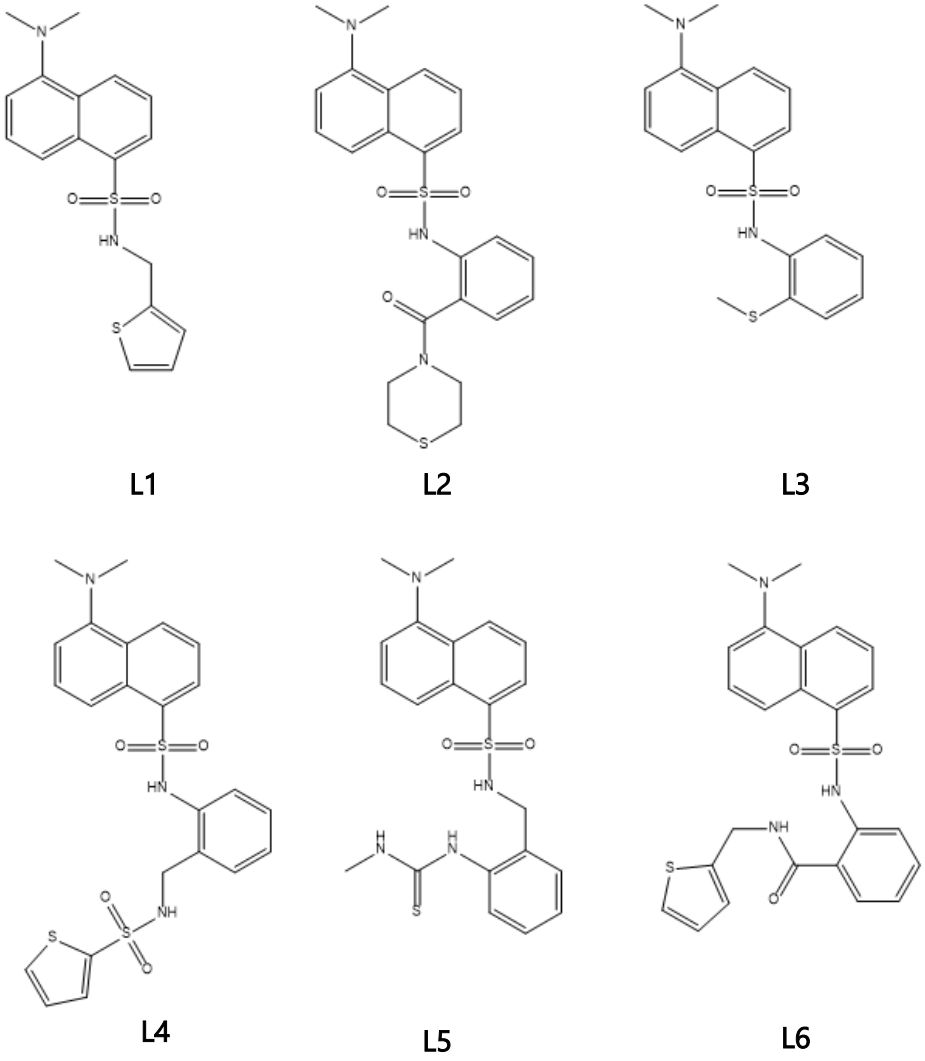

Figure 19 - Chemical structures of dansyl-derivatives **L1-L6.**

3

EXPERIMENTAL PROCEDURES

3.1 Chemicals and Starting Materials

Solvents

Acetonitrile (Merck Millipore, Darmstadt, Germany, 99.5%, CAS 75-05-8), Chloroform (Honeywell, Minneapolis, MN, USA, 99.0–99.4%, CAS 67-66-3), DMSO (Honeywell, 99.5%, CAS 67-68-5), Ethanol (Honeywell, 99.9%, CAS 64-17-5), Tetrahydrofuran (THF) (PanReac, Barcelona, Spain, 99.0%, CAS 109-99-9), Acetone (Honeywell, 99.5%, 67-64-1), H_2O (Milli-Q ultrapure).

Reagents

Ethylenediamine tetraacetic acid (EDTA) (Alfa Aesar, Ward Hill, MA, USA, CAS 194491-31-1, , LUDOX® AS-30 colloidal silica (SiO2, Sigma-Aldrich, 30 wt.% suspension in water, CAS 7631-86-9), Poly(methyl methacrylate) (PMMA) (Sigma-Aldrich, St, Louis, MO, USA, MW ~350,000, CAS 9011- 14-7), Zinc trifluoromethanesulfonate (Sigma-Aldrich, St, Louis, MO, USA, CAS 54010-75-2), Silver trifluoromethanesulfonate (Sigma-Aldrich, St, Louis, MO, USA, CAS 2923-28-6), Mercury trifluoromethanesulfonate (Sigma-Aldrich, St, Louis, MO, USA, CAS 49540-00-3), Copper trifluoromethanesulfonate (Sigma-Aldrich, St, Louis, MO, USA, CAS 34946-82-2), Tetrabutylammonium bromide (Sigma-Aldrich, St, Louis, Mo, USA, CAS 1643-19-2), Tetrabutylammonium chlorine (Sigma-Aldrich, St, Louis, Mo, USA, CAS 1112-67-0), Tetrabutylammonium cyanide (Sigma-Aldrich, St, Louis, Mo, USA, CAS 10442-39-4), Tetrabutylammonium fluoride (Sigma-Aldrich, St, Louis, Mo, USA, CAS 22206-57-1), Acridine Yellow G (Sigma-Aldrich, St, Louis, MO, USA, CAS 135-49-9), Hydrochloric acid (Honeywell, 37%, CAS 7647-01-0), Ammonia (Sigma-Aldrich, St, Louis, MO, USA, CAS 7664-41-7).

3.2 Instrumental methods of analysis

The absorption spectra were recorded on a JASCO V-650 UV-Vis Spectrophotometer and the fluorescence emission spectra on a Horiba Jobin-Yvon Scientific Fluoromax-4, both at room temperature with a 1cm optical path length quartz cells.

The spectra of solid samples were collected with a Horiba-Jobin-Yvon Fluoromax-4® spectrofluorometer using an optic fiber connected to the equipment, by exciting the solid compounds at appropriated λ (nm).

Lifetime studies were carried out on TemPro, Deltahub Nanoled of Horiba Jobin-Yvon, with a 390 nm Nanoled. All instruments were provided by PROTEOMASS-BIOSCOPE facility.Synthesis of compounds L1-L6

All compounds **L1-L6** were provided by the group of Dr. Atanas Kurutos and Dr. Georgi Dobrikov from the Bulgarian Academy of Sciences in Sofia, Bulgaria. These compounds have been characterized by ^{1}H and ^{13}C NMR, 2-D COSY, 2-D HSQC, 2D-HMBC NMR techniques, elemental analysis and completely by FTIR and mass spectrometry MS in the Biological Mass Spectrometry Lab Isabel Moura by PROTEOMASS BIOCOPE Facility.

The synthetic methodology was reported in the publication.

3.3 Photophysical characterization: Methodology

3.3.1 In solution

Stock solutions of each compound were prepared weighing 1 mg of compound and dissolving them in 10mL of the appropriate solvent. Then, several dilutions were prepared to the concentrations, $3x10^{-6}$, $6x10^{-6,}$ and $1x10^{-5}$ M using the stock solutions.

For the UV-Vis absorption spectra, we filled the reference cell with 3mL of the respective solvent and the sample cell with 3mL of the corresponding solution. Between each measurement, the cells were cleaned to avoid contamination and to guarantee lower error in the measurement. All measurements have been done in a climatized room at 22ºC.

3.3.2 Fluorescent quantum yields

Firstly, the absorption spectra of the sample and the standard was measured in the same solvent. For the standard compounds, the solution was prepared using 3mL of absolute

ethanol with the standard compound. The spectra were measured below 0.2 absorbance to reduce self-quenching and re-absorption effects. All samples were measured and a wavelength where both spectra intersect was chosen. Afterwards, emission spectra were obtained at the intersection wavelength. The emission spectrum area was then used to calculate the quantum yield with equation 6.

The fluorescence quantum yields of compounds **L1-L6** were measured using a solution of acridine yellow in absolute ethanol as the reference standard [ϕ_f = 0.37][61]

3.3.3 Lifetime studies

For the lifetime studies, we prepared all solutions of each compound as previously described and their absorption spectra were measured with the objective of obtaining a maximum of absorbance below 0.2. Subsequently a standard solution was prepared using 3mL of milliQ H_2O and 2µL of LUDOX AS-30 colloidal silica.

3.3.4 Solid-state studies

The emission spectra of solid samples were collected with a Horiba-Jobin-Yvon Fluoromax-4® spectrofluorometer using an optic fiber connected to the equipment, by exciting the sample at appropriated λ (nm).

3.4 Preparation of doped polymeric films

A hundred mg of polymer was weighed in a vial, and 1mg of compound **L1**-**L6** was weighed in a separate vial. The polymer was dissolved in 5mL of chloroform, and the selected compound in 1mL of chloroform. Then, the compound solution was added to the vial with the polymer solution, and they were mixed for 10 minutes. All solutions were filtered with a cotton pipette before casting.

Subsequently, the solution was poured into a 15mL perfluoroalkoxy alkane (PFA) plate from the trademark Bohlender, GmbH, Germany. Finally, we covered the plate with an aluminum foil and left it to slow evaporate at room temperature for 24h. For spectroscopic measurements, a 1x1cm square of polymer was cut and immobilized between two quartz glass lamellae.

3.5 Doped polymer acidity assays

3.5.1 Acid immersion studies

In the acid dipping assays, the doped polymer sample was submerged in a 12M solution of hydrochloric acid (HCl) for 5 minutes before each spectral measurement. The doped polymer sample was thoroughly dried before each measurement to prevent any interference.

3.5.2 Acid vapours assays

For the acid vapor assays, the doped polymer sample was placed in a closed glass vessel where it was exposed to 12M HCl acid vapors for 25 minutes before each spectral measurement. Various tests were conducted with time intervals of 5, 10, 15, and 20 minutes before determining that a 25-minute exposure was the most suitable timeframe for observing the fluorescence emission quenching effect caused by the acid vapors.

3.5.3 Reversibility studies

To investigate reversibility, a series of cycle studies were conducted. The polymer sample was immersed in a 12M HCl solution for 20 minutes until the emission was completely quenched. Subsequently, it was dipped in a 12M ammonia (NH_3) solution, leading to an instant enhancement of emission intensity back to the initial levels. This procedure was repeated for a total of 10 cycles. The 20-minute time interval was chosen as it proved to be the ideal duration for achieving full quenching of emission, based on prior tests with intervals of 5, 10, and 15 minutes of immersion.

3.5.4 Acid concentration gradient studies

Concentration gradient studies were conducted using hydrochloric acid (HCl) solutions at various concentrations, including 2M, 4M, 6M, 8M, 10M, and 12M. Polymer samples were immersed in each of these solutions for 20 minutes, and their emissions were measured.

3.6 Metal ion and pH Titrations

Titrations of compounds **L1-L6** were carried out in a $2x10^{-5}$M acetonitrile solution by the addition of microliter amounts of standard metal solutions of Zn^{2+}, Ag^{+}, Hg^{2+}, Cu^{2+}, Br^{-}, Cl^{-}, F^{-}

and CN^- in acetonitrile, and HCl and NH_3 in H_2O. In the data analysis step, a correction for the absorbed light and for the dilution factor was performed when necessary.

4

RESULTS AND DISCUSSION

4.1 Photophysical Characterization

The six compounds, **L1** to **L6**, were characterized using UV-Vis and fluorescence emission spectroscopy in various solvents (DMSO, CH_3CN, EtOH, THF, $CHCl_3$) at 298K. Moreover, they were also characterized in solid state, with the main results displayed in Table 1.

Focusing on the results obtained for acetonitrile, which was the selected solvent for the further studies in solution, compounds **L1** to **L6** exhibited an absorption band of 341 nm, 345, 320, 345, 337 and 333 nm, which is characteristic of the π-π* transition of the dansyl chromophores that contributes to the colorless appearance of these compounds to the naked eye, as evidenced previously by our group in recent works [8,62]. The observed red shift in the absorption maximum bands of the compounds **L2**, **L3**, **L4**, and **L6**, which contain a benzene ring directly attached to the dansyl unit, is likely due to the increased number of donor atoms and the longer side chain. Such changes can result in an alteration of the electronic structure of the molecule, leading to a shift in the absorption wavelength. This red shift is consistent with the effects of donor groups in conjugated systems, as documented in the literature[63,64]. Compounds **L1** and **L5** which contain a CH_2 group bonded to the dansyl's amine group acting as a spacer, displayed no significant changes in the absorption.

The six compounds displayed a yellow emission in CH_3CN, as visible in Figure 20, with maximum bands at 519, 528, 535, 530, 520 and 528 nm, from **L1** to **L6**, however, in the excited state there weren't significant changes for compounds **L2**, **L3**, **L4** and **L6**. In contrast, compounds **L1** and **L5** which contain the forementioned CH_2 spacer displayed a 10 nm blue shift in the emission bands. In addition, the highest fluorescence quantum yield was observed for

compounds **L1** and **L5** (ϕ =ca. 35-36%), which suggests that the introduction of the spacer stabilizes the molecules in the excited state.

For the solid-state results, there was a red shift in the emission spectra for compounds **L4** and **L5** which can be explained due to the presence of a high number of donor atoms that also lead to the stabilization of the excited state.

The obtained UV-Vis and fluorescence emission spectra for the photophysical characterization of compounds **L1**-**L6** in the five solvents are presented in Annexes 1 to 6.

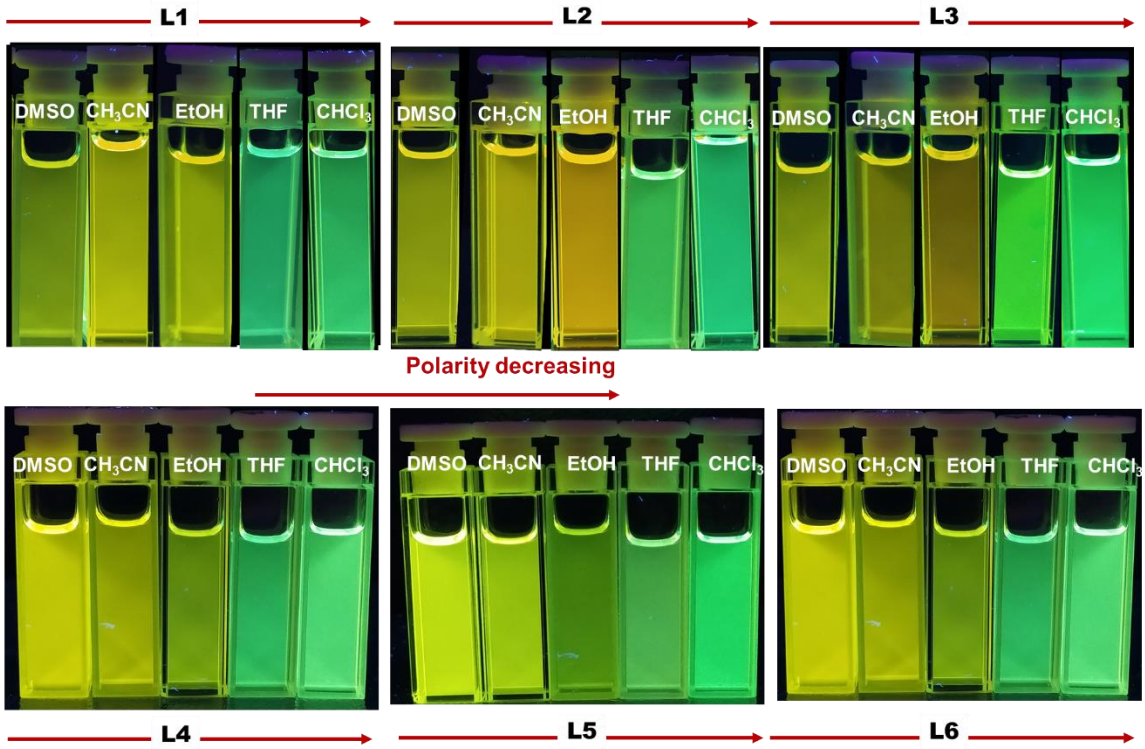

Figure 20. Images of **L1**-**L6** in 5 different solvents, with polarity decreasing from DMSO to $CHCl_3$. Pictures taken under a 365nm UV light lamp

Table 1. Photophysical properties of compounds **L1** to **L6** in various solvents

Cpd.	Solv.	λ_{abs} [nm]	λ_{em} [nm]	ε [10^3 cm^{-1} M^{-1}]	Stokes shift [cm^{-1}]	$\lambda_{em.solid}$ [nm]	Φ (%)	Brightness (ε X ϕ) [cm^{-1} M^{-1}]	t[ns]
	DMSO	337	522	5.765	54054		22	1291	17
	CH_3CN	341	519	5.531	56179		35	1941	10
L1	EtOH	335	516	4.873	55248	484	31	1506	13
	THF	334	498	4.969	60975		21	1048	12
	$CHCl_3$	345	496	4.721	66225		35	1671	14
	DMSO	353	540	5.950	53475		11	666	13
L2	CH_3CN	345	528	5.519	54644	478	29	1606	12
	EtOH	346	520	4.983	57471		38	1913	13

	THF	334	504	5.201	58823		39	200	13
	$CHCl_3$	345	499	5.204	64935		37	1951	15
L3	DMSO	340	536	5.397	51020	486	10	550	13
	CH_3CN	320	535	5.454	46511		28	1538	11
	EtOH	340	531	5.052	52356		32	1596	11
	THF	339	511	4.921	58139		32	1555	13
	$CHCl_3$	346	503	4.057	63694		32	1282	15
L4	DMSO	343	533	4.254	52631	505	21	914	15
	CH_3CN	345	530	4.471	54054		27	1211	10
	EtOH	345	522	3.780	56497		17	646	13
	THF	343	502	4.653	62893		27	1261	13
	$CHCl_3$	345	504	4.482	62893		29	1313	15
L5	DMSO	339	524	4.640	54054	500	30	1378	17
	CH_3CN	337	520	5.674	54644		36	2048	11
	EtOH	338	515	3.968	56497		22	877	13
	THF	337	497	4.940	62500		26	1304	13
	$CHCl_3$	343	500	0.3593	63694		34	1210	15
L6	DMSO	347	537	4.279	52631	486	17	740	14
	CH_3CN	333	528	4.817	51282		28	1354	11
	EtOH	329	525	7.164	51020		17	1189	13
	THF	341	501	4.370	62500		29	1280	13
	$CHCl_3$	341	497	4.782	64102		34	1616	14

As observed previously in other dansyl derivatives in our group, we can observed a positive solvatochromic effect in compounds **L1**-**L6**, with a notable variation in emission color from yellow to green (as visible in Figure 20) as the solvent polarity increases, due to the red shift in the maximum emission bands, varying from 496 to 522 nm for **L1**, 499 nm to 540 nm for **L2**, 503 to 536 nm for **L3**, 504 to 533 nm for **L4**, 500 nm to 524 nm to **L5** and 497 nm to 537 nm for **L6**, respectively. As more polar solvents enhance the stability of molecules in their excited state, this leads to the lowering of their energy, causing the observed red shift. To quantify the interactions between solute and solvent in compounds **L1-L6** a multiparametric fit using the Kamlet-Taft equation (equation 4) was carried out. Table 2 displays the fitted parameters (υ_0, a, b and p), the slope and correlation coefficients based on the fitting linear plots of $\upsilon_{exp.}$ versus υ_{calc}.

The analysis of the data in Table 2 indicates a correlation between solvatochromism and electronic interactions, specifically, the polarizability and dipolarity of the solvent. The p-values associated with these interactions are significantly higher, spanning one to two orders of magnitude when compared to a. Furthermore, it becomes evident that the hydrogen bond

accepting behavior of the solvent exerts a more dominant influence on solvatochromism, surpassing the impact of hydrogen bond donating behavior. This is discerned from the b values, which exhibit a one-order-of-magnitude difference when compared to a.

Table 2. Kamlet-Taft equation multiparametric fitting results from emission data. υ_0, a, b, and p values are expressed in cm^{-1}

	υ_0	a	b	p	Slope	R^2
L1	33032	-533	-4770	-17808	1.00	1
L2	35386	-350	-5804	-21300	1.00	1
L3	35354	-432	-6116	-21414	1.00	1
L4	35581	-638	-5444	-21838	1.00	1
L5	32841	-629	-4363	-17796	1.00	1
L6	36665	-672	-6248	-22877	1.00	1

4.2 Acid-base sensing

4.2.1 In a CH_3CN solution

The six compounds underwent acid-base sensing tests involving spectrophotometric and spectrofluorimetric titrations with HCl and NH_3. As exhibited in Annexes 7 to 29, the results were consistent in all compounds, except for compound **L3**, which exhibited no response to the addition of HCl. **L1** was chosen as a representative case and as depicted in Figure 21, the titration with HCl resulted in a decrease in the absorption band at 345nm as well as the emergence of a new band at 293nm. This was accompanied by a decrease in emission intensity in the band centered at 519 nm. In contrast, when ammonia was introduced, we observed an increase at 345 nm and a decrease at 519 nm bands, in the absorption and emission spectra, respectively. Additionally, there was an approximately 60% increase in the intensity of the 519 nm emission band.

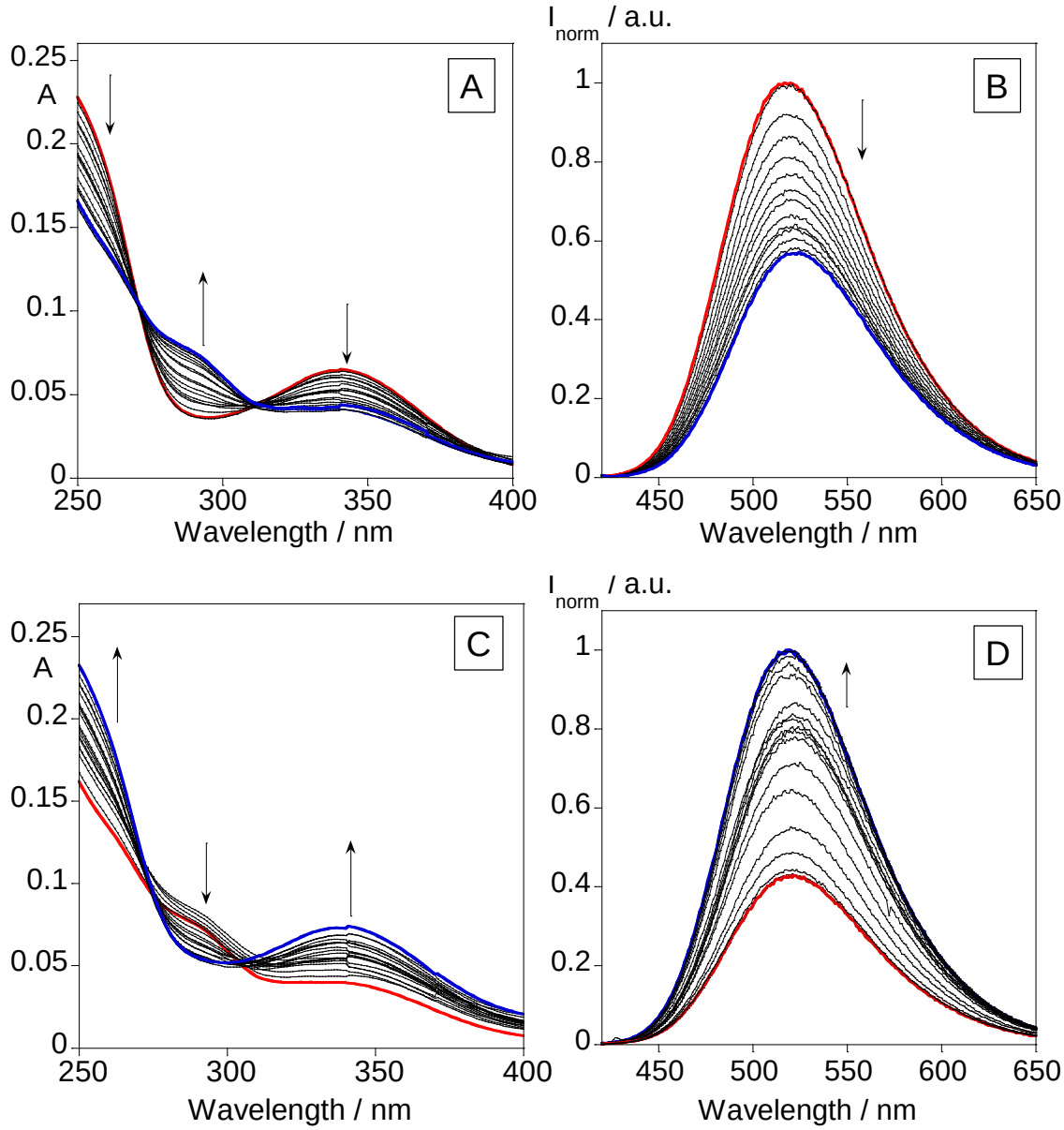

Figure 21. Spectrophotometric and spectrofluorimetric titrations of **L1** with increased additions of HCl (A,B) and NH_3 (C,D). [**L1**]=20 μM, $\lambda_{exc\mathbf{L1}}$=345 nm, T = 295 K

4.2.2 In a PMMA polymer matrix

Based on the results obtained for the dansyl derivatives in a CH_3CN solution, which suggested their sensitivity to acidic conditions, PMMA polymers doped with these compounds were successfully synthesized and investigated as acid sensors to further explore this phenomenon and expand their range of applications. Figure 22 showcases the results for **L1** as a representative case, while the remaining compounds are depicted in the corresponding Annexes 11 to 14, 17 to 19, 22 to 24 and 27 to 29. Initially, the **L1**@PMMA polymer was immersed in a

12M solution of HCl, and emission spectra were recorded every 5 minutes. As depicted in Figure 22A, this immersion led to a gradual reduction in the emission intensity of the main band centered at 463 nm, resulting in complete quenching. This decrease in emission intensity coincided with the disappearance of the bright blue emission color characteristic of the **L1**@PMMA system, which is evident from the color differences between the start and the end of the experiment in Figure 22. Furthermore, emission spectra were collected at 20-minute intervals after exposing the **L1**@PMMA polymer to a closed system containing HCl vapors (Figure 22B). In this case, the emission intensity of the band at 463 nm also decreased progressively with increasing exposure time. To assess the impact of varying HCl concentrations on emission intensity, spectra were acquired after immersing the polymer system in HCl solutions with increasing concentrations ranging from 0 to 12M. It can be observed that as the HCl concentration increased, there was a gradual reduction in emission intensity (Figure 22D). The progressive reduction in emission intensity is visually evident in the images displayed in Figure 22C where notably the blue emission color vanishes when the concentration reaches values of 4M and higher.

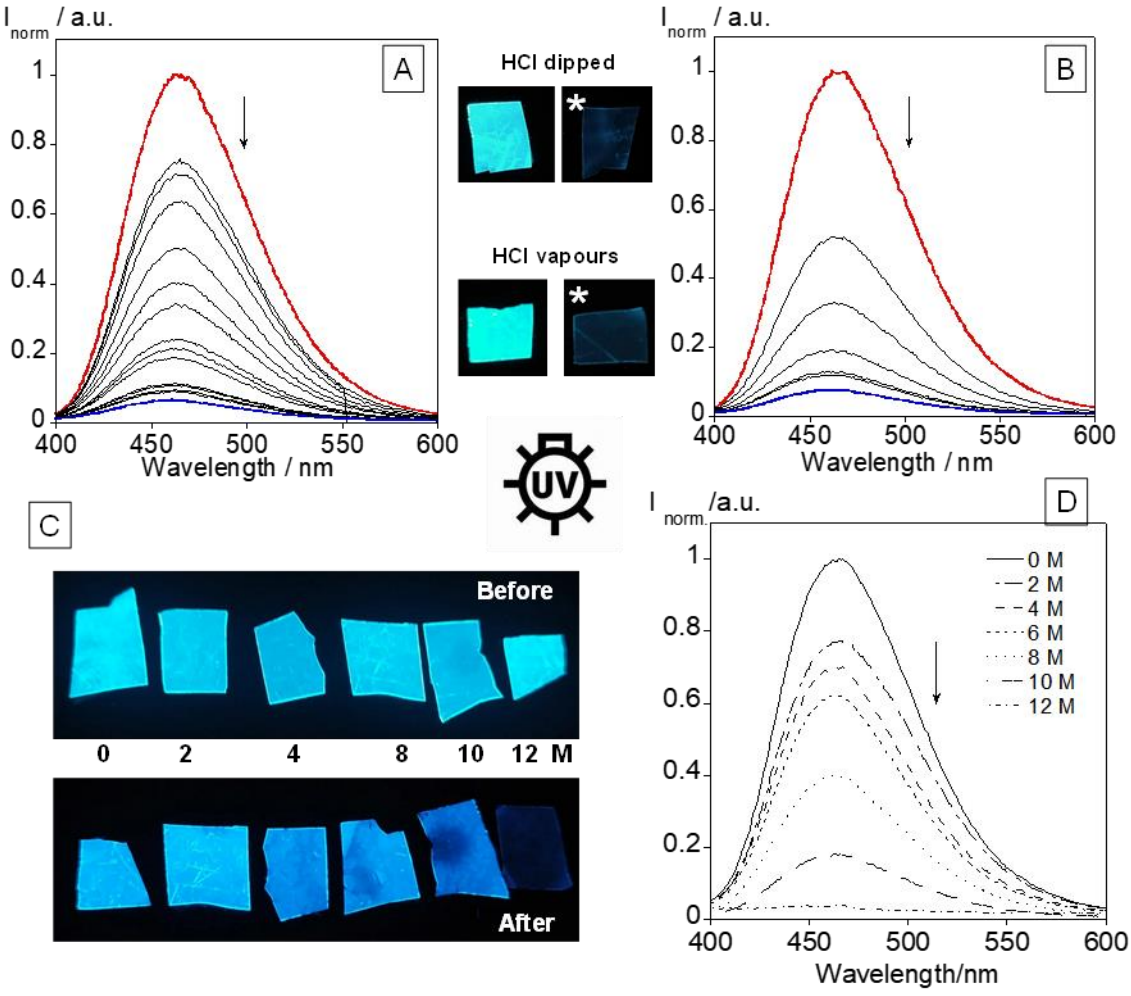

Figure 22. (A) Emission spectra of successive immersion of **L1** doped PMMA polymer film in a concentrated HCl solution (5m in 5min). (B) Emission spectra of exposure of **L1** to HCl vapours (20m in 20m), T = 298 K. Images under a UV lamp (C) and emission spectra (D) of **L1** immersion in the HCl concentrations from 0 to 12 M.

The promising results obtained for the polymer systems in acid sensing applications prompted an assessment of their stability and reversibility. This evaluation involved immersing the systems in a 12M acid solution for 20 minutes, resulting in complete emission quenching, followed by immersion in a 12M ammonia solution to achieve an immediate increase in emission intensity back to the initial levels. The results, presented in Figure 23, affirm that the system maintains stability and does not experience degradation following repeated immersions in high-concentration acid and base solutions. This finding is particularly valuable for environmental applications, as it ensures the system's reusability without compromising the quality of results obtained.

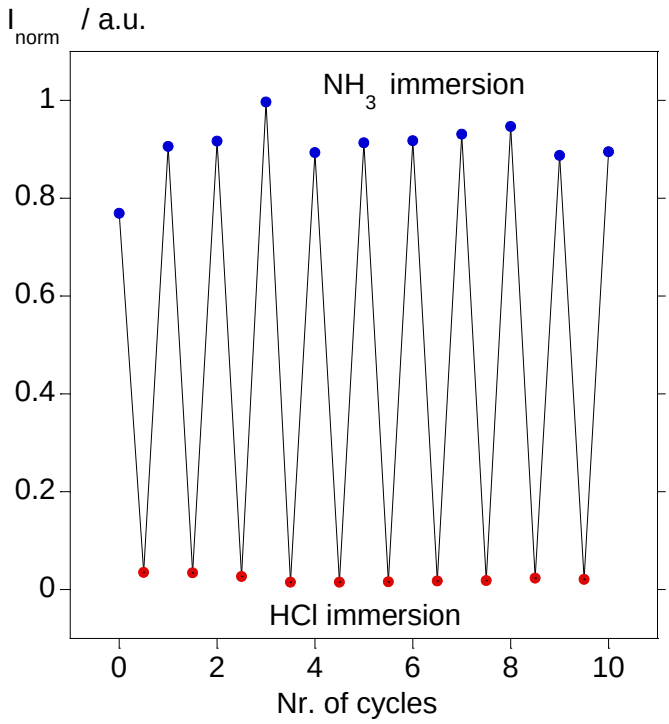

Figure 23. Emission intensity of **L1**@PMMA at λ_{463nm} after successive cycles of HCl/NH_3 immersion

4.3 Metal sensing studies

The metal sensing abilities of compounds **L1** to **L6** towards Zn^{2+}, Cd^{2+}, Hg^{2+}, Ag^{+} and Cu^{2+} in acetonitrile were assessed through titrations of the free ligands with small quantities of these metal ions. The spectral behavior in all compounds was quite similar and thus **L1** and **L5** were chosen as a representative example, while the results for the remaining compounds are available in Annexes 30 to 43. Figure 24 illustrates the maximum emission intensities at 519nm and 521nm of **L1** and **L5**, respectively, following the addition of 1, 2 and 10 equivalents of the metal ions. The observed reduction in emission intensity indicates that these compounds exhibit exceptional sensibility to Cu^{2+} and Hg^{2+}. Compound **L5** also showed sensitivity to Ag^{+}, as a 60% reduction in emission intensity was noted after the addition of 10 equivalents, compared to complete quenching observed with Cu^{2+} and Hg^{2+} upon the addition of up to 2 equivalents. Figure 25 presents the absorption and emission spectral changes for **L1** when Cu^{2+} and Hg^{2+} were added in acetonitrile.

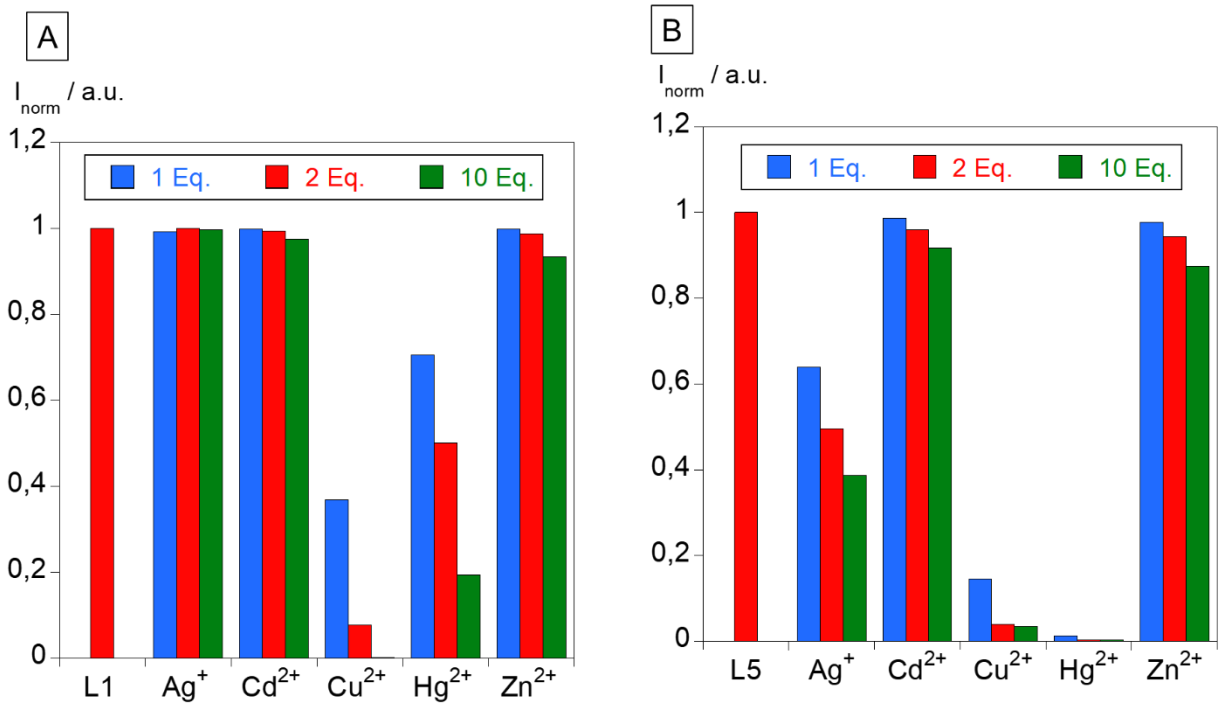

Figure 24. Maximum emission intensities of **L1** (A) and **L5** (B) following the addition of 1, 2 and 10 equivalents of Ag^{+}, Cd^{2+}, Cu^{2+},Hg^{2+}, Zn^{2+}metal ions. ([**L1**] = [**L5**] = 20 μM, λ_{em}**L1**= 519 nm, λ_{em}**L5** = 521 nm, T = 298 K).

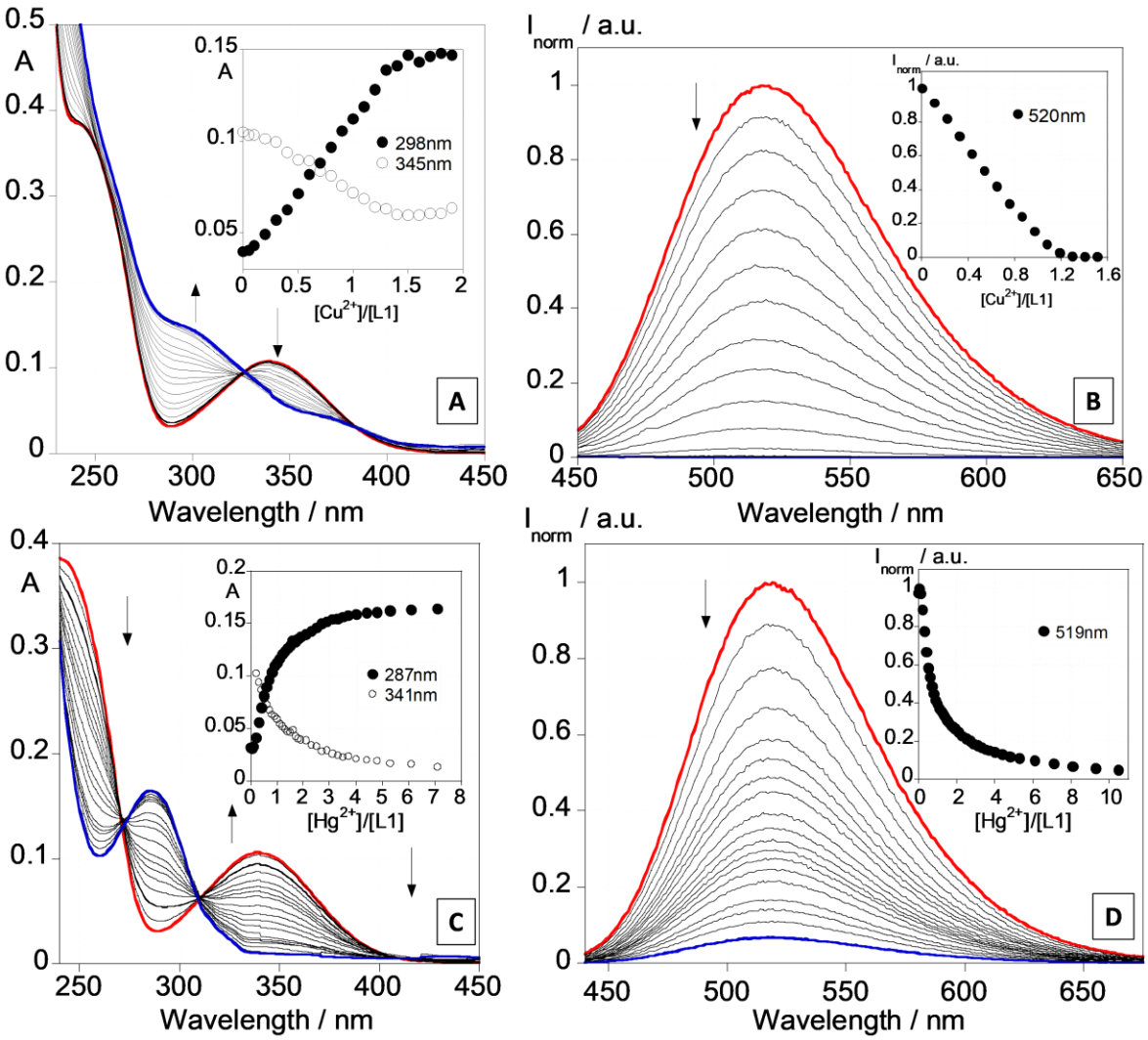

Figure 25. Spectrophotometric and spectrofluorimetric titrations of dansyl derivative **L1** with additions of Cu^{2+} (A, B), and Hg^{2+} (C, D) in CH_3CN. The inset illustrates the absorption (A, C) and emission intensity (B-D) in relation to $[Cu^{2+}]/[\mathbf{L1}]$ and $[Hg^{2+}]/[\mathbf{L1}]$, respectively. [**L1**] = 20 μM, λ_{exc}**L1**=341 nm, T = 298 K).

Comparing the effects of Cu^{2+} and Hg^{2+} in the absorption spectra in Figures 25A and 25B, it is evident similarities, such as, the increase in the concentration of both ions results on a decrease in the absorption at 341nm and an increase at 298nm (for Cu^{2+}) and 287nm (for Hg^{2+}). In the case of the emission spectra, results are also similar, where a decrease in the emission intensity at 519nm is observed in both cases. The sensing mechanism for these ions can be elucidated by considering their electronic configurations. Cu^{2+} ions are paramagnetic transition metals with unfilled d orbital shells, rendering them susceptible to the chelation

enhancement of quenching (CHEQ) effect through either an electron or energy-transfer mechanism. However, Hg^{2+} behaves differently since it is a diamagnetic metal with a filled d^{10} configuration. In this case, quenching can also arise from spin-orbit coupling, attributed to its large atomic number, acting as the primary pathway for non-radiative deactivation (k_{nr}).[65]

As shown in Figure 26, the spectral changes observed in compound **L5** are in line with those seen in other compounds when exposed to Cu^{2+} and Hg^{2+}. However, this compound exhibited a significant response to the addition of Ag^{+}, resulting in a decrease in emission intensity, although no changes were observed in the absorption spectra, as depicted in Figures 26E and 26F. The observed quenching of emission can be attributed to the photoinduced electron transfer effect induced by Ag^{+}. This response is consistent with the structure of **L5**, which features a higher number of nitrogen atoms.

In order to provide more insights into the interactions between the dansyl derivatives **L1**-**L6** with the tested metal ions and quantify the strength of these interactions, their stability constants were computed using the HypSpec program[66].The summarized results are presented in Table 3. The stability constants indicate the formation of mononuclear species for $Cu^{2+}$and Hg^{2+} in the case of **L1-L6** and also for Ag^{+} in the case of compound **L5**. Notably, **L3** exhibits the highest stability constant among the derivatives with a value of $LogK_{ass.}$ = 11.40±0.02 for its interaction with Hg^{2+}. We can observe that compounds **L1**, **L2**, and **L3** exhibit higher stability constants towards Cu^{2+} and Hg^{2+} than compounds **L4**, **L5** and **L6**. These results are in agreement with other dansyl derivatives studied previously in our group, being Hg(II) or Cu(II) the higher values observed.

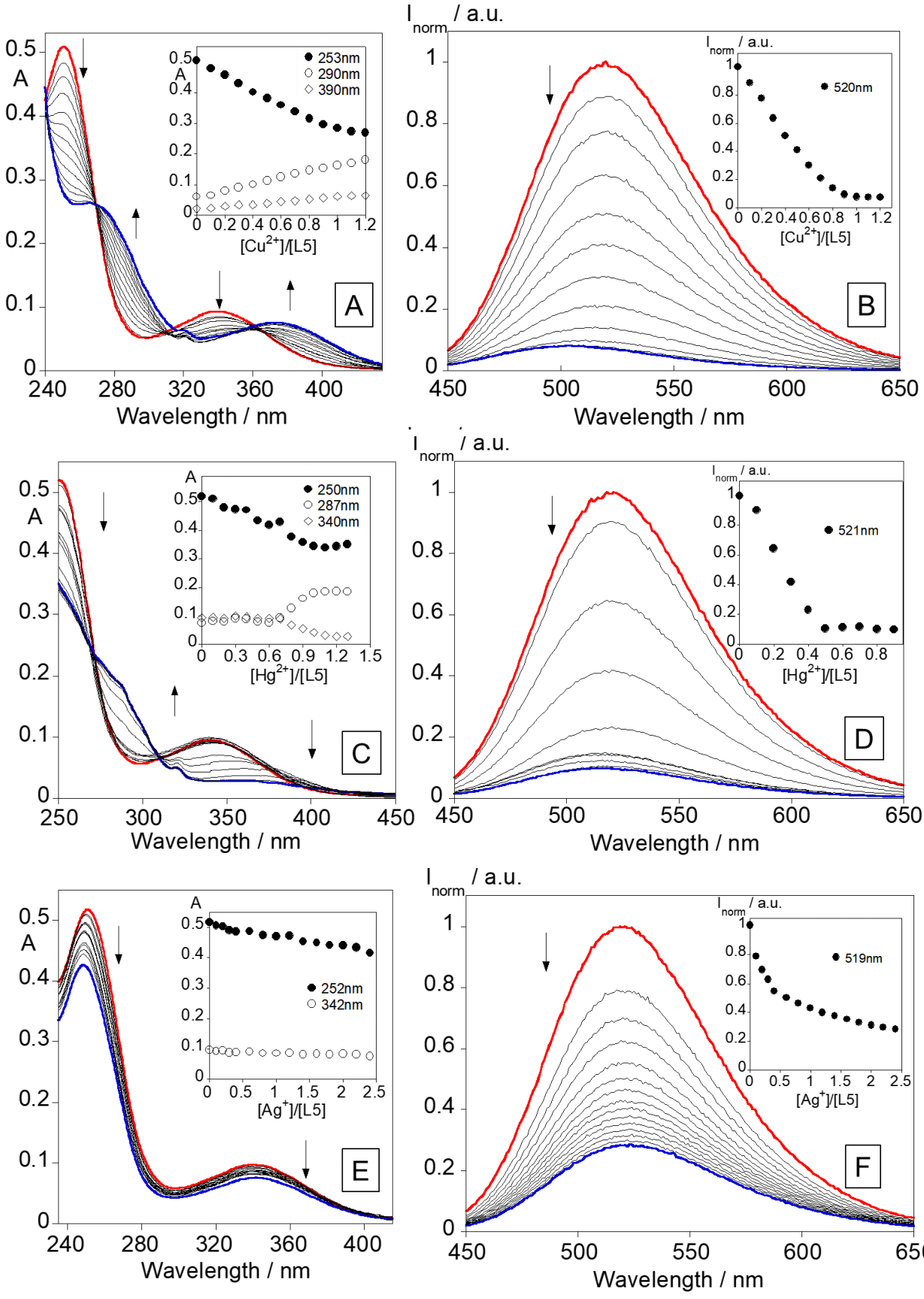
A
0.5
0.4
0.3
0.2
0.1
0
240 280 320 360 400
Wavelength / nm
253nm
290nm
390nm
[Cu2+]/[L5]
B
I norm / a.u.
1
0.8
0.6
0.4
0.2
0
450 500 550 600 650
Wavelength / nm
520nm
[Cu2+]/[L5]
C
250 300 350 400 450
Wavelength / nm
250nm
287nm
340nm
[Hg2+]/[L5]
D
521nm
[Hg2+]/[L5]
E
252nm
342nm
[Ag+]/[L5]
F
519nm
[Ag+]/[L5]

Figure 26. Spectrophotometric and spectrofluorimetric titrations of dansyl derivative **L5** with increased additions of Cu^{2+} (A, B), Hg^{2+} (C, D), and Ag^{+} (E, F) in CH_3CN. The inset illustrates the absorption (A,C,E) and emission intensity (B,D,F) in relation to [Cu^{2+}]/[**L5**], [Hg^{2+}]/[**L5**] and [Ag^{+}]/[**L5**], respectively. [**L5**] = 20 μM, λ_{exc}**L5**=340 nm, T = 295 K).

Table 3. Stability association constants and complex stoichiometry for the interactions of **L1** to **L6** with Cu^{2+}, Hg^{2+}, Ag^{+} ions, in CH_3CN.

Compounds (L)	Metal (M)	Association constants ($LogK_{ass.}$)	L:M
L1	Cu^{2+}	7.22±0.06	1:1
	Hg^{2+}	9.10±0.01	1:1
L2	Cu^{2+}	10.54±0.01	1:1
	Hg^{2+}	8.96±0.01	1:1
L3	Cu^{2+}	11.40±0.02	1:1
	Hg^{2+}	9.44±0.01	1:1
L4	Cu^{2+}	5.34±0.01	1:1
	Hg^{2+}	5.76±0.01	1:1
L5	Cu^{2+}	5.92±0.01	1:1
	Hg^{2+}	5.20±0.01	1:1
	Ag^{+}	5.30±0.01	1:1
L6	Cu^{2+}	7.15±0.02	1:1
	Hg^{2+}	5.67±0.01	1:1

4.4 Anion sensing studies

Similar to the procedure used for metal sensing, the anion-sensing capabilities of compounds **L4** to **L6** towards Br^-, Cl^-, CN^-, and F^- in acetonitrile were assessed by titrating the free ligand with small quantities of these anions. The spectral behavior was again quite similar among the tested compounds, leading to the selection of **L4** as a representative example. Results for compounds **L5** and **L6** are depicted in Annexes 44 to 50. In Figure 27, we can observe the maximum emission intensities at 519nm for **L4** upon the addition of 1, 2, and 10 equivalents of the anions. The significant decrease in emission intensity indicates that **L4** exhibits exceptional sensitivity to CN^- and F^-.

Figure 28 illustrates the changes in absorption and emission spectra of **L4** when CN^- and F^- are added in acetonitrile. Comparing the effects of both anions, we can observe their remarkably similar behavior. As the concentration of CN^- and F^- in solution increases, the 307nm and 303nm (respectively) increases in absorption, while the 375nm and 378nm band shows a slight decrease in absorption. Analyzing the emission spectra, we can observe that the results are consistent for both anions, with a significant decrease in the emission intensity of the 520nm band (for CN^-) and the 531nm band (for F^-). The mechanism underlying the detection of these anions can be explained by examining the molecular structure of compounds **L4** to **L6**, which contain multiple amine groups. As the anion concentration in the solution increases, the anions interact with the amine groups, acting as a base and causing their deprotonation. This deprotonation alters the electronic structure of the dansyl derivatives, resulting in the observed quenching of emission intensity as non-radiative decay pathways are promoted. Additionally, deprotonation can disrupt hydrogen bond interactions between the dansyl derivative and surrounding solvent molecules, leading to changes in the electronic structure and subsequent quenching of emission.

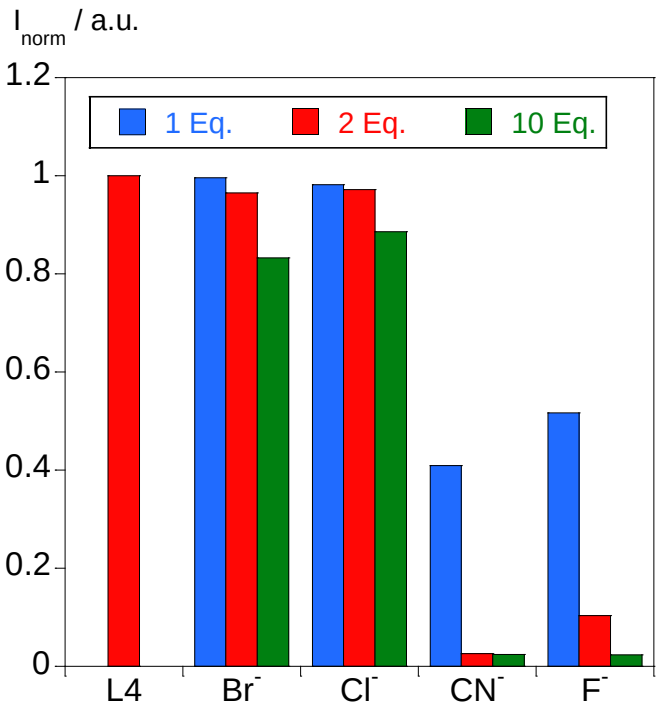

Figure 27. Maximum emission intensities of **L4** upon the addition of 1, 2 and 10 equivalents of Br^-, Cl^-, CN^- and F^- anions. ([**L4**] = 20 μM, λ_{em}**L4**= 519 nm, T = 295 K).

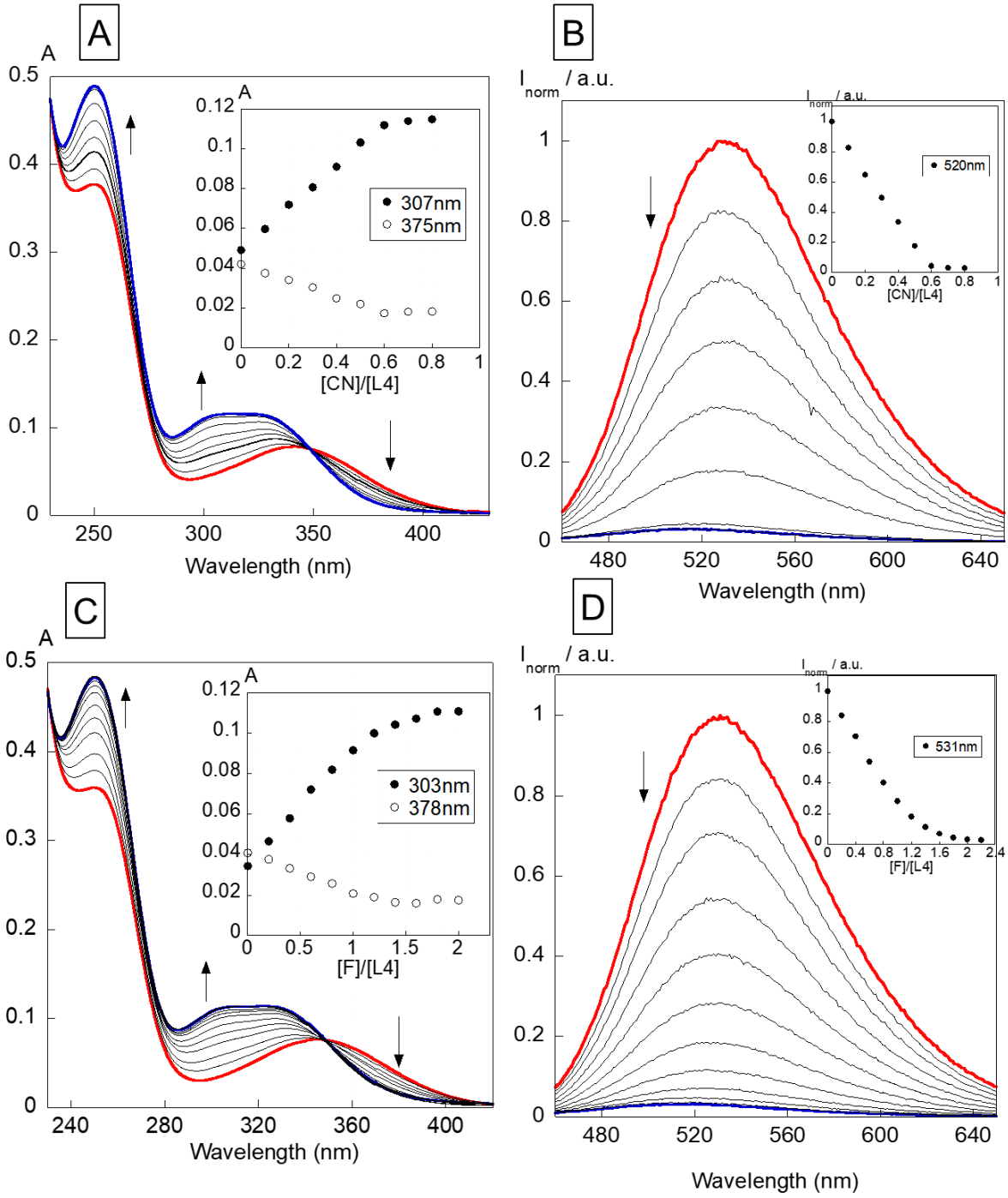

Figure 28. Spectrophotometric and spectrofluorimetric titrations of dansyl derivative **L4** with increased additions of CN^- (A, B), and F^- (C, D) in CH_3CN. The inset illustrates the absorption (A, C) and emission intensity (B-D) in relation to $[CN^-]/[\mathbf{L4}]$ and $[F^-]/[\mathbf{L4}]$, respectively. [**L4**] = 20 μM, λ_{exc}**L4**=340 nm, T = 298 K).

5

General Conclusions

Six novel dansyl-based compounds **L1**-**L6** have been thoroughly characterized through UV-Vis absorption and fluorescence emission steady-state and excited state spectroscopy in various states: solution, solid-state, and when doped into PMMA polymers. The comprehensive photophysical characterization of these compounds included determining fluorescence quantum yields and fluorescence lifetimes in five different solvents. These compounds exhibited a positive solvatochromic effect, causing a shift in emission color from yellow to green as solvent polarity increased, accompanied by red-shifts of 30-40nm in emission maximum wavelength.

The acid-sensing studies conducted showed that all six compounds, except **L3**, hold substantial potential for developing cost-effective systems to detect acidic environments. They displayed significant emission intensity quenching and recovery when titrated with HCl and NH_3, respectively, in solution. In PMMA polymer matrices, gradual intensity reductions were observed after successive immersions in HCl and exposure to HCl vapors, and these systems exhibited good emission intensity reversibility after ten cycles, underscoring their reusability.

Given the vital role of heteroatoms in sensing applications, compounds **L1** to **L6** were investigated as sensors for various metal ions, including Cd^{2+}, Cu^{2+}, Zn^{2+}, Ag^{+}, and Hg^{2+}, by adding 1 to 10 equivalents these metal ions to each compound. The studies revealed the sensitivity of these compounds to Cu^{2+} and Hg^{2+}, with complete emission intensity quenching upon the addition of no more than 2 equivalents of each metal. After full spectrophotometric and spectrofluorimetric titrations, it was observed that these compounds modulate their optical properties in the presence of Hg^{2+} and Cu^{2+}, leading to emission signal quenching and changes in absorption bands. This information highlights their potential for environmental applications. Stability association constants and stoichiometry suggested the formation of

mononuclear species for both metals with high affinity. Similar results were obtained for **L5** with Ag^+ ions.

Moreover, due to the presence of multiple amine groups in the chemical structure, which is crucial for anion sensing, compounds **L4** to **L6** were tested for various anions, including Br^-, Cl^-, CN^-, and F^-. The results revealed that these compounds exhibit exceptional sensitivity to cyanide and fluoride anions. Further titrations were conducted with these anions, demonstrating that compounds **L4** to **L6** undergo photophysical changes when exposed to CN^- and F^-, resulting in variations in their absorption spectra and quenching of fluorescence emission spectra.

In summary, this work provides valuable insights into the photophysical properties and toxic ion sensing capabilities of the six novel dansyl-based compounds, **L1** to **L6**, making them promising candidates for a wide range of applications in environmental monitoring.

REFERENCES

1. Broekaert, J. A. C. Daniel C. Harris: Quantitative chemical analysis, 9th ed. *Anal Bioanal Chem* **407**, 8943–8944 (2015).
2. Skoog, D. A., West, D. M., Holler, F. J. & Crouch, S. R. *Fundamentals of Analytical Chemistry*. (Cengage Learning, 2013).
3. Levitus, M. Handbook of Fluorescence Spectroscopy and Imaging. From Ensemble to Single Molecules. Edited by Markus Sauer, Johan Hofkens and Jörg Enderlein. *Angewandte Chemie International Edition* **50**, 9017–9018 (2011).
4. Marini, A., Muñoz-Losa, A., Biancardi, A. & Mennucci, B. What is Solvatochromism? *J Phys Chem B* **114**, 17128–17135 (2010).
5. Oliveira, E., Baptista, R. M. F., Costa, S. P. G., Raposo, M. M. M. & Lodeiro, C. Synthesis and solvatochromism studies of novel bis(indolyl)methanes bearing functionalized arylthiophene groups as new colored materials. *Photochemical & Photobiological Sciences* **13**, 492–498 (2014).
6. Oliveira, E., Baptista, R. M. F., Costa, S. P. G., Raposo, M. M. M. & Lodeiro, C. Synthesis and solvatochromism studies of novel bis(indolyl)methanes bearing functionalized arylthiophene groups as new colored materials. *Photochemical & Photobiological Sciences* **13**, 492–498 (2014).
7. Pedro, G. *et al.* Exploring Coumarin-Based Boron Emissive Complexes as Temperature Thermometers in Polymer-Supported Materials. *Sensors* **23**, 1689 (2023).
8. Duarte, F. *et al.* Enhancing water sensing via aggregation-induced emission (AIE) and solvatofluorochromic studies using two new dansyl derivatives containing a disulfide bound: Pollutant metal ions detection and preparation of water-soluble fluorescent polymeric particles. *Dyes and Pigments* **218**, 111428 (2023).

9. Berlman, I. B. *Handbook of Fluorescence Spectra of Aromatic Molecules*. (Elsevier, 1971). doi:10.1016/B978-0-12-092656-5.X5001-1.
10. Lakowicz, J. *Principles of Fluorescence Spectroscopy*. (Springer US, 2006). doi:10.1007/978-0-387-46312-4.
11. Gao, G. *et al.* A simple and effective dansyl acid based "turn-on" fluorescent probe for detecting labile ferrous iron in physiological saline and live cells. *Talanta* **215**, 120908 (2020).
12. Wang, P. *et al.* A peptide-based fluorescent chemosensor for measuring cadmium ions in aqueous solutions and live cells. *Dalton Transactions* **44**, 18057–18064 (2015).
13. Li, P. *et al.* Quantitative Fluorescence Ratio Imaging of Intralysosomal Chloride Ions with Single Excitation/Dual Maximum Emission. *Chemistry - A European Journal* **20**, 11760–11767 (2014).
14. Ogrizek, M., Kroflič, A. & Šala, M. Determination of trace concentrations of simple phenols in ambient PM samples. *Chemosphere* **303**, 135313 (2022).
15. Sha, C., Li, Z., Lu, S., Hu, X. & Xu, D. A dansyl-based fluorescent probe for turn-off and turn-on detection of Hg2+ in a full water system. *Research on Chemical Intermediates* **48**, 5227–5241 (2022).
16. Zhou, S. *et al.* A dansyl based fluorescence chemosensor for Hg2+ and its application in the complicated environment samples. *Spectrochim Acta A Mol Biomol Spectrosc* **148**, 348–354 (2015).
17. Su, P. *et al.* A biomolecule-based fluorescence chemosensor for sequential detection of Ag+ and H2S in 100% aqueous solution and living cells. *Sens Actuators B Chem* **273**, 93–100 (2018).
18. Martynov, V. I., Pakhomov, A. A., Popova, N. V., Deyev, I. E. & Petrenko, A. G. Synthetic Fluorophores for Visualizing Biomolecules in Living Systems. *Acta Naturae* **8**, 33–46 (2016).
19. Martynov, V. I., Pakhomov, A. A., Popova, N. V., Deyev, I. E. & Petrenko, A. G. Synthetic Fluorophores for Visualizing Biomolecules in Living Systems. *Acta Naturae* **8**, 33–46 (2016).
20. Stuart, M. A. C. *et al.* Emerging applications of stimuli-responsive polymer materials. *Nat Mater* **9**, 101–113 (2010).
21. Zhang, H.-J. *et al.* Preparation, characterization, and properties of PMMA-doped polymer film materials: a study on the effect of terbium ions on luminescence and lifetime enhancement. *Dalton Transactions* **44**, 2871–2879 (2015).

22. Bejaoui, M., Galai, H., Touati, F. & Kouass, S. Multifunctional Roles of PVP as a Versatile Biomaterial in Solid State. in *Dosage Forms - Innovation and Future Perspectives* (IntechOpen, 2023). doi:10.5772/intechopen.99431.
23. Hinojosa-Meza, R. *et al.* Cost-Effective and Portable Instrumentation to Enable Accurate pH Measurements for Global Industry 4.0 and Vertical Farming Applications. *Applied Sciences* **12**, 7038 (2022).
24. Niu, W. *et al.* A novel pH fluorescent probe based on indocyanine for imaging of living cells. *Dyes and Pigments* **126**, 224–231 (2016).
25. Li, Z., Li, L.-J., Sun, T., Liu, L. & Xie, Z. Benzimidazole-BODIPY as optical and fluorimetric pH sensor. *Dyes and Pigments* **128**, 165–169 (2016).
26. Lodeiro, C. & Pina, F. Luminescent and chromogenic molecular probes based on polyamines and related compounds. *Coord Chem Rev* **253**, 1353–1383 (2009).
27. Lodeiro, C. *et al.* Light and colour as analytical detection tools: A journey into the periodic table using polyamines to bio-inspired systems as chemosensors. *Chem Soc Rev* **39**, 2948 (2010).
28. Galhano, J. *et al.* Development of low-cost colourimetric and pH sensors based on PMMA@Cyanine polymers. *Dyes and Pigments* **200**, 110154 (2022).
29. Yan, C., Qu, Z., Wang, J., Cao, L. & Han, Q. Microalgal bioremediation of heavy metal pollution in water: Recent advances, challenges, and prospects. *Chemosphere* **286**, 131870 (2022).
30. Jomova, K. *et al.* Essential metals in health and disease. *Chem Biol Interact* **367**, 110173 (2022).
31. Estrada-Aldrete, J., Hernández-López, J. M., García-León, A. M., Peralta-Hernández, J. M. & Cerino-Córdova, F. J. Electroanalytical determination of heavy metals in aqueous solutions by using a carbon paste electrode modified with spent coffee grounds. *Journal of Electroanalytical Chemistry* **857**, 113663 (2020).
32. Bernhoft, R. A. Mercury Toxicity and Treatment: A Review of the Literature. *J Environ Public Health* **2012**, 1–10 (2012).
33. U.S. Environmental Protection Agency. What EPA is Doing to Reduce Mercury Pollution, and Exposures to Mercury. https://www.epa.gov/mercury/what-epa-doing-reduce-mercury-pollution-and-exposures-mercury (2023).
34. Chopra, T., Sasan, S., Devi, L., Parkesh, R. & Kapoor, K. K. A comprehensive review on recent advances in copper sensors. *Coord Chem Rev* **470**, 214704 (2022).

35. Marcelo, G. A. *et al.* New dual colorimetric/fluorimetric probes for Hg2+ detection & extraction based on mesoporous SBA-16 nanoparticles containing porphyrin or rhodamine chromophores. *Dyes and Pigments* **161**, 427–437 (2019).
36. Cuerva, C. *et al.* Columnar discotic Pt(<scp>ii</scp>) metallomesogens as luminescence multifunctional materials with chemo and thermosensor abilities. *J. Mater. Chem. C* **2**, 9167–9181 (2014).
37. Cuerva, C. *et al.* Aggregation-induced emission enhancement (AIEE)-active Pt(II) metallomesogens as dyes sensitive to Hg2+ and dopant agents to develop stimuli-responsive luminescent polymer materials. *Dyes and Pigments* **175**, 108098 (2020).
38. Gunnlaugsson, T., Glynn, M., Tocci (née Hussey), G. M., Kruger, P. E. & Pfeffer, F. M. Anion recognition and sensing in organic and aqueous media using luminescent and colorimetric sensors. *Coord Chem Rev* **250**, 3094–3117 (2006).
39. Bianchi, E., Bowman-James, K. & Gracia-Espannia, E. *Supramolecular Chemistry of Anions*. (1997).
40. Busschaert, N., Caltagirone, C., Van Rossom, W. & Gale, P. A. Applications of Supramolecular Anion Recognition. *Chem Rev* **115**, 8038–8155 (2015).
41. Santos, C. I. M. *et al.* New gallium(III) corrole complexes as colorimetric probes for toxic cyanide anion. *Inorganica Chim Acta* **417**, 148–154 (2014).
42. Prodi, L., Bolletta, F., Montalti, M. & Zaccheroni, N. Searching for New Luminescent Sensors: Synthesis and Photophysical Properties of a Tripodal Ligand Incorporating the Dansyl Chromophore and of Its Metal Complexes. *Eur J Inorg Chem* **1999**, 455–460 (1999).
43. Tong, A.-J. *et al.* Selective extraction of alkali metal cations with proton-ionizable dibenzo-16-crown-5 fluoroionophores. *Anal Chim Acta* **420**, 57–64 (2000).
44. Dey, K. R., Wong, B. M. & Hossain, Md. A. Rational design of a macrocycle-based chemosensor for anions. *Tetrahedron Lett* **51**, 1329–1332 (2010).
45. Suzuki, Y. & Komatsu, Y. Environmentally Responsive and Bright Fluorescent Probes Possessing Dansyl-Modified Oligonucleotides Under Hybridization of DNA and RNA. in 145–159 (2015). doi:10.1007/978-3-319-17305-4_7.
46. Pavan Kumar, Y. *et al.* Fluorescent Dansyl-Guanosine Conjugates that Bind *c-MYC* Promoter G-Quadruplex and Downregulate *c-MYC* Expression. *ChemBioChem* **17**, 388–393 (2016).
47. Nasomphan, W., Tangboriboonrat, P., Tanapongpipat, S. & Smanmoo, S. Selective Fluorescent Detection of Aspartic Acid and Glutamic Acid Employing Dansyl Hydrazine Dextran Conjugate. *J Fluoresc* **24**, 7–11 (2014).

48. Wang, P., An, Y. & Liao, Y. A novel peptide-based fluorescent chemosensor for Cd(II) ions and its applications in bioimaging. *Spectrochim Acta A Mol Biomol Spectrosc* **216**, 61–68 (2019).
49. Matsuura, K. *et al.* Turn-On Fluorescent Probe Based on a Dansyl Triarginine Peptide for Ganglioside Imaging. *ACS Organic & Inorganic Au* **1**, 60–67 (2021).
50. Maiti, D. *et al.* Dansyl-appended Cu^{II} -complex-based nitroxyl (HNO) sensing with living cell imaging application and DFT studies. *Dalton Transactions* **48**, 2760–2771 (2019).
51. Murov, S. L., Carmichael, I. & Hug, G. L. *Handbook of Photochemistry*. (CRC Press, 1993).
52. Li, Y.-H. *et al.* Solvent effects on the fluorescence of 1-(dimethylamino)-5-naphthalenesulfonic acid and related compounds. *J Am Chem Soc* **97**, 3118–3126 (1975).
53. Schnute, M. E. *et al.* Discovery of a Potent and Selective Sphingosine Kinase 1 Inhibitor through the Molecular Combination of Chemotype-Distinct Screening Hits. *J Med Chem* **60**, 2562–2572 (2017).
54. Park, E.-Y. *et al.* Synthesis of dansyl labeled sphingosine kinase 1 inhibitor. *Chem Phys Lipids* **215**, 29–33 (2018).
55. Li, K.-B. *et al.* A colorimetric/fluorescence dual-channel probe for highly discriminating detection of cysteine. *Talanta* **194**, 803–808 (2019).
56. Knighton, R. C. *et al.* Fluorogenic dansyl-ligated gold nanoparticles for the detection of sulfur mustard by displacement assay. *Chemical Communications* **49**, 2293 (2013).
57. Liu, Y., Wang, Y., Zhao, L. & Xu, B. Development of a Simple Dansyl-Based PH Fluorescent Probe in Acidic Medium and Its Application in Cell Imaging. *J Fluoresc* **32**, 227–233 (2022).
58. Sha, C., Chen, Y., Chen, Y. & Xu, D. An easily Prepared Fluorescent pH Probe Based on Dansyl. *J Fluoresc* **26**, 1709–1714 (2016).
59. Jeong, E., Yoon, S., Lee, H. S., Kumar, A. & Chae, P. S. TURN-ON fluorescence detection of cyanide using an ensemble system consisting of a dansyl-based cationic probe and dicyanovinyl derivative. *Dyes and Pigments* **162**, 348–357 (2019).
60. Kwanmuang, P., Songsasen, A., Sirisaksoontorn, W. & Wannalerse, B. Synthesis of a novel sensor based on orcinol-dansyl derivative for fluoride ion detection. in *Proceedings of International Exchange and Innovation Conference on Engineering & Sciences (IEICES)* 49–52 (2019).
61. Montalti, M., Credi, A., Prodi, L. & Gandolfi, M. T. *Handbook of Photochemistry*. (CRC Press, 2006). doi:10.1201/9781420015195.

62. Duarte, F. *et al.* Development of fluorochromic polymer doped materials as platforms for temperature sensing using three dansyl derivatives bearing a sulfur bridge. *J Photochem Photobiol A Chem* **445**, 115033 (2023).
63. Jia, L. & Liu, Y. The effects of electron-withdrawing and electron-donating groups on the photophysical properties and ESIPT of salicylideneaniline. *Spectrochim Acta A Mol Biomol Spectrosc* **242**, 118719 (2020).
64. Tahir, M. H., Mubashir, T., Shah, T. & Mahmood, A. Impact of electron-withdrawing and electron-donating substituents on the electrochemical and charge transport properties of indacenodithiophene-based small molecule acceptors for organic solar cells. *J Phys Org Chem* **32**, (2019).
65. Oliveira, E., Baptista, R. M. F., Costa, S. P. G., Raposo, M. M. M. & Lodeiro, C. Exploring the Emissive Properties of New Azacrown Compounds Bearing Aryl, Furyl, or Thienyl Moieties: A Special Case of Chelation Enhancement of Fluorescence upon Interaction with Ca^{2+}, Cu^{2+}, or Ni^{2+}. *Inorg Chem* **49**, 10847–10857 (2010).
66. GANS, P., SABATINI, A. & VACCA, A. Investigation of equilibria in solution. Determination of equilibrium constants with the HYPERQUAD suite of programs. *Talanta* **43**, 1739–1753 (1996).

A

Annexes

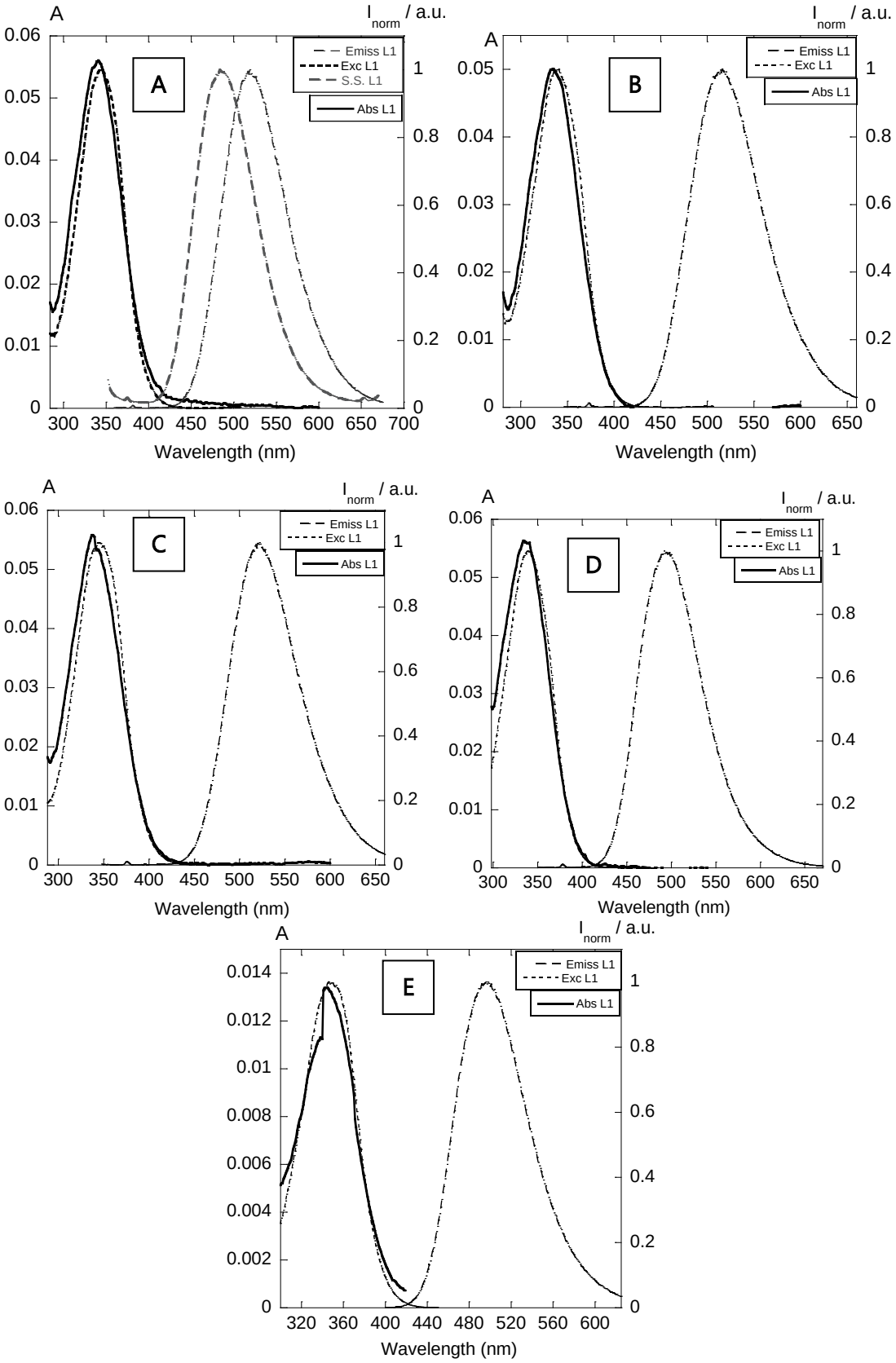

Annex 1. Photophysical characterization of compound L1 in A) CH_3CN B) EtOH, C) DMSO, D) THF ([L] = 10 μM) and E) $CHCl_3$ ([L] = 3 μM)

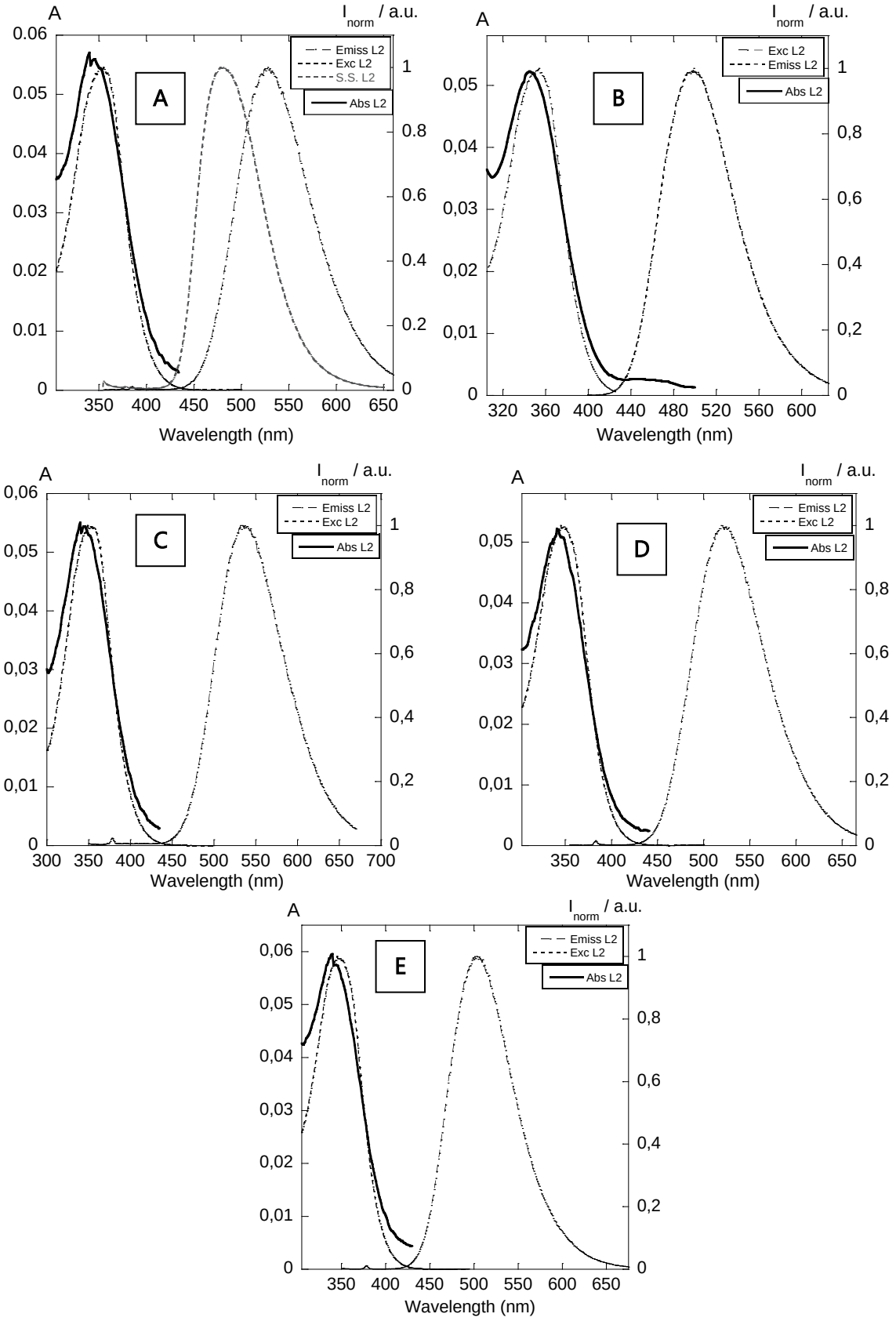

Annex 2. Photophysical characterization of compound L2 in a) CH_3CN b) $CHCl_3$, c) DMSO, d) EtOH, e) THF ([L] = 10 μM)

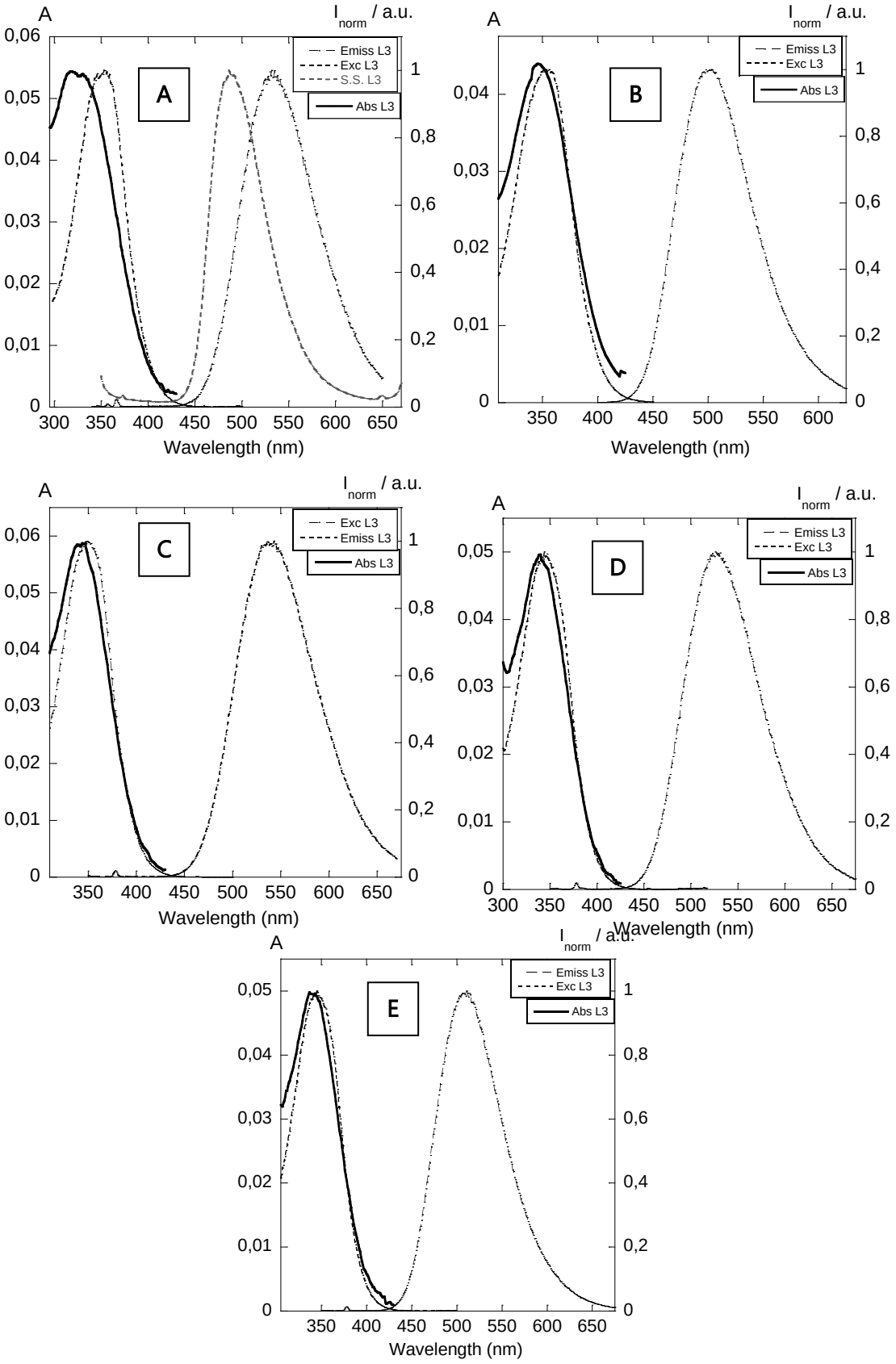

Annex 3. Photophysical characterization of compound L3 in a) CH3CN b) CHCl3, c) DMSO, d) EtOH, e) THF ([L] = 10 mM)

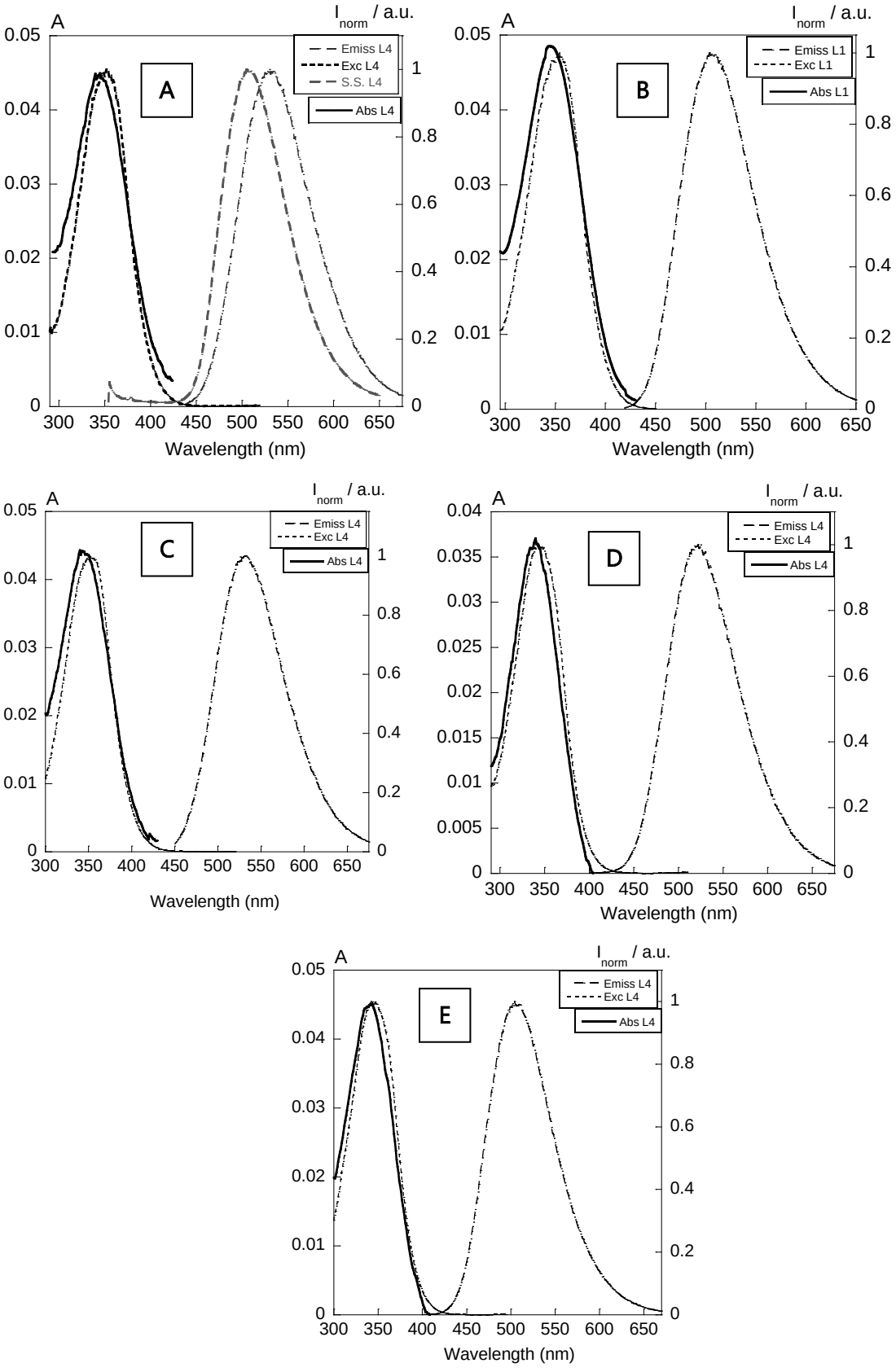

Annex 4. Photophysical characterization of compound L4 in a) CH_3CN b) $CHCl_3$, c) DMSO, d) EtOH, e) THF ([L] = 10 μM)

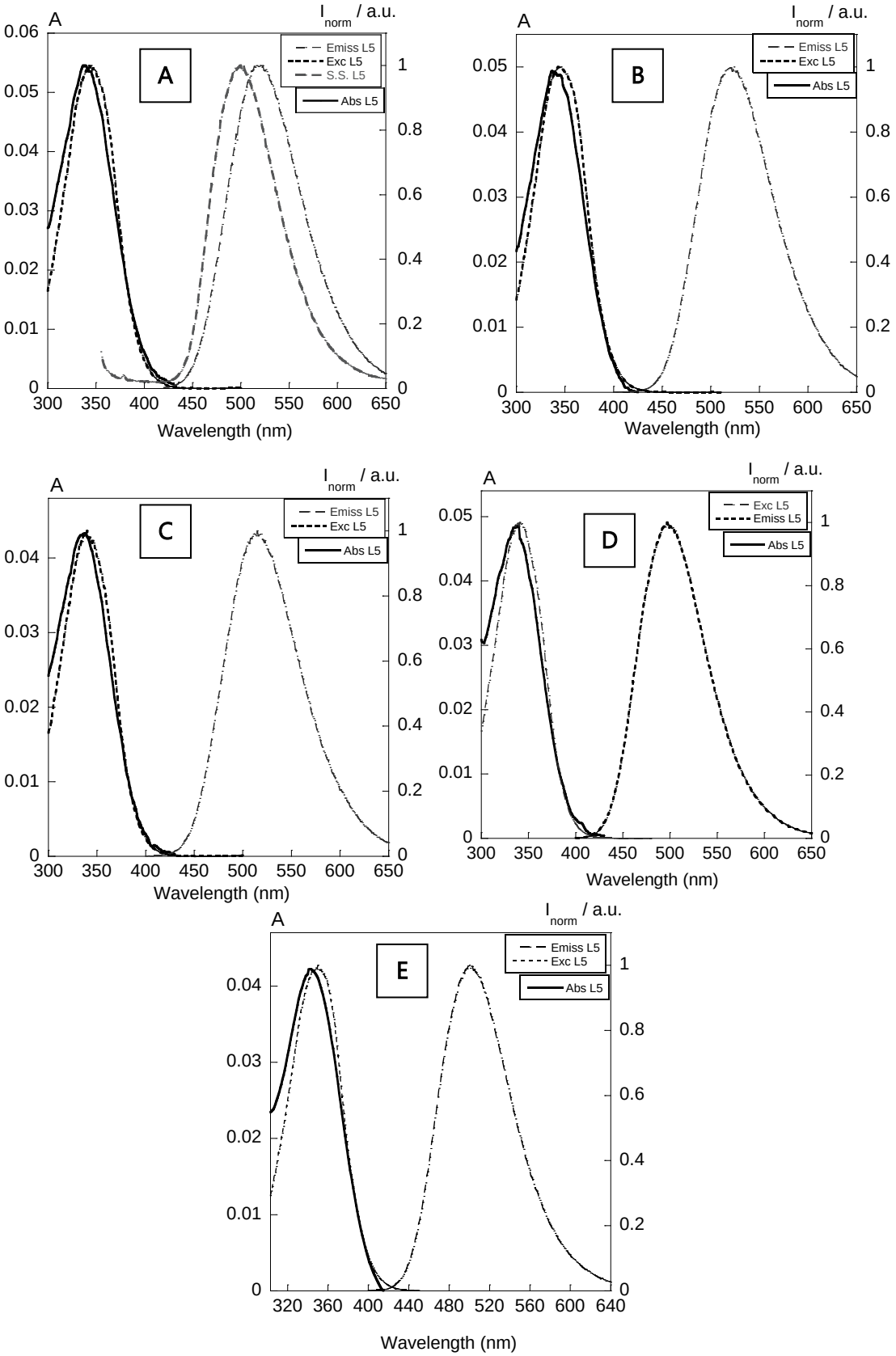

Annex 5. Photophysical characterization of compound L5 in a) CH_3CN b) $CHCl_3$, c) DMSO, d) EtOH, e) THF ([L] = 10 μM)

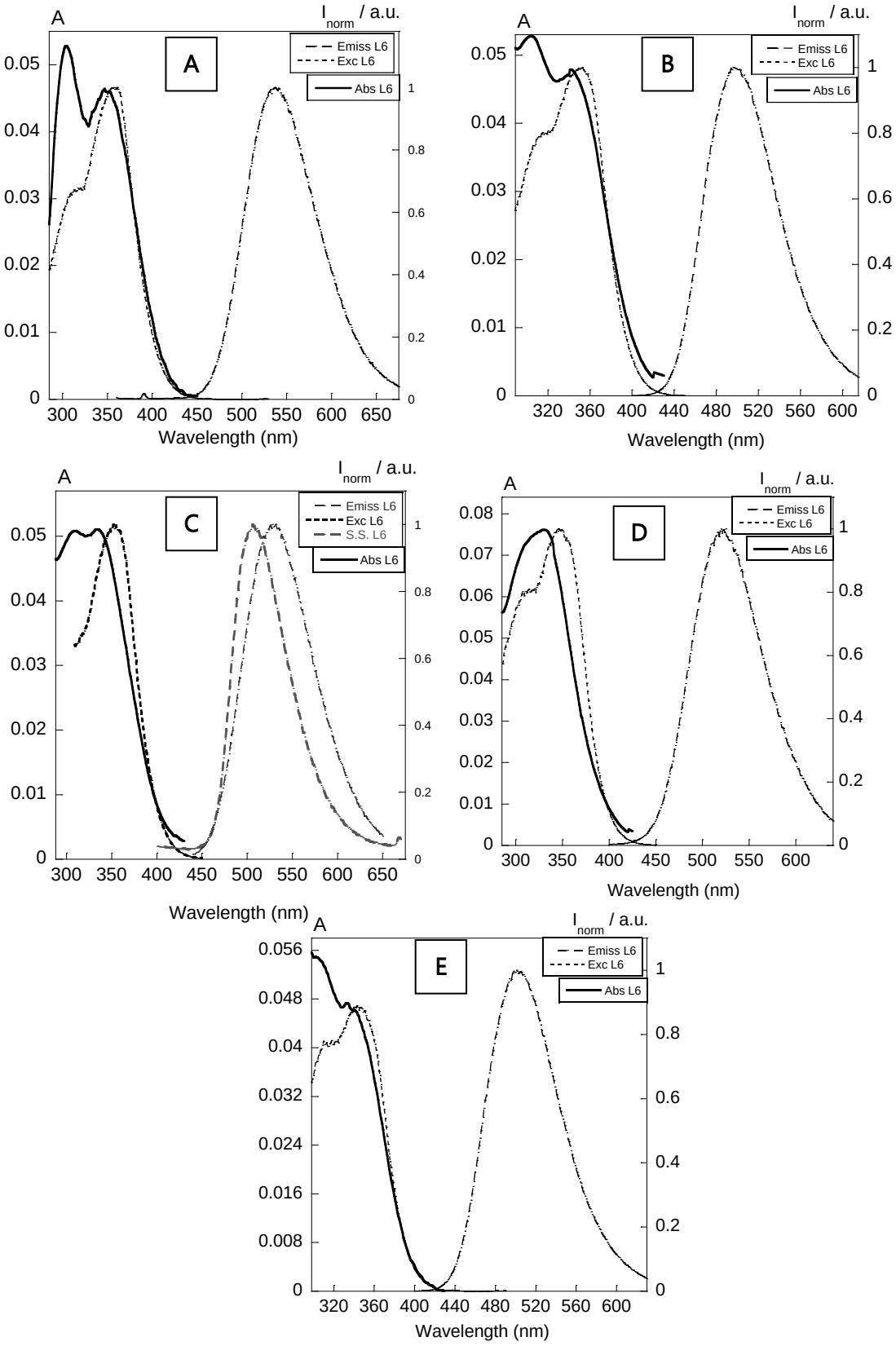

Annex 6. Photophysical characterization of compound L6 in a) CH_3CN b) $CHCl_3$, c) DMSO, d) EtOH, e) THF ([L] = 10 μM

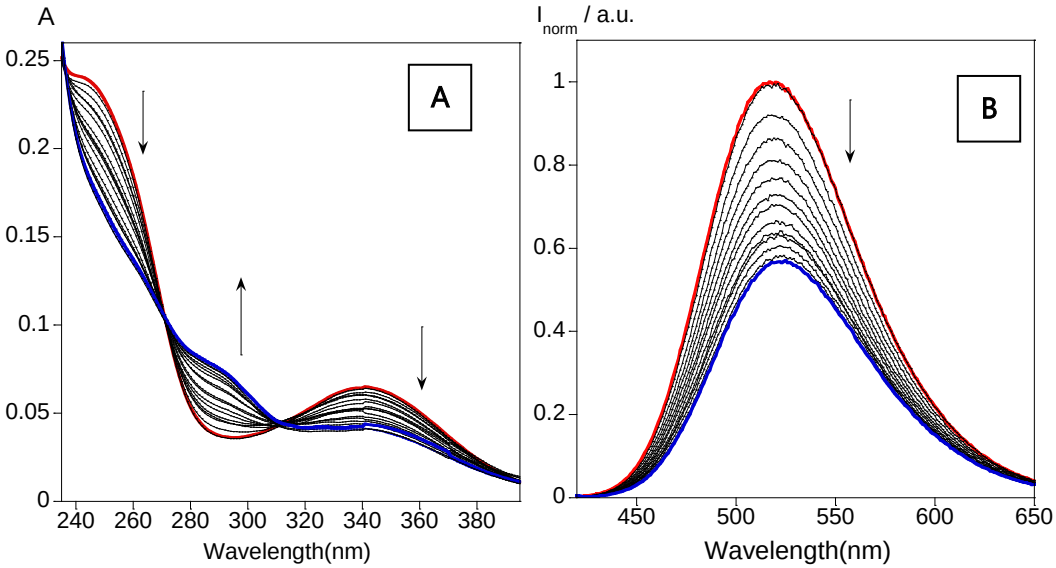

Annex 7. (A) Spectrophotometric and (B) spectrofluorimetric titrations of L1 with the addition of HCl (aq).

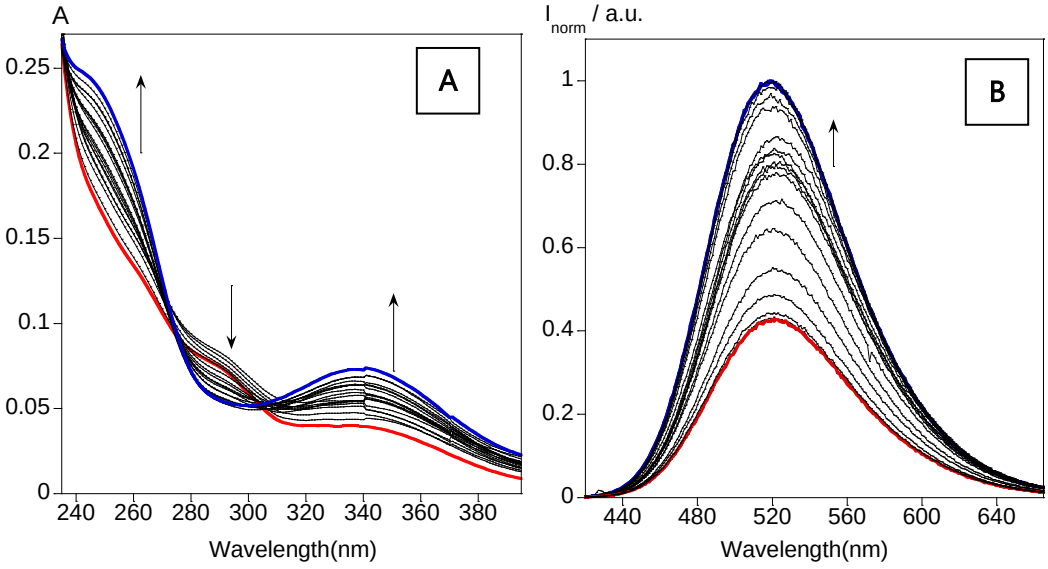

Annex 8. (A) Spectrophotometric and (B) spectrofluorimetric titrations of L1 with the addition of NH_3 (aq).

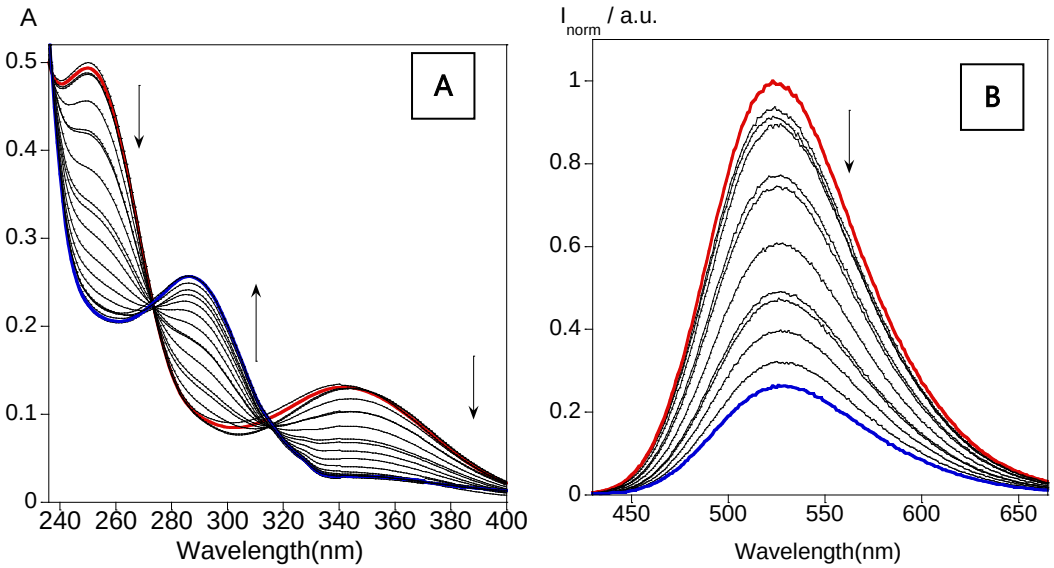

Annex 9. (A) Spectrophotometric and (B) spectrofluorimetric titrations of L2 with the addition of HCl (aq).

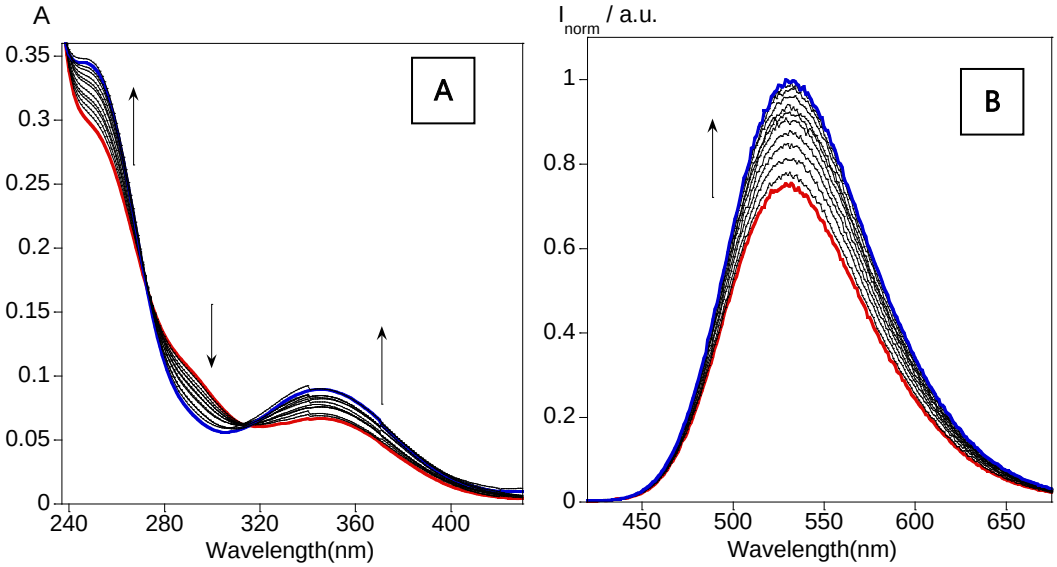

Annex 10. (A) Spectrophotometric and (B) spectrofluorimetric titrations of L2 with the addition of NH_3 (aq).

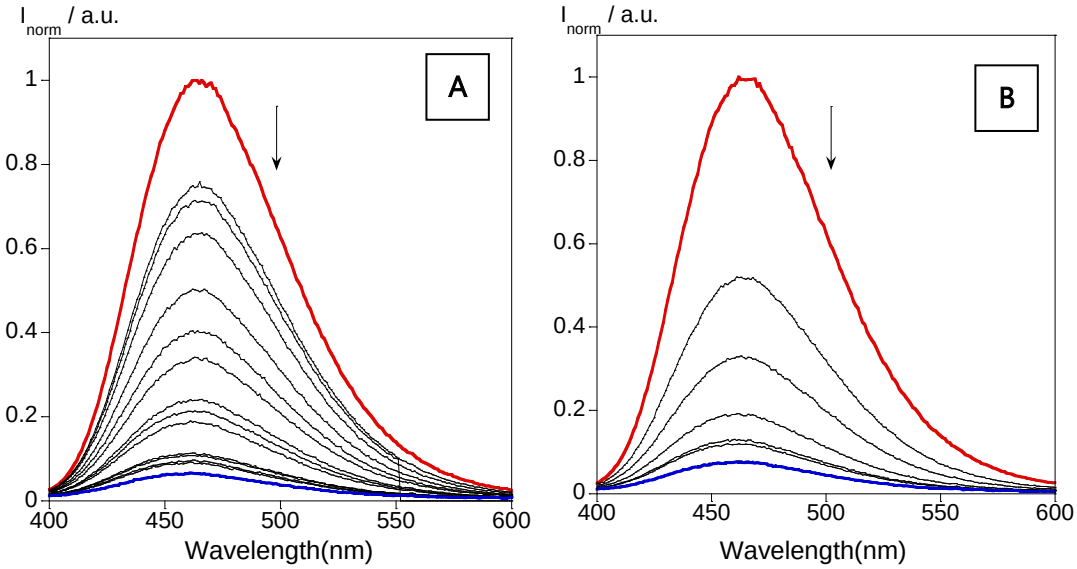

Annex 11. (A) Emission spectra of successive immersion of L1 doped PMMA polymer film in a conc. HCl solution (5m in 5min) (B) Emission spectra of exposure to HCl vapors (20m in 20m)

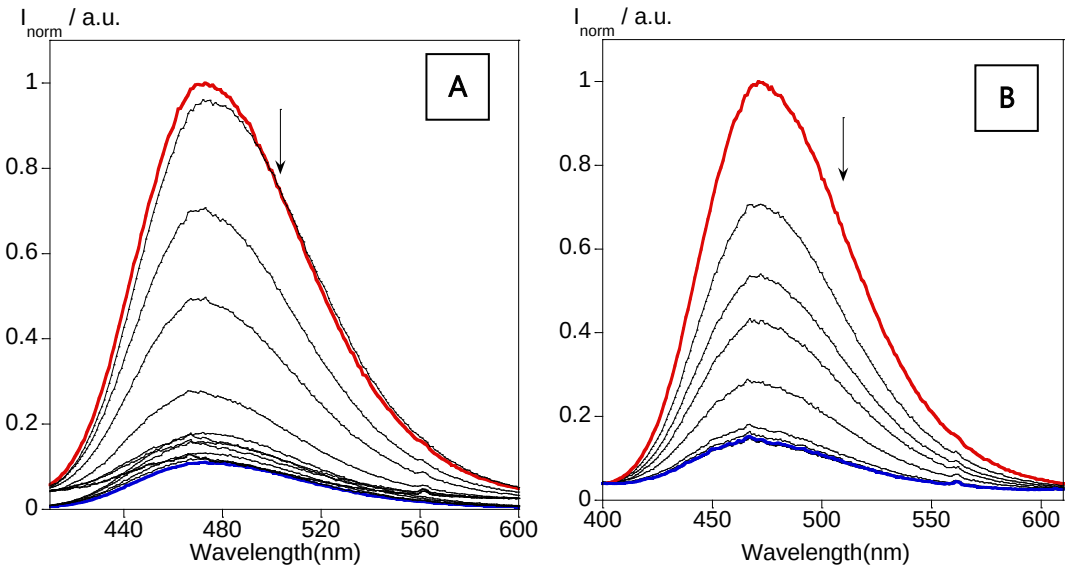

Annex 12. (A) Emission spectra of successive immersion of L2 doped PMMA polymer film in a conc. HCl solution (5m in 5min) (B) Emission spectra of exposure to HCl vapors (20m in 20m)

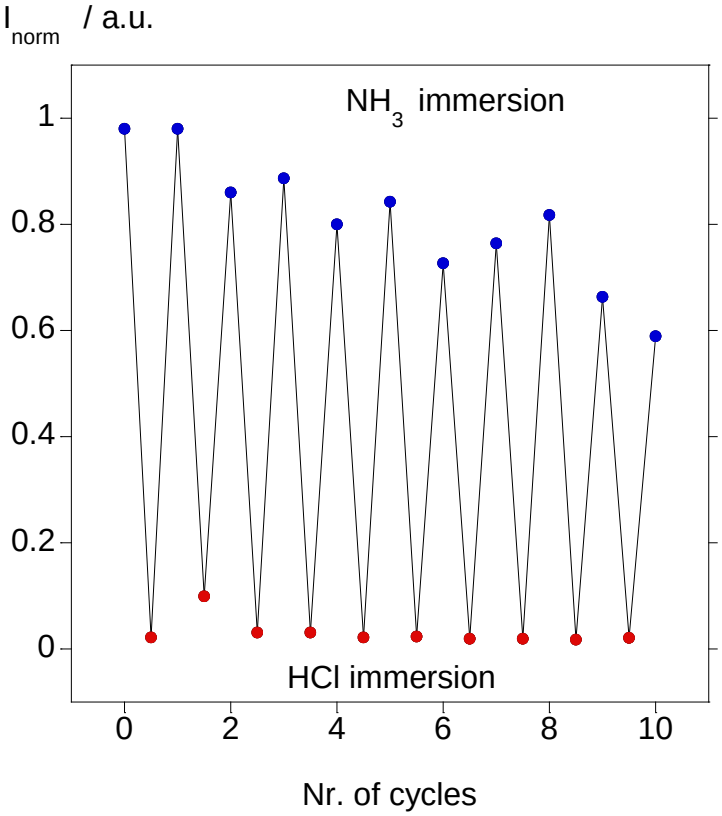

Annex 13. Emission intensity of **L2**@PMMA at λ_{476nm} after successive cycles of HCl/NH_3 immersion

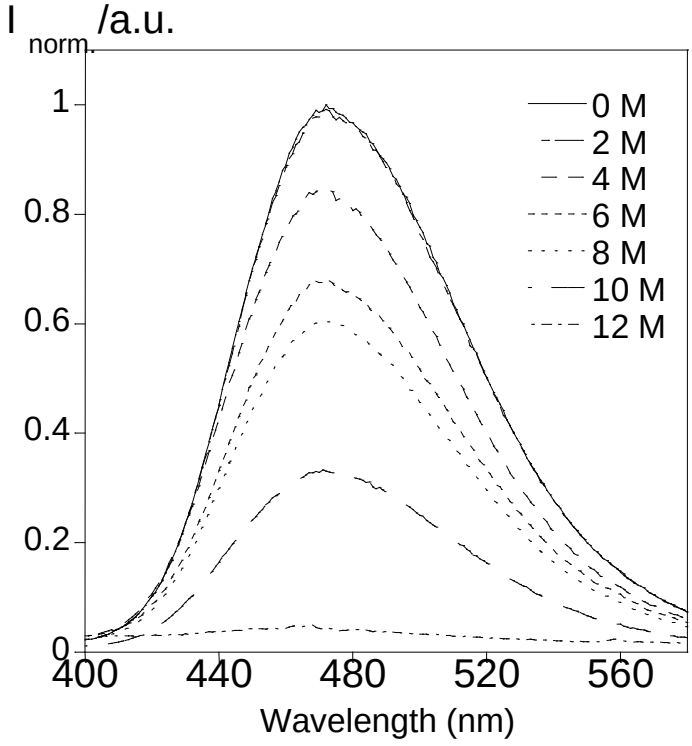

Annex 14. Emission spectra of **L2** immersion in the HCl concentrations from 0 to 12 M

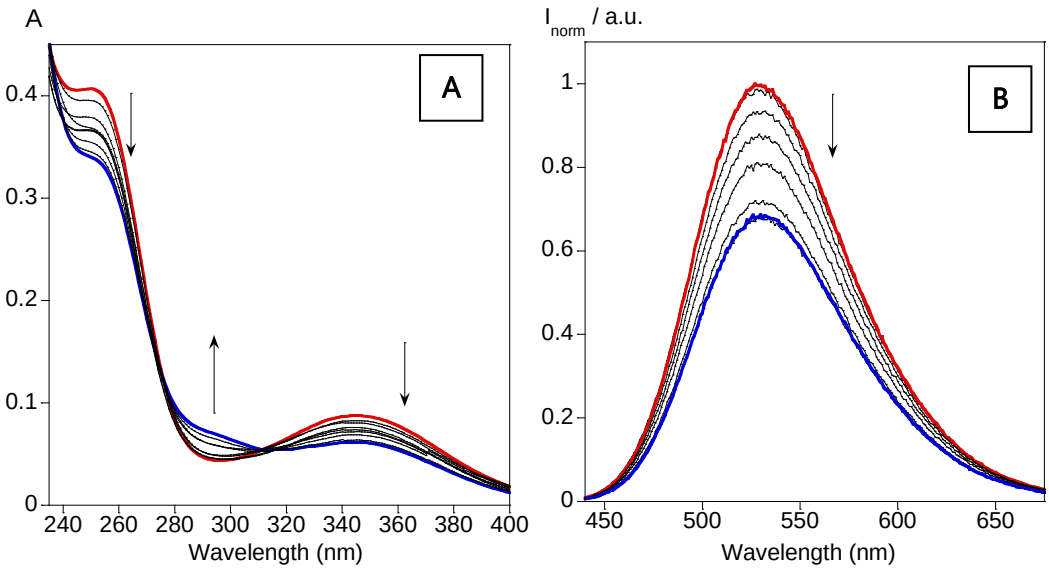

Annex 15. (A) Spectrophotometric and (B) spectrofluorimetric titrations of L4 with the addition of HCl (aq) ([HCl]= 10^{-3}M).

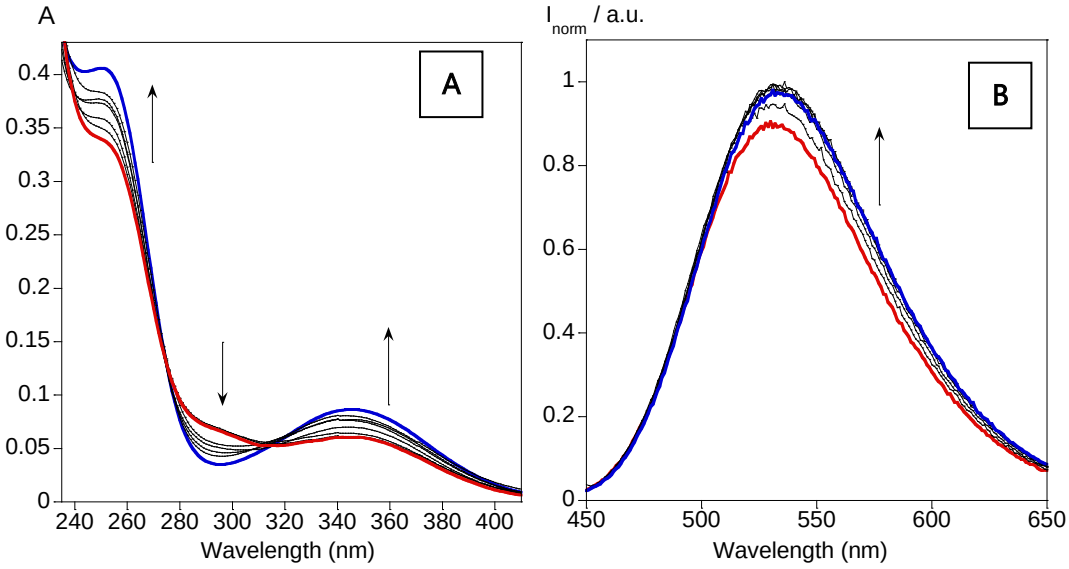

Annex 16. (A) Spectrophotometric and (B) spectrofluorimetric titrations of L4 with the addition of NH_3 (aq) ([NH_3]= 10^{-3}M).

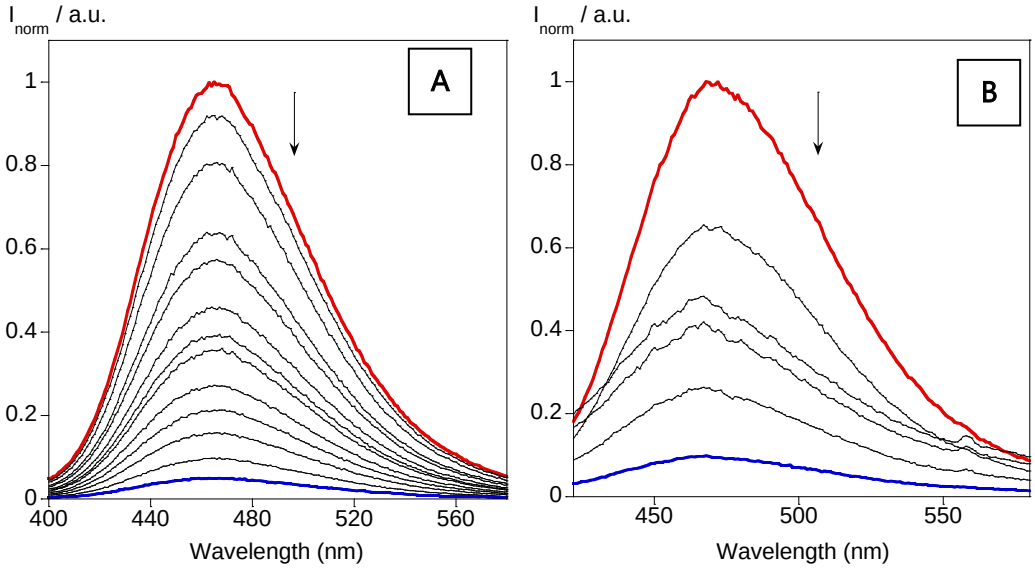

Annex 17. (A) Emission spectra of successive immersion of **L4** doped PMMA polymer film in a conc. HCl solution (5m in 5min) (B) Emission spectra of exposure to HCl vapors (20m in 20m)

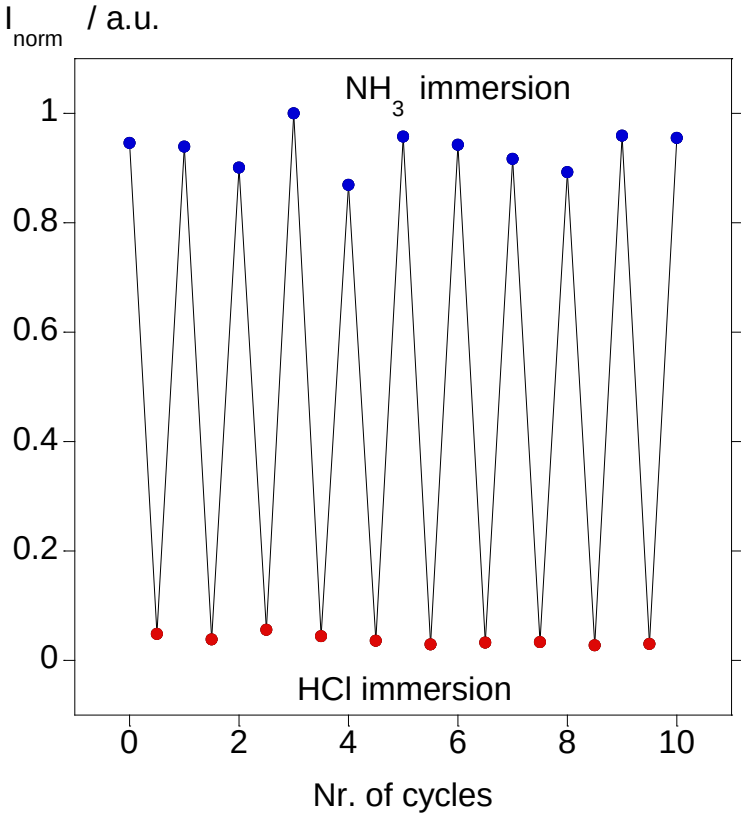

Annex 18. Emission intensity of **L4**@PMMA at λ_{476nm} after successive cycles of HCl/NH_3 immersion

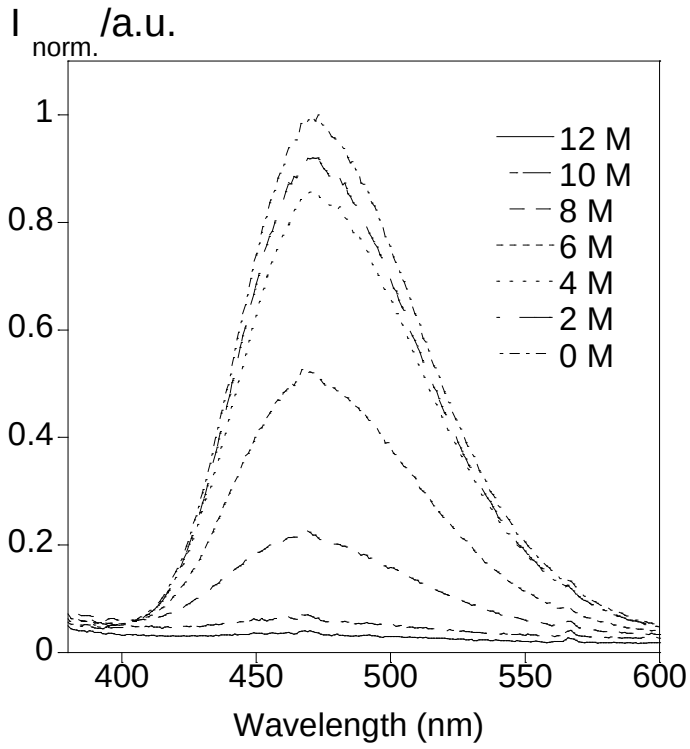

Annex 19. Emission spectra of **L4** immersion in the HCl concentrations from 0 to 12 M

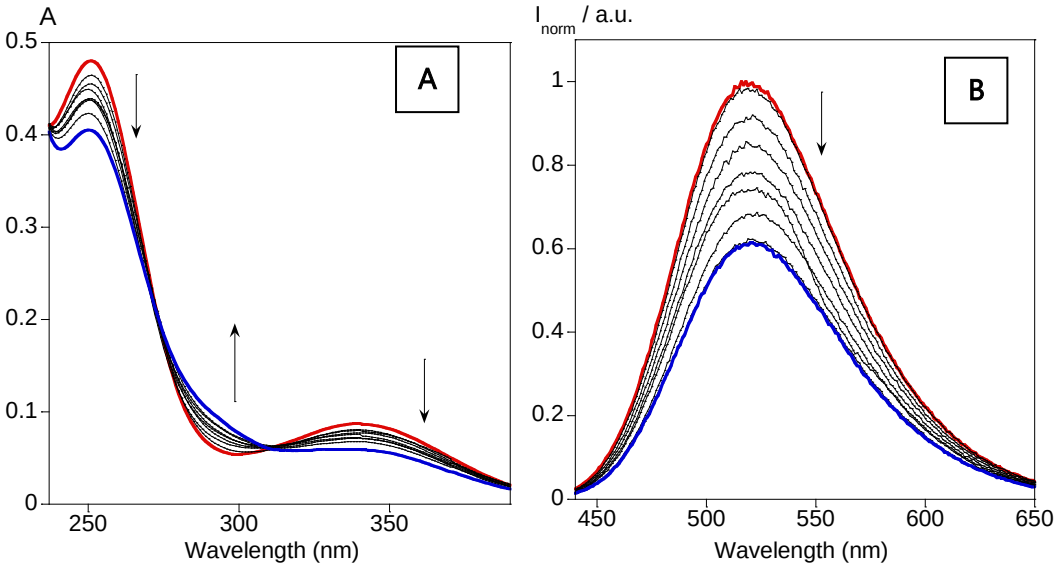

Annex 20. (A) Spectrophotometric and (B) spectrofluorimetric titrations of L5 with the addition of HCl (aq) ([HCl]= 10^{-3}M).

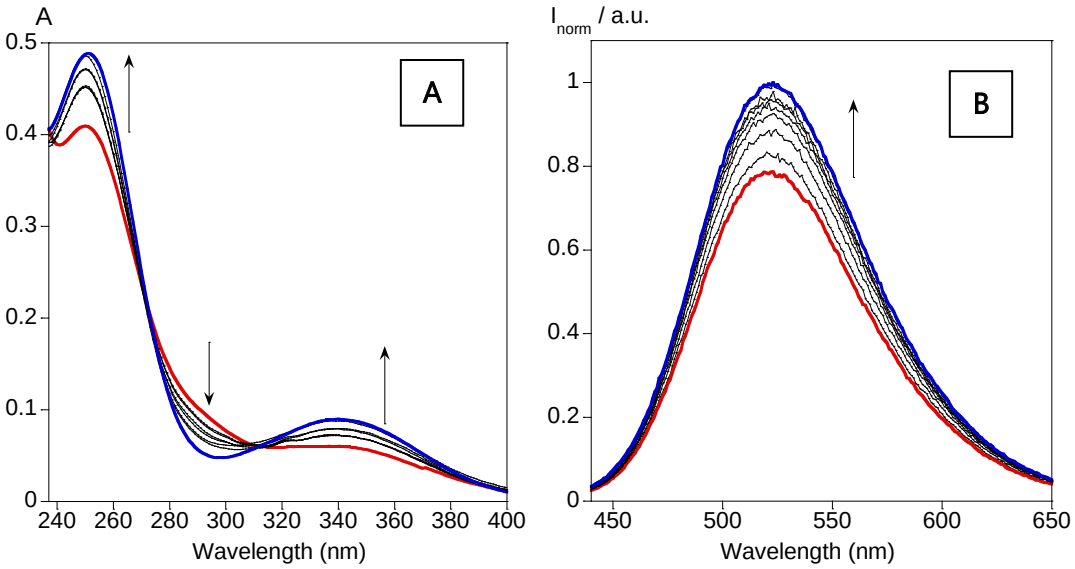

Annex 21. (A) Spectrophotometric and (B) spectrofluorimetric titrations of L5 with the addition of NH_3 (aq) ([NH_3]= 10^{-3}M).

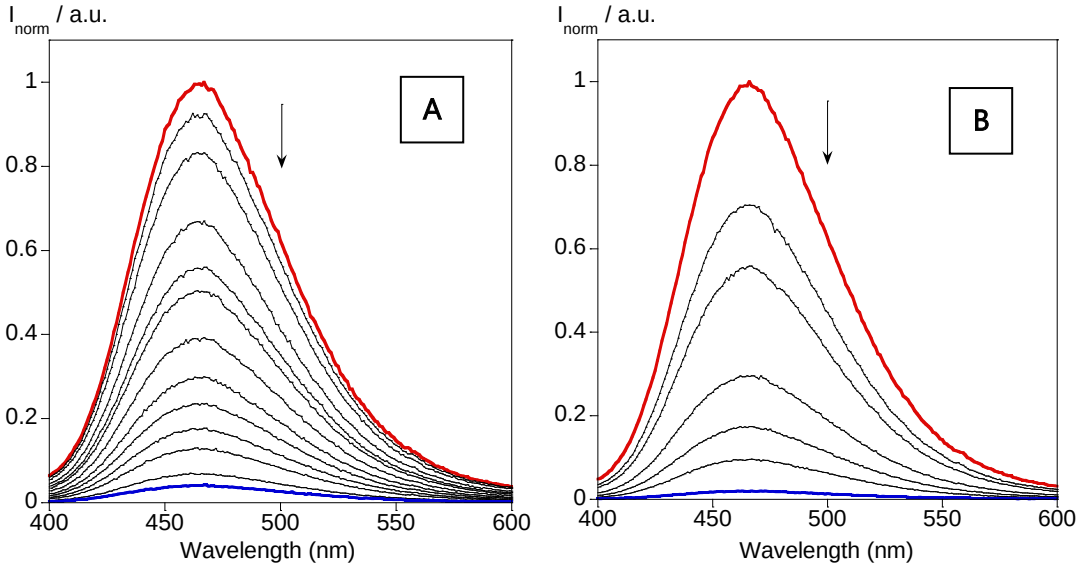

Annex 22. (A) Emission spectra of successive immersion of L5 doped PMMA polymer film in a conc. HCl solution (5m in 5min) (B) Emission spectra of exposure to HCl vapors (20m in 20m)

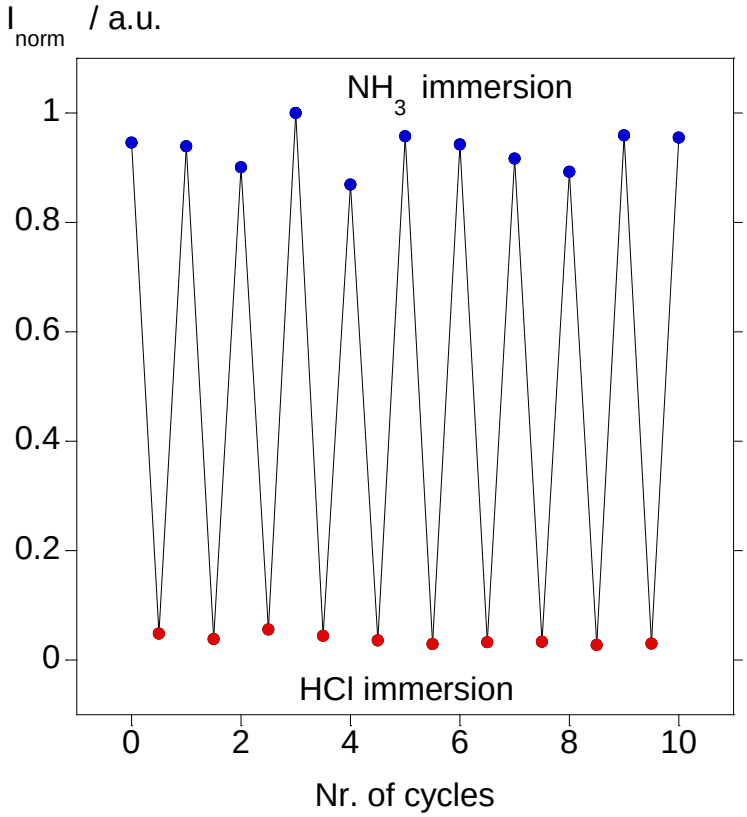

Annex 23. Emission intensity of **L5**@PMMA at λ_{464nm} after successive cycles of HCl/NH_3 immersion

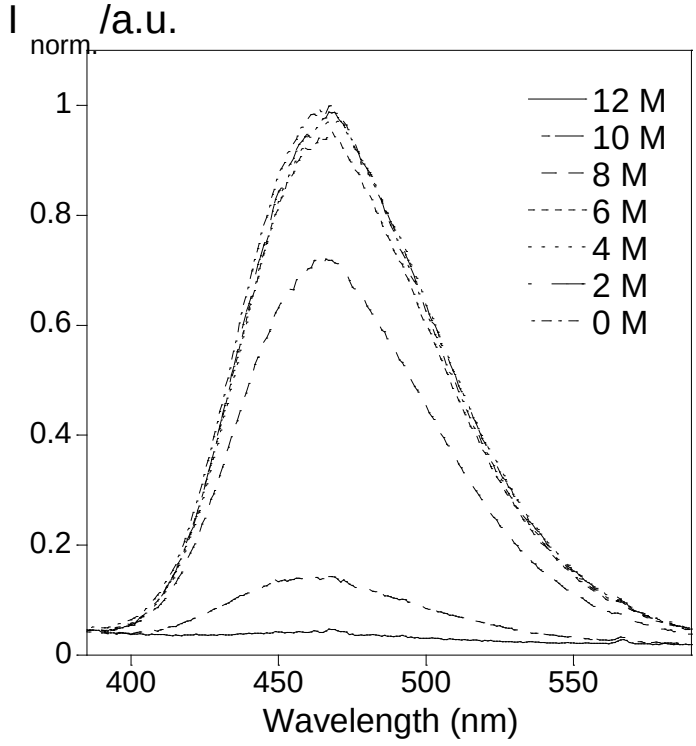

Annex 24. Emission spectra of **L5** immersion in the HCl concentrations from 0 to 12 M

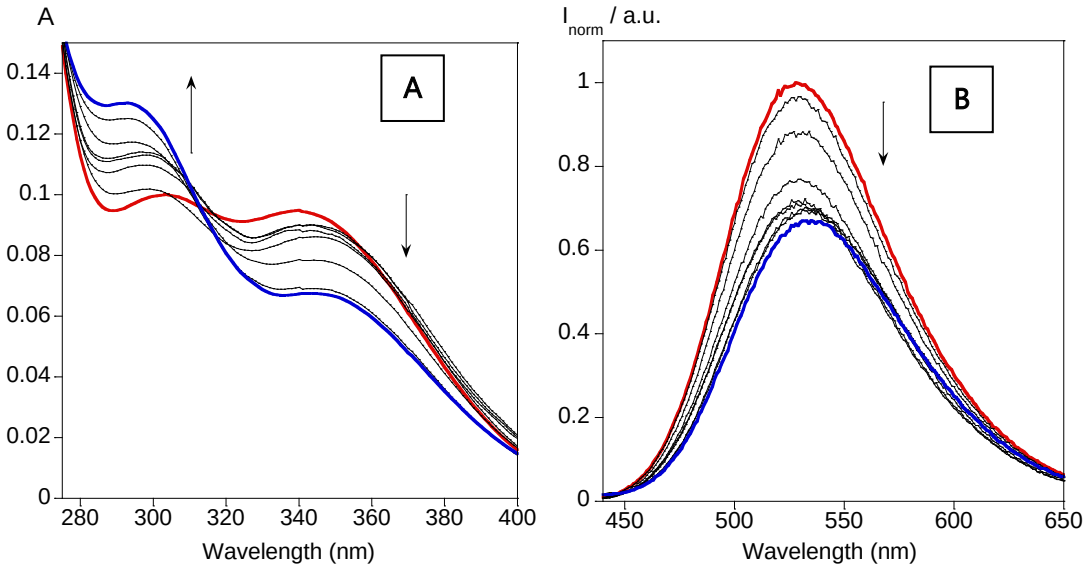

Annex 25. (A) Spectrophotometric and (B) spectrofluorimetric titrations of L6 with the addition of HCl (aq) ([HCl]= 10^{-3}M).

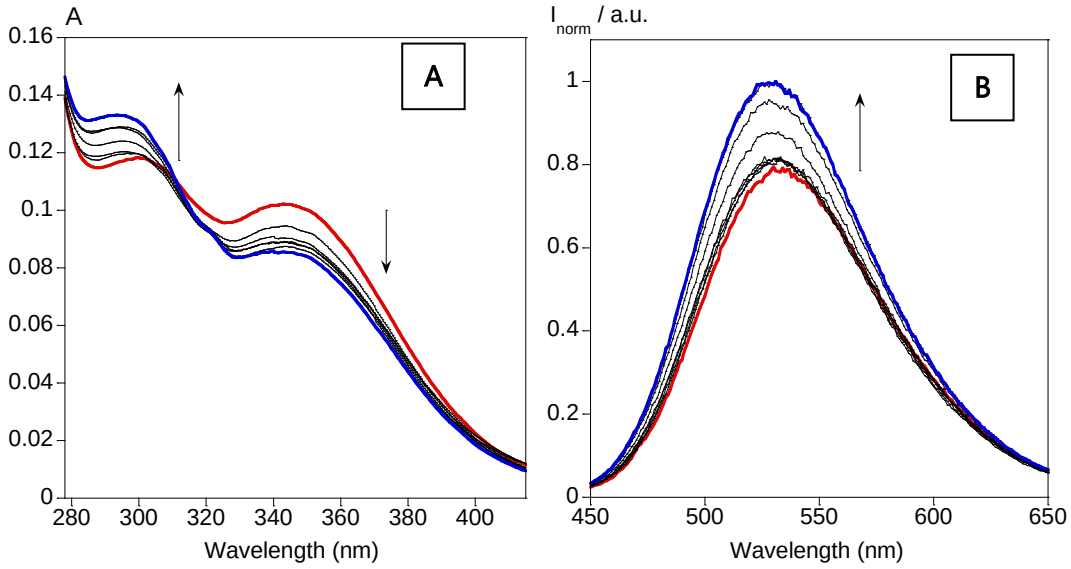

Annex 26. (A) Spectrophotometric and (B) spectrofluorimetric titrations of L6 with the addition of NH_3 (aq) ([NH_3]= 10^{-3}M).

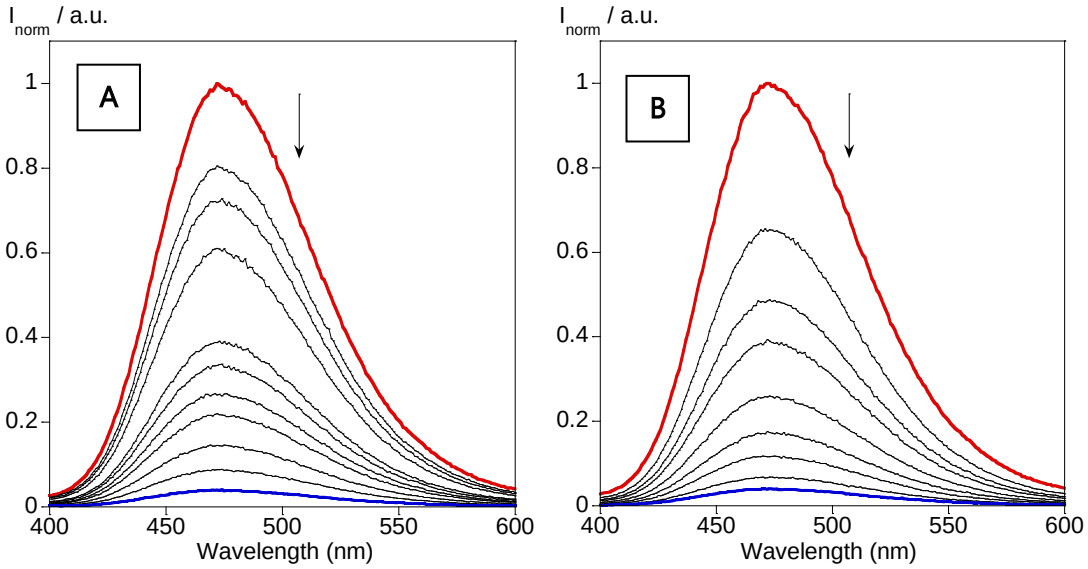

Annex 27. (A) Emission spectra of successive immersion of L6 doped PMMA polymer film in a conc. HCl solution (5m in 5min) (B) Emission spectra of exposure to HCl vapors (20m in 20m)

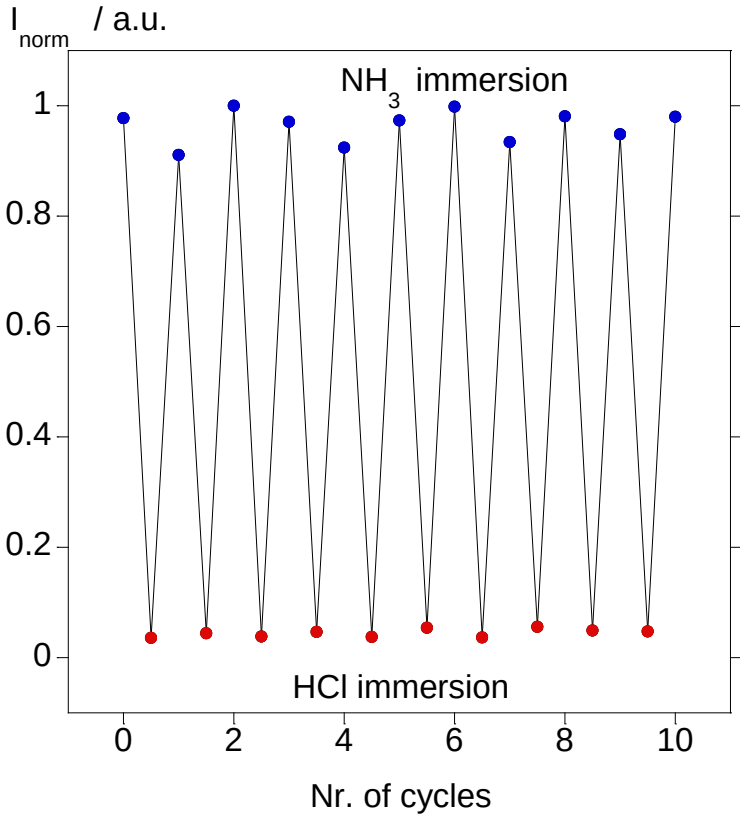

Annex 28. Emission intensity of **L6**@PMMA at λ_{473nm} after successive cycles of HCl/NH_3 immersion

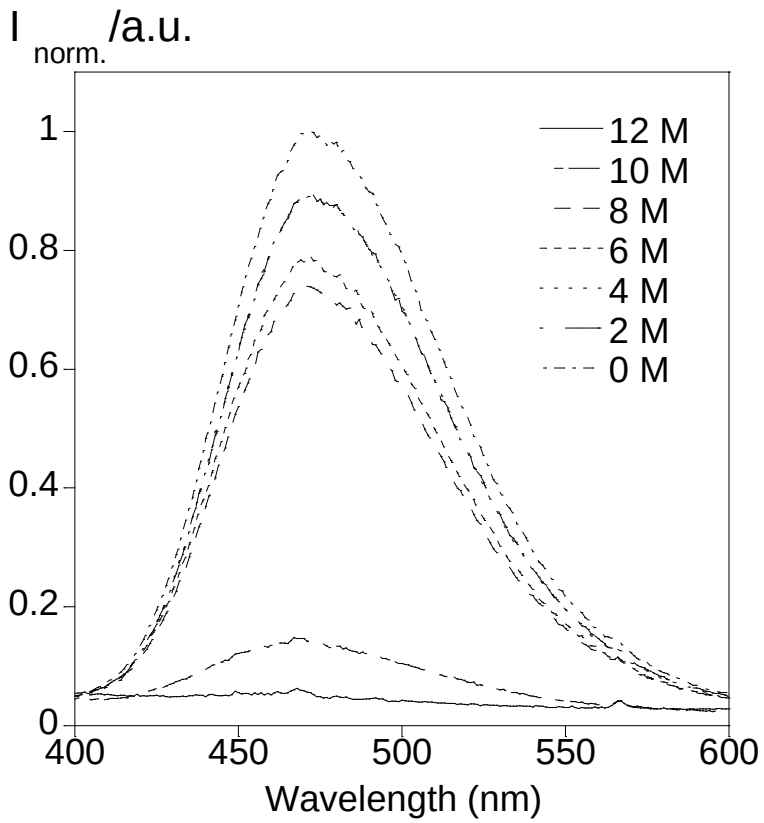

Annex 29. Emission spectra of **L6** immersion in the HCl concentrations from 0 to 12 M

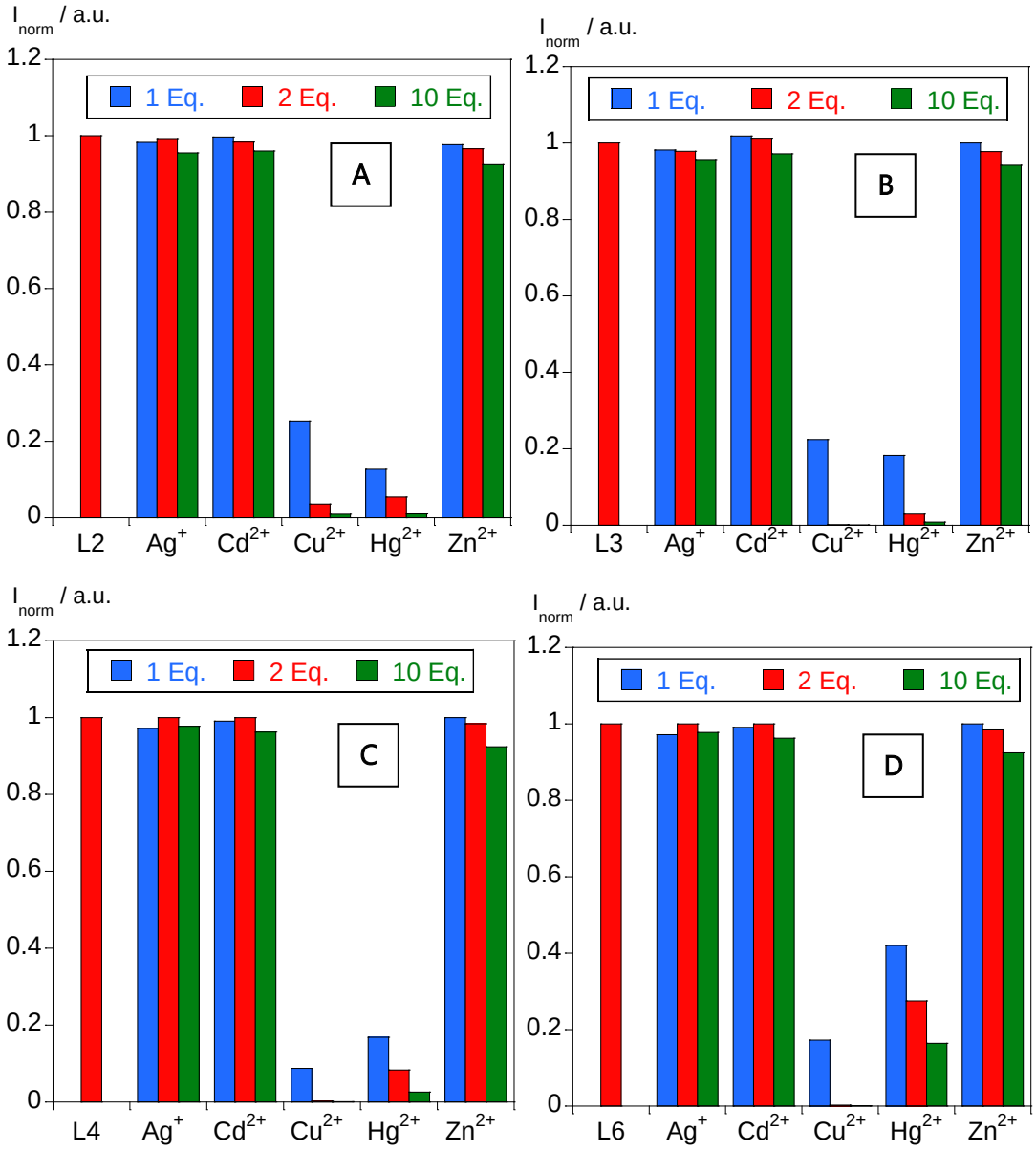

Annex 30. Maximum emission intensities of **L2** A), **L3** (B), **L4** (C), **L6** (D) upon the addition of 1, 2 and 10 equivalents of Ag^{+}, Cd^{2+}, Cu^{2+},Hg^{2+}, Zn^{2+}metal ions. ([**L**] = 20 μM, λ_{em}**L2**= 527 nm, λ_{em}**L3** = 521 nm , λ_{em}**L4** = 530 nm, λ_{em}**L6** = 532 nm T = 298 K).

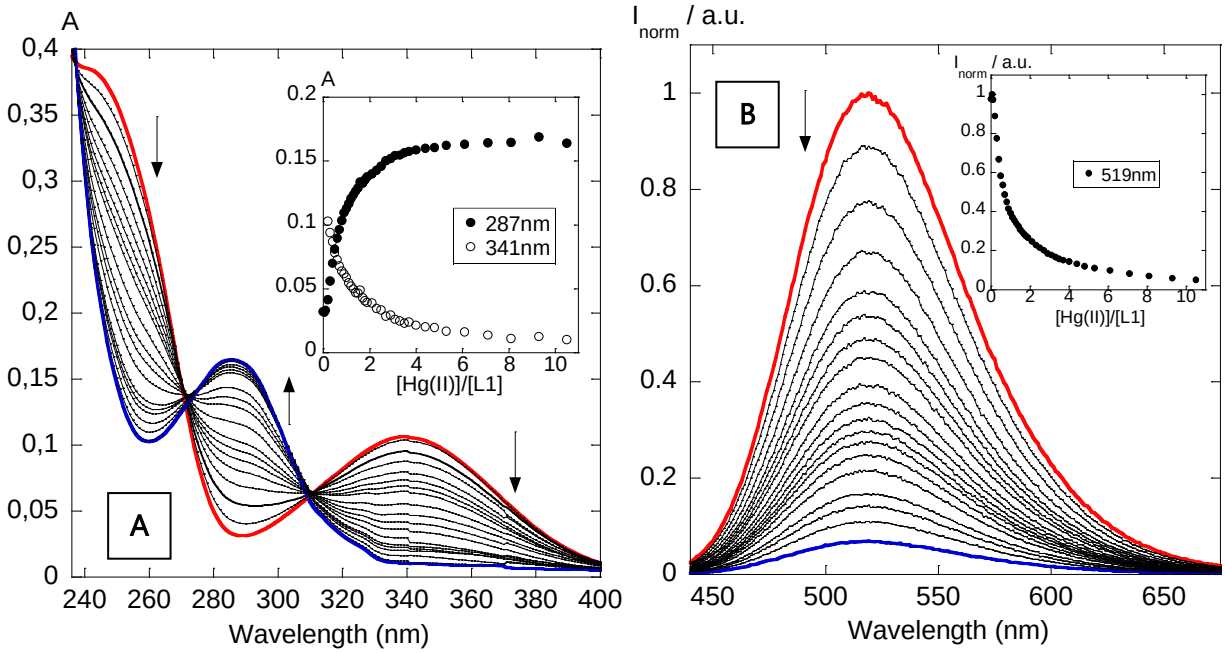

Annex 31. (A) Spectrophotometric and (B) spectrofluorimetric titrations of L1 with the addition of Hg in CH_3CN

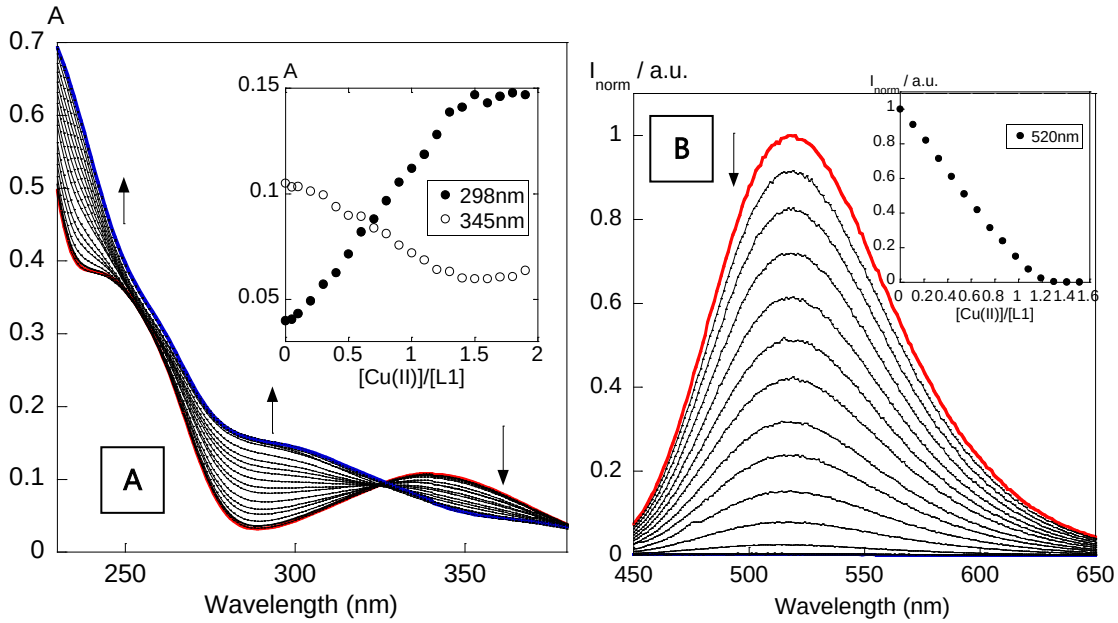

Annex 32. (A) Spectrophotometric and (B) spectrofluorimetric titrations of L1 with the addition of Cu in CH_3CN

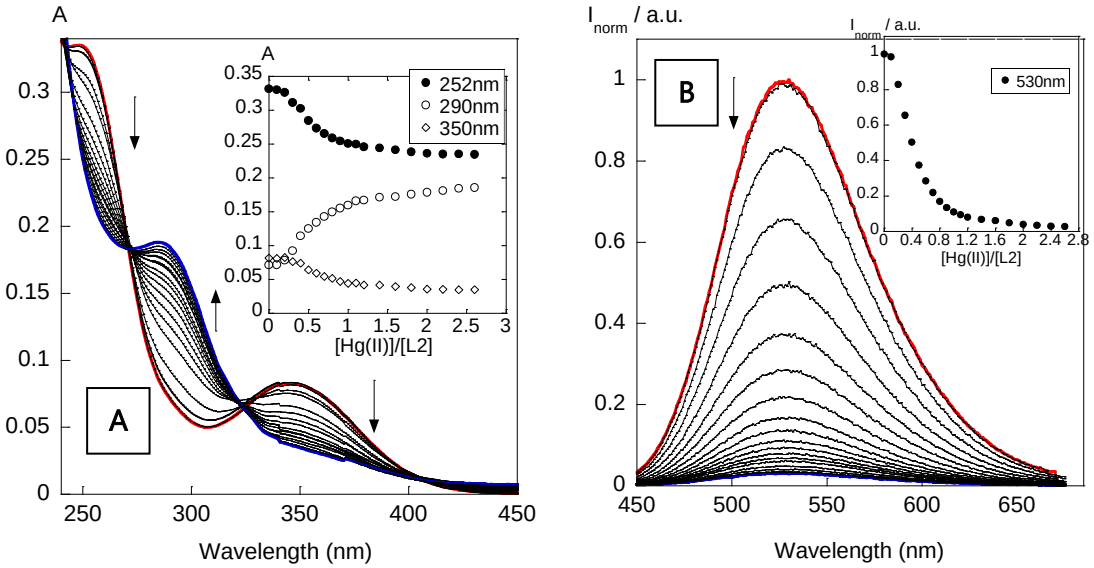

Annex 33. (A) Spectrophotometric and (B) spectrofluorimetric titrations of L2 with the addition of Hg in CH_3CN

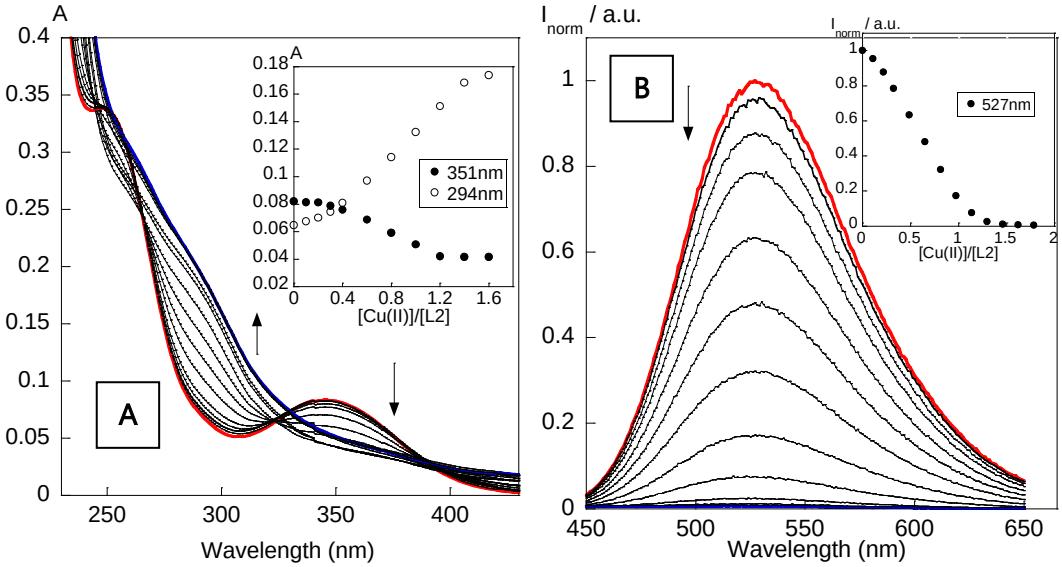

Annex 34. (A) Spectrophotometric and (B) spectrofluorimetric titrations of L2 with the addition of Cu in CH_3CN

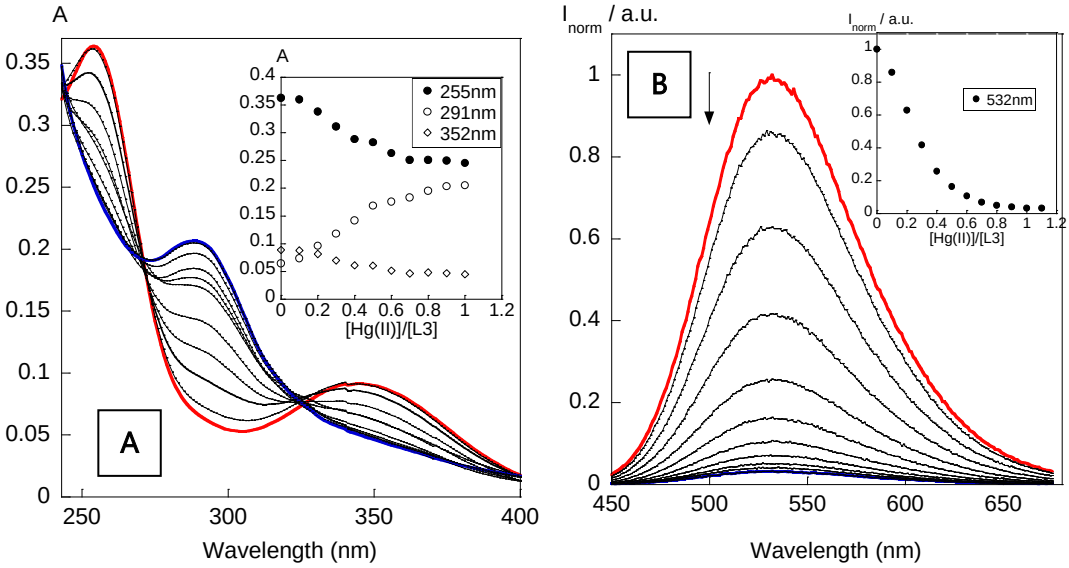

Annex 35. (A) Spectrophotometric and (B) spectrofluorimetric titrations of L3 with the addition of Hg in CH_3CN

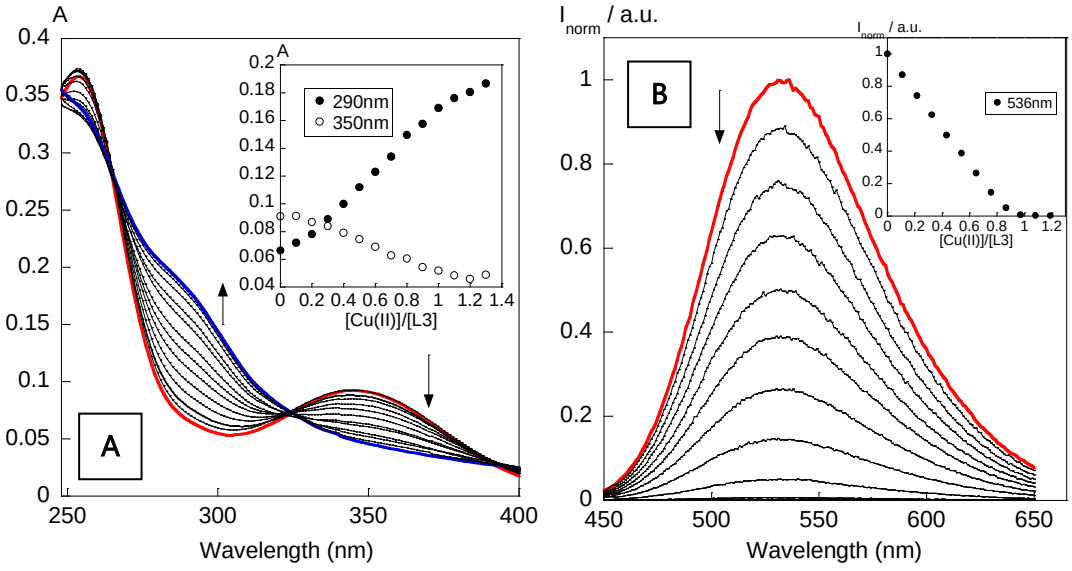

Annex 36. (A) Spectrophotometric and (B) spectrofluorimetric titrations of L3 with the addition of Cu in CH_3CN

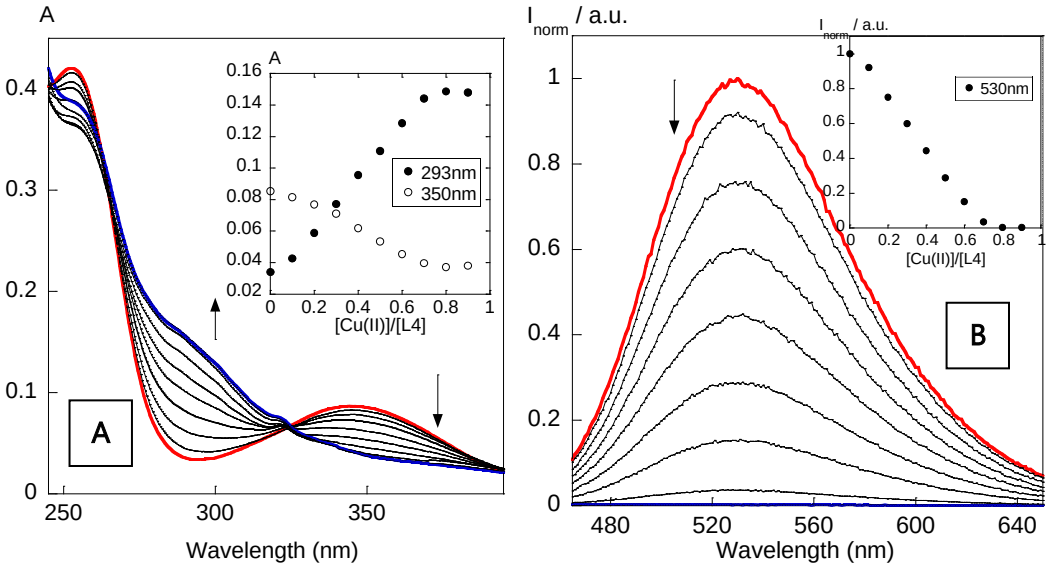

Annex 37. (A) Spectrophotometric and (B) spectrofluorimetric titrations of L4 with the addition of Cu(II) in CH_3CN

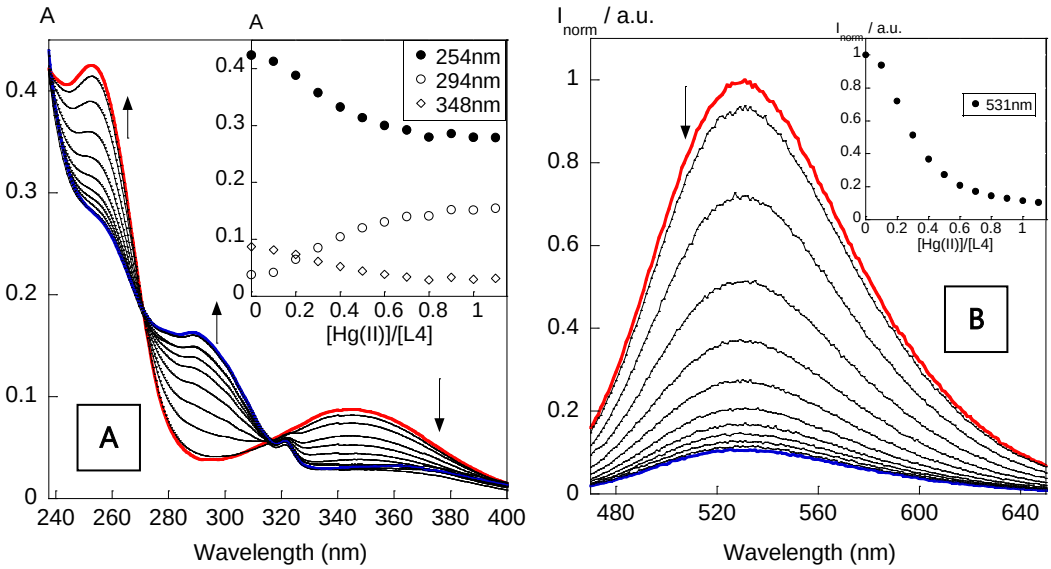

Annex 38. (A) Spectrophotometric and (B) spectrofluorimetric titrations of L4 with the addition of Hg(II) in CH_3CN

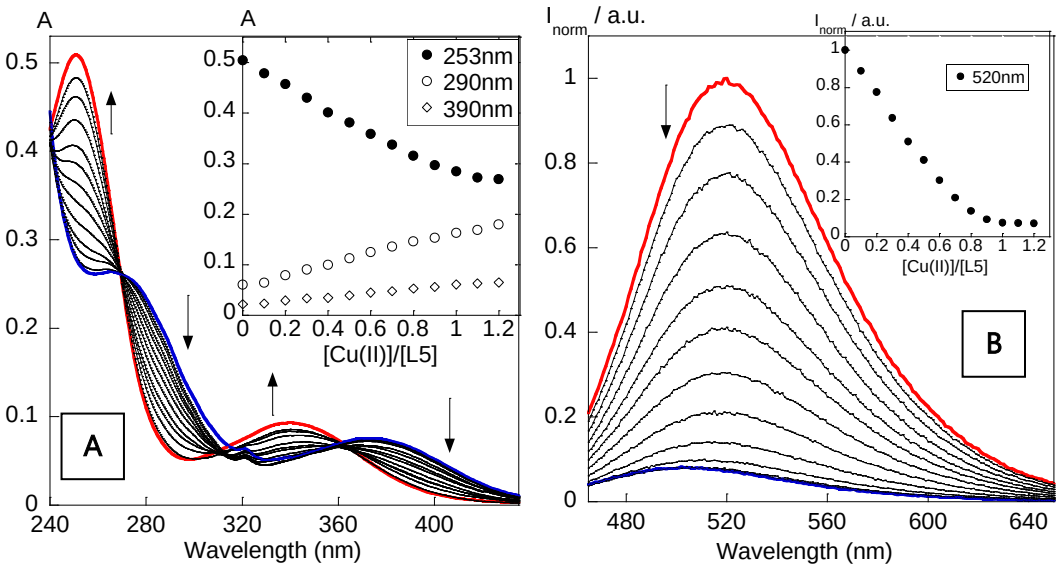

Annex 39. (A) Spectrophotometric and (B) spectrofluorimetric titrations of L5 with the addition of Cu(II) in CH_3CN

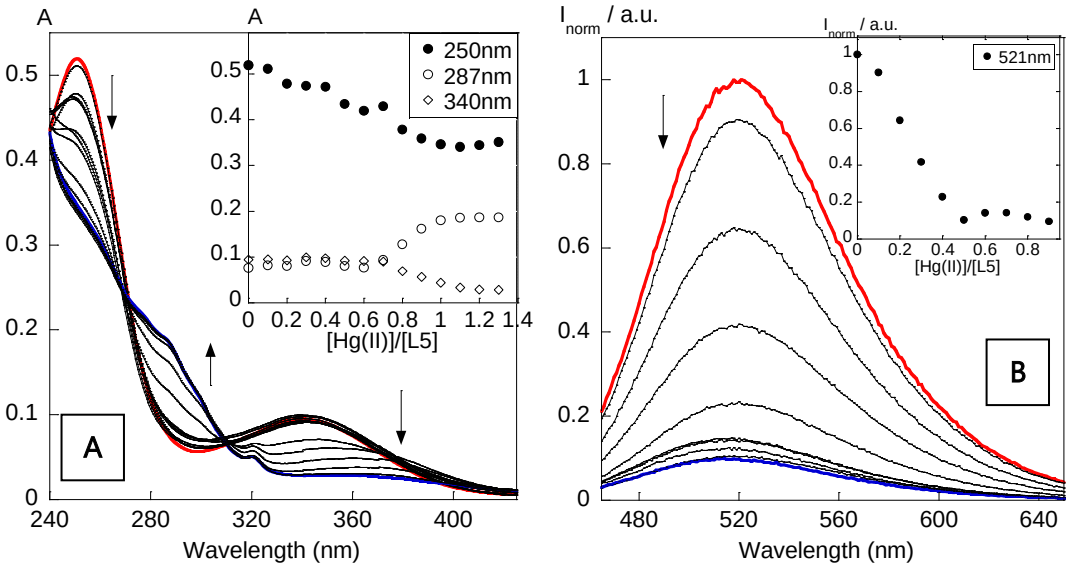

Annex 40. (A) Spectrophotometric and (B) spectrofluorimetric titrations of L5 with the addition of Hg(II) in CH_3CN

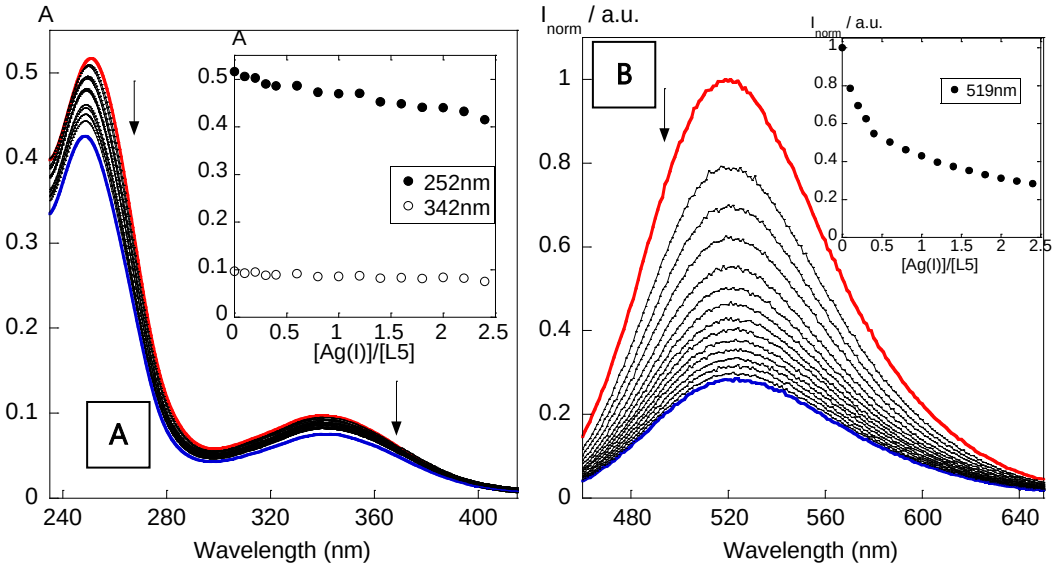

Annex 41. (A) Spectrophotometric and (B) spectrofluorimetric titrations of L5 with the addition of Ag(I) in CH_3CN

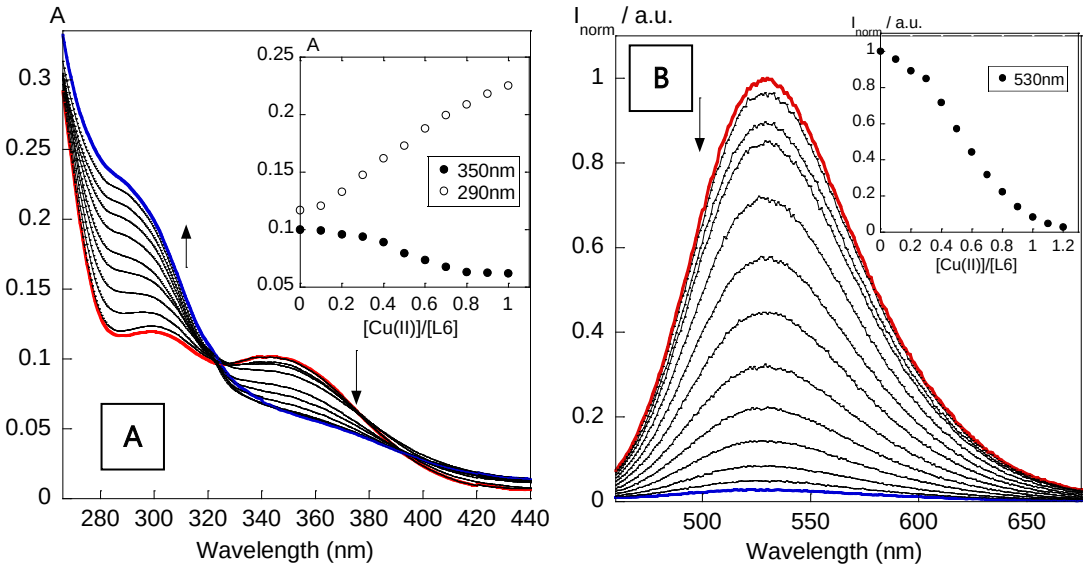

Annex 42. (A) Spectrophotometric and (B) spectrofluorimetric titrations of L6 with the addition of Cu(II) in CH_3CN

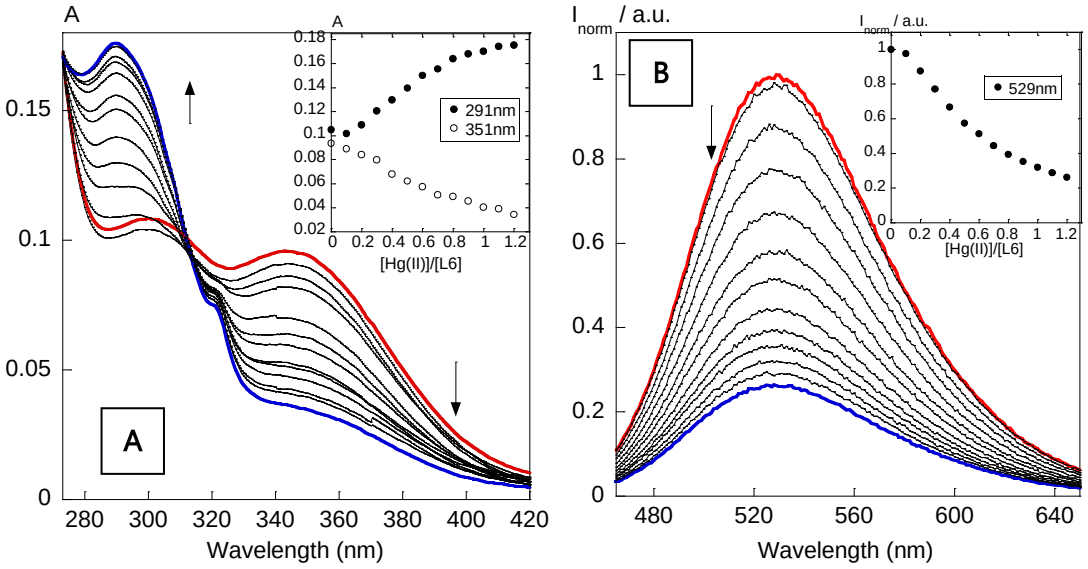

Annex 43. (A) Spectrophotometric and (B) spectrofluorimetric titrations of L6 with the addition of Hg(II) in CH_3CN

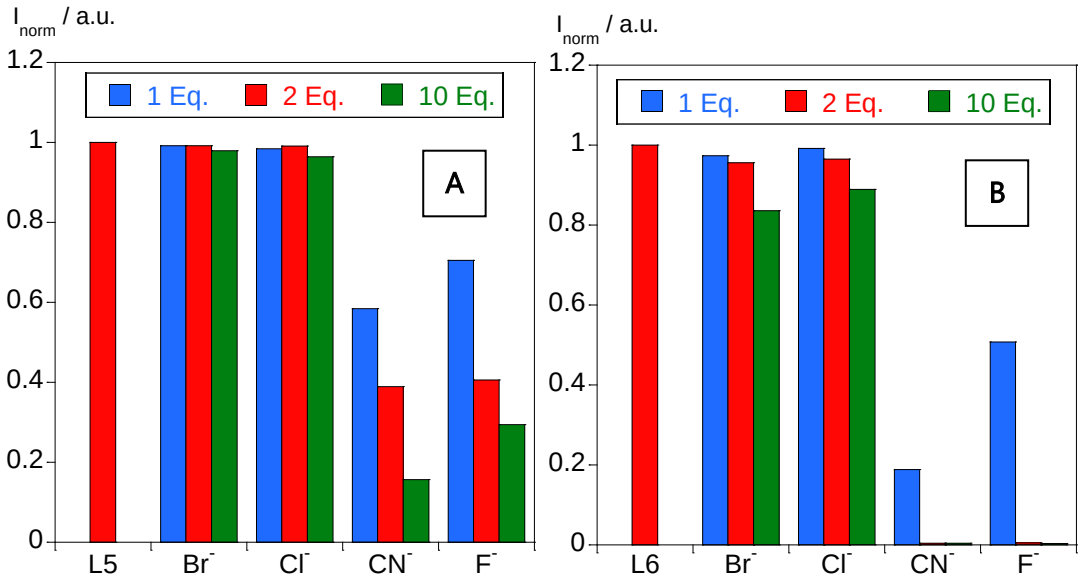

Annex 44. Maximum emission intensities of **L5** (A) and **L6** (B) upon the addition of 1, 2 and 10 equivalents of Br^-, Cl^-, CN^- and F^- anions. ([**L5**]= [**L6**] = 20 µM, λ_{em}**L5**= 519 nm, λ_{em}**L6**= 527 nm T = 295 K).

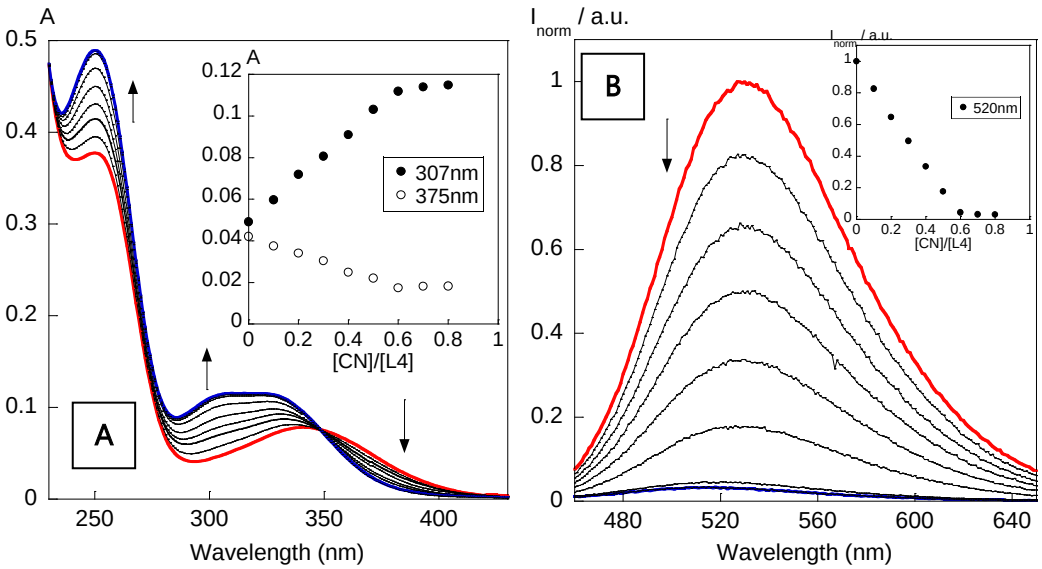

Annex 45. (A) Spectrophotometric and (B) spectrofluorimetric titrations of L4 with the addition of CN^- in CH_3CN

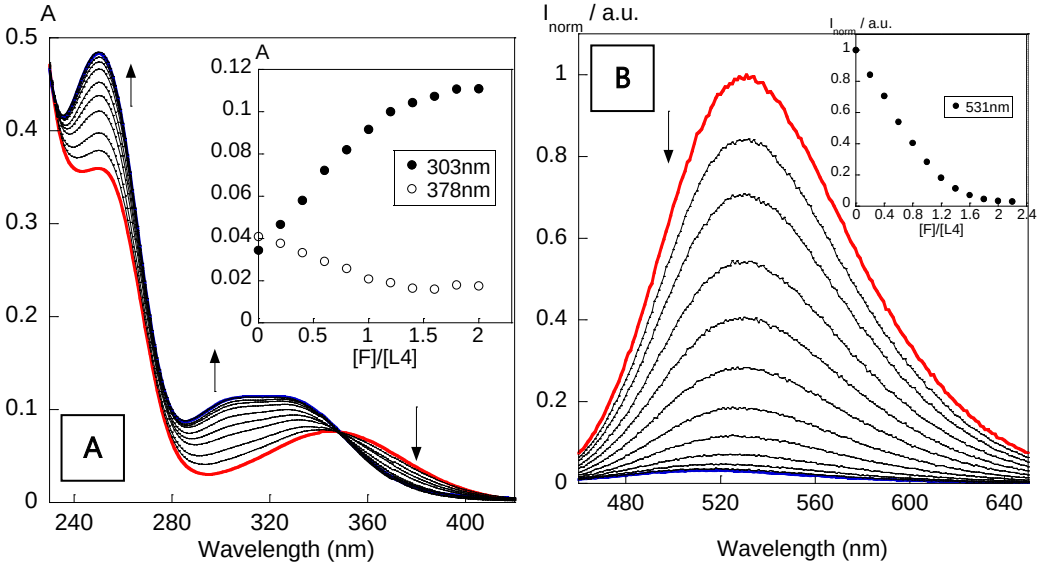

Annex 46. (A) Spectrophotometric and (B) spectrofluorimetric titrations of L4 with the addition of F^- in CH_3CN

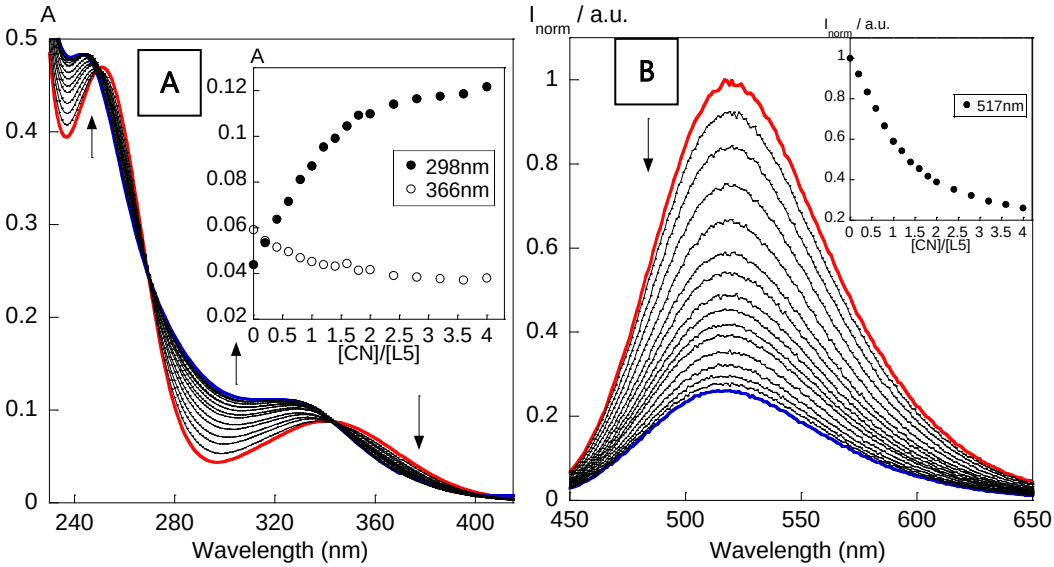

Annex 47. (A) Spectrophotometric and (B) spectrofluorimetric titrations of L5 with the addition of CN^- in CH_3CN

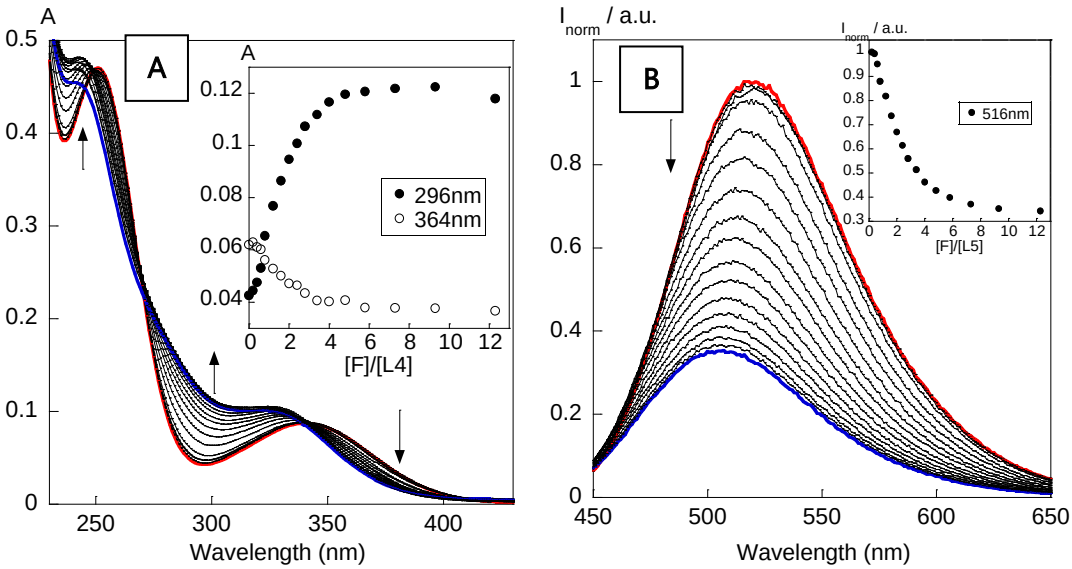

Annex 48. (A) Spectrophotometric and (B) spectrofluorimetric titrations of L5 with the addition of F^- in CH_3CN

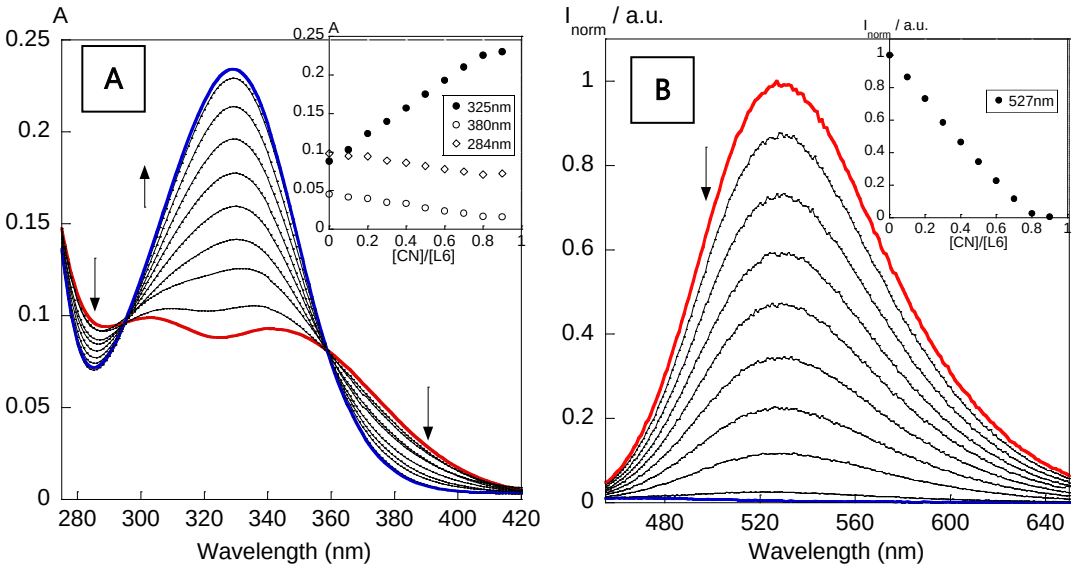

Annex 49. (A) Spectrophotometric and (B) spectrofluorimetric titrations of L6 with the addition of CN^- in CH_3CN

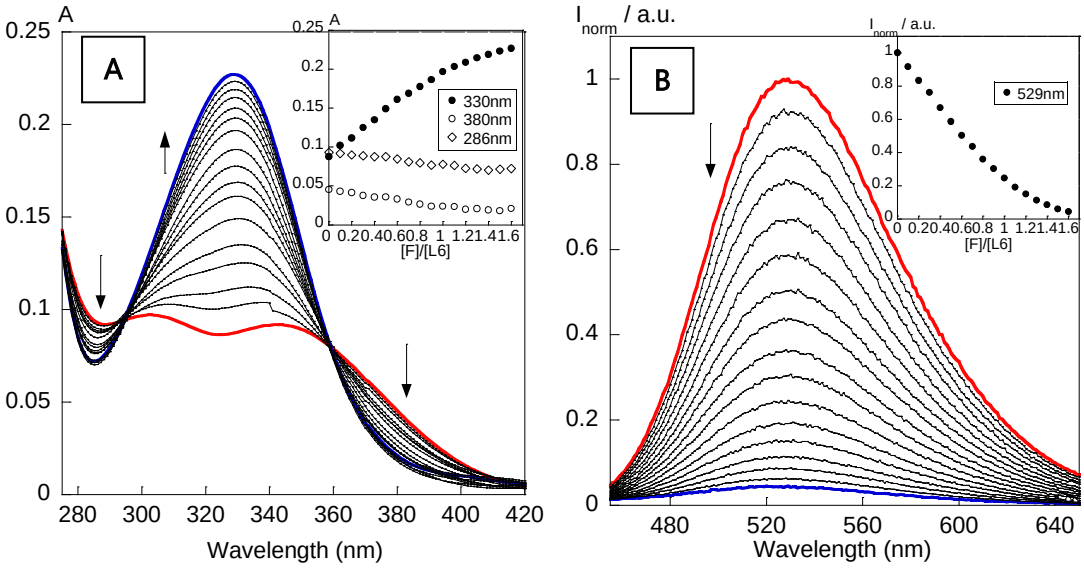

Annex 50. (A) Spectrophotometric and (B) spectrofluorimetric titrations of L6 with the addition of F^- in CH_3CN